# Design and Control of Dairy Housing Microclimate using Advanced Sensor Networks and Simulation Tools to Mitigate Heat Stress of Dairy Cows

By

Hanwook Chung

A dissertation submitted in partial fulfillment of

the requirements for the degree of

Doctor of Philosophy

(Biological Systems Engineering)

at the

UNIVERSITY OF WISCONSIN-MADISON

2023

Data of final oral examination: 11/01/2023

The dissertation is approved by the following members of the Final Oral Committee:

Christopher Y. Choi, Professor, Biological Systems Engineering

Younghyun Kim, Associate Professor, Electrical and Computer Engineering

Neslihan Akdeniz Onuki, Assistant Professor, Biological Systems Engineering

Zhou Zhang, Assistant Professor, Biological Systems Engineering

# DEDICATION

I am who I am due to my countless interactions with many amazing people throughout my life. However, I would like to dedicate this work mostly to Dr. Christopher Y. Choi, my family, and God. I am the product of their support, care, and love, and I wouldn't exist here today without them.

# ACKNOWLEDGEMENTS

I recognize that my dissertation work and where I am right now in my career are not because of my own. These are all the people, excluding my co-authors and committee members, that I would like to mention who directly supported me (big or small) along my PhD journey (in alphabetical order):

**Animal Science:** *Joao Dorea, Ariana Negreiro, Minh Ngo, Kim Reuscher, Faith Reyes, Stephen Switzer, Jennifer Van Os*

**Arlington Research Station:** *Michael Grott*

**Biological Systems Engineering:** *Rob Anex, Julie Garvin, Kody Habeck, Terry Meye, Susan Reinen, Pam Spahn, Trey Standiford, Betsy Wood*

**College of Agriculture and Life Science:** *Eric Dieckman*

**Dairy Cattle Center:** *Jessica Cederquist, Melanie Eck*

**Electrical and Computer Engineering:** *Omkar Prabhune*

**Veterinary Science:** *Thomas Bennett, Sabrina Brounts, Nigel Cook*

Beyond the academic related works, these are the people who also made my PhD journey more special:

*Jiansong Chen, Derek Ho, Yuanye Jiang, Larryn Smerling, Doee Yang, Yoonhong Yi*

All these mentioned people are associated with UW-Madison. Any non-UW people who were part of my journey as well, you know who you are.

# ABSTRACT

Amidst escalating production scales, sustainability imperatives, and heightened awareness of animal welfare with increasingly extreme weather conditions, heat stress in livestock has emerged as a paramount concern for the U.S. dairy industry. Conventional cross- and tunnel-ventilation systems, which have become the standard mechanical system for cow cooling and barn ventilation in large dairy barn facilities, might no longer meet the requirements per cow, given the expanding numbers of cows accommodated within single facilities. This dissertation proposed a series of elements that all pertain to one overarching goal of developing an intelligent animal-centric ventilation system design and control that could address some of the identified concerns with mechanical ventilation in large-scale dairy barns while meeting animal-specific cooling requirements. Solving this problem requires many different interdisciplinary efforts to perfect. However, the studies presented in this dissertation aim to serve as a foundation for future studies. Due to the nature of interdisciplinary studies, many of the presented solutions contain technical knowledge from various disciplines (e.g. Machine Learning, Computational Fluid Dynamics, and Internet of Things).

The two major components required for developing an effective animal-centric ventilation system are a sound method to retrieve animal-based heat stress index and an appropriate targeted cooling ventilation design that can efficiently be controlled using that direct heat stress index. Chapter Two delves into the real-time monitoring of dairy cow heat stress by employing an Internet of Things-infused rechargeable ear tag. This wireless device tracks the subcutaneous ear temperature, offering a minimally invasive proxy to gauge core body temperatures. Chapter Four describes the design optimization and cooling performance evaluation of PPPV. Design parameter optimization and performance prediction using CFD are crucial, especially in a newly proposed system without

a direct predecessor. Lastly, Chapter Three delineates the conception of a machine-learning-augmented computational fluid dynamics (CFD-ML) simulator. This CFD-ML model, which can "simulate" heat and mass transfer phenomena in a dairy barn with much less required computational cost, can be a blueprint for smart simulation tools that can eventually support and aid in ventilation design processes, as described in Chapter Three. In the future, these individual efforts should come together to attain the ultimate goal of developing a smarter, animal-centric dairy barn ventilation system.

# Table of Contents

# CHAPTER 1: INTRODUCTION

## 1.1. Heat Stress Trends in the U.S.

Heat stress emerges as the paramount and most economically detrimental challenge faced by dairy farms in the U.S. Defined as a state wherein animals experience thermal discomfort, prompting the activation of physiological and behavioral defense mechanisms that work against thermal irritation (Bianca, 1968), heat stress triggers a cascade of responses in dairy cows. When subjected to such stress, cows undergo alterations in both physiology and behavior (stemming from elevated body temperatures), and these reactions subsequently impact their rate of heat generation and dissipation.

Physiologically, cows manifest increased respiration and perspiration rates to augment the exchange of heat with the surrounding air through water vapor (Gebremedhin et al., 2008). Concurrently, vasodilation enhances blood flow, channeling heat from the core to the extremities, promoting heat dissipation across the body surface. This heightened thermal stress also precipitates declines in estrus activity and milk synthesis—key metabolic processes produce substantial heat (St. Pierre et al., 2003).

Behavioral adaptations, manifested primarily through reductions in Dry Matter Intake (DMI), are aimed at minimizing digestive processes and ruminal fermentation, thus diminishing internal heat production. Lying time serves as a reliable indicator of a cow's comfort levels, and in periods of elevated temperatures, cows tend to stand longer to augment body surface area exposure to the air, optimizing convective heat loss (Cook et al., 2007). These multifaceted changes converge to diminish overall productivity and compromise the well-being of the animals. To safeguard animal welfare and mitigate the onset of illnesses and diseases, thermal comfort must be maintained (West, 2003).

Recent shifts in both environmental patterns and industry practices are poised to intensify heat stress experienced by dairy cows. Firstly, the anticipated persistence of violent weather patterns, characterized by frequent and severe heat waves, could substantially diminish dairy productivity due to heightened exposure

to heat stress (Rosenstock et al., 2006; Key et al., 2014). Secondly, the consolidation of smaller farms into larger entities for economic and operational gains has led to the construction of large-scale dairy barn structures. In the Upper Midwest, for example, the proportion of milk produced by farms with over 500 cows has seen a more than threefold increase from 2000 to 2012, rising from 9.0% to 38.1% in Wisconsin alone (Evink & Endres, 2017). These larger facilities present significant challenges and escalated costs in ensuring uniform and adequate ventilation and cooling for the animals (Shields, 2010; Mondaca et al., 2019). This trend towards expanding dairy operations in the U.S. to meet the burgeoning global demand for dairy products has amplified the consequences of heat stress. The establishment of dairies in warmer regions and efforts to cultivate more productive bovine breeds have further compounded these challenges as well (Key et al., 2014). Given these developments, there is a pressing need to reassess and refine traditional guidelines for ventilation design and control strategies to accommodate better the requirements and complexities of modern large-scale dairy barns.

## 1.2. Large-scale Dairy Cooling Systems and Their Concerns

### 1.2.1. Baisc Principles

In the endeavor to mitigate the adverse effects of heat stress on livestock, particularly bovines, industry practitioners and infrastructural developers have increasingly turned to sophisticated mechanical ventilation systems. These systems synergistically integrate electrical fans with water spray units to engender an environment conducive to the well-being of the livestock. Through the strategic deployment of such ventilation methodologies, there is a pronounced enhancement of both the sensible and the latent cooling mechanisms that affect the epidermal surface of cows (Van Os, 2019). The foundational principle behind these systems pertains to the propulsion of air currents, a propulsion typically facilitated by electric fans strategically situated in the airspace above livestock resting zones. Also, exhaust fans are used to create a negative-pressure air trajectory that further improves circulation patterns. Water—having undergone a cooling process—is subsequently amalgamated into the ventilation schema to bolster the cooling efficiency.

This is typically achieved either through evaporative cooling pads or through systematic deployment of sprinkler systems.

Architecturally, the barns equipped with these mechanical ventilation systems generally exhibit a low-profile design characterized by their fully enclosed structural parameters. Furthermore, these infrastructures can be categorized (based on their ventilation alignment) as either tunnel-ventilated or cross-ventilated, both of which types dictated by the directionality of the airflow vis-à-vis the barn's ridgeline. It is should be noted that, predicated upon the barn's specific design and geographical positioning, the advocated air velocity can vary, with recommendations ranging from 1.5 m $s^{-1}$ (Tyson et al., 2004) to 3.6 m $s^{-1}$ (Bucklin et al., 2009).

### 1.2.2. Dairy Barn Ventilation Control

In contemporary agricultural practices, cooling systems have traditionally been either manually controlled or automated. The automated system typically depends on a predetermined air temperature setpoint, with activation thresholds generally ranging from 20 to 24 °C (Holmes, 2013; Brouk et al., 1999). While the automated approach offers distinct advantages over its manual counterpart, it presents an array of imperfections. Primarily, the exclusive reliance on air temperature as an activation metric must encapsulate the comprehensive nature of environmental determinants that affect heat load. An equally salient determinant, relative humidity, has been largely marginalized within this systemic framework. Zimbelman et al. (2009) posited that a more holistic approach, incorporating a temperature-humidity index (THI) exceeding 68, would be optimal for cows that maintain a production rate of 35 kg per day. Second, the current mode of temperature acquisition often requires a probe, which, unfortunately, must be positioned sub-optimally and thus yields a generalized reading, overlooking the nuanced microclimates pervading the barn. Furthermore, recent scholarly endeavors (Chen et al., 2016a; Chen et al., 2013; Atkins et al., 2018) have illuminated the differences between environmental heat and actual bovine heat stress, suggesting a need for more direct, precise indicators beyond the prevailing air-temperature or THI paradigms. Additionally, it is pivotal to recognize the heterogeneity in the heat stress responses of individual bovines,

which are contingent upon many factors, including breed, age, production level, reproductive status, health profile, and socio-hierarchical positioning within the herd. Such factors can substantially influence the cow's access to essential resources. Moreover, operational inefficiencies arise when cooling systems continue to function in bovine resting areas during milking sessions and consume resources unnecessarily.

Such practices become particularly salient when considering the resource-intensive nature of cow-cooling systems. Ortiz et al. (2015) pointed out that in regions like Saudi Arabia, daily, per-cow, resource consumption can reach alarming levels of approximately 370 L of water and 4 kWh of electricity. Given the intrinsic linkage between resource utilization and control parameters, even marginal modifications can engender profound shifts in consumption, particularly in expansive facilities equipped with intricate cooling systems. Consequently, there has been a burgeoning interest within the academic community to explore alternative control parameters that align more closely with bovine health, behavior, and physiological metrics (Van Os, 2019). Nevertheless, successfully deploying such parameters necessitates real-time monitoring, and the traditional methodologies, which are limited by technological constraints, cannot perform such tasks reliably. One salient example involves the assessment of core body temperature—a quintessential metric of acute heat stress—which, historically, could only be ascertained via laborious and invasive intravaginal techniques that rendered it impractical for real-time data procurement (Sellier et al., 2014).

### 1.2.3. Dairy Barn Ventilation Design

While effective in augmenting air velocity and enhancing convective heat transfer, the widely adopted negative-pressure exhaust system has its intricacies when deployed within large dairy barns employing crosswind-based ventilation. In such environments, achieving a homogenous air velocity remains a formidable challenge. Specifically, the air velocity tends to diminish within the animal-occupied zone (AOZ) due to the inherent tendency of air currents to follow the path of least resistance. This often results in air movement in the spaces above the cattle rather than directly through the AOZ, as elucidated by Mondaca (2019). Moreover, the unidirectional airflow within these systems invariably compounds air quality

concerns. As the air traverses through the barn's length, it accrues temperature and becomes laden with particulate matter and many microorganisms. Such air quality deterioration can heighten the risk of respiratory ailments within livestock populations (Zhou et al., 2019). A consequential issue associated with this design is the positioning of exhaust fans at the terminal end of the barn to draw this degraded air out of the barn. Over time, debris accumulates on the fans, necessitating cleaning and escalating labor requirements. Further compounding the challenges, the operation of the negative pressure system means that any ingress or egress, such as for feeding or manure handling equipment, inadvertently becomes a prominent air inlet. This transient alteration in airflow dynamics disrupts the established patterns in adjacent barn areas during the door's usage. Recognizing these challenges, contemporary dairies have increasingly incorporated interior recirculating fans, aiming for more uniform air speeds. However, this solution comes at a financial cost. The energy demands of these fans are substantial and, as evidenced by Sharpe et al. (2020), can account for upwards of a third of a dairy's total electricity consumption.

## 1.3. Modern Technologies for Dairy Barn Ventilation Advancement

### 1.3.1. Advanced Sensor Network and Internet of Things

Leveraging the capabilities of advanced sensor network technologies, notably the Internet of Things (IoT), facilitates a granular, per-animal strategy for modulating dairy barn ventilation. By persistently monitoring various metrics in real time—animal health, welfare, and productivity inclusive of reproductive metrics—as well as the vicissitudes in the environment, a dairy producer can adopt Precision Livestock Farming (PLF) (Berckmans, 2017). At its essence, PLF amalgamates contemporary livestock management practices with avant-garde technological innovations such as IoT to accentuate the efficacies of bovine management. Modern electronics' miniaturization and enhanced energy efficiency facilitate the development of pragmatic wearable biosensors. Such devices are adept at continually assessing the physiological health of cows. For instance, parameters such as subcutaneous temperature can be meticulously gauged to ascertain the onset of heat stress, a capability demonstrated by Chung et al. (2020). Given this unprecedented ease of access to granular animal data, it becomes tenable to incorporate big data and machine learning frameworks. Such

integrations allow for the automation of the dairy barn's ventilation systems. They do so by modeling operations imbedded in temporal animal-centric and environmental datasets.

### 1.3.2. Computational Fluid Dynamics for Dairy Barn Ventilation Design

In contemporary literature concerning dairy-housing research, the need for a computational modeling paradigm capable of assessing and improving dairy barn ventilation systems has become increasingly pronounced, especially given the escalating size of ventilation mechanisms and facilities. By harnessing precise models encompassing mass, momentum, and heat transfer dynamics, research engineers can elucidate the intricate interrelations between livestock, spatial configurations, cooling strategies, and environmental conditions. Such an approach obviates the need for expensive physical construction and testing, and such is especially beneficial when pioneering novel ventilation strategies. In this context, computational fluid dynamics (CFD) emerges as a pivotal tool, particularly when modeling large dairy facilities.

The CFD methodology has historically been instrumental in generating airflow simulations across diverse livestock enclosures. For instance, Wu et al. (2012) leveraged a CFD-centric approach to gauge multiple air exchange rate methodologies in naturally ventilated dairy barns. This approach was repeated by Rojano et al. (2015, 2016), who employed CFD simulations to ascertain the environmental impact of air discharged from poultry houses. Expanding upon this, Tomasello et al. (2019) innovated a CFD model to simulate natural ventilation within semi-open freestall barns housing dairy cattle, while Mondaca et al. (2019) underscored the utility of CFD in evaluating microclimates within tunnel-ventilated dairy structures. Furthermore, Zhou et al. (2019) adeptly utilized CFD to model a sectional cross-ventilation barn, offering insights into optimal baffle placements vis-à-vis heat transfer rates occurring on bovine epidermal surfaces.

There has been a prolific corpus of research aiming to refine the CFD methodology used to create livestock housing simulations. A notable study by Mondaca and Choi (2016) scrutinized diverse modeling strategies, focusing on their potential to curtail computational costs. They assessed the efficacy of using simplified bovine geometries and porous mediums to replicate livestock presence in the AOZ. Beyond mere airflow

simulations, a group of researchers has probed into gas emissions and the intricacies of heat and mass transfers occurring within animal enclosures (Rojano et al., 2015; Rojano et al., 2016; Drewry et al., 2018). Rong et al. (2016) further enriched the literature by delineating best practices for CFD modeling, which becomes especially pertinent when selecting optimal turbulent flow models and numerical solvers for livestock buildings. Comprehensive overviews of CFD applications used to predict indoor airflows have also been articulated by research engineers such as Sørensen and Nielsen (2003) and Nielsen (2015).

### 1.3.3. Vision of Machine-learning and Computational Fluid Dynamics in Ventilation

Deep Learning (DL), a subset of Machine Learning (ML), has gained substantial traction in research endeavors that grapple with intricate and voluminous data structures. Its ascendancy can be attributed to its capacity to manage non-linearity through a layered learning paradigm. Computational Fluid Dynamics (CFD) often entails significant computational demands, necessitating extensive CPU, RAM, and GPU resources. When simulating a full-scale dairy barn, the complexities become even more pronounced, rendering CFD approaches less accessible to non-experts. Nevertheless, interdisciplinary research groups have begun to adopt a data-driven strategy. This approach capitalizes on DL, which depends on the metadata derived from CFD simulations. By leveraging such a technique, DL can deliver outcomes that are not only congruent with CFD simulations but can also be achieved with markedly greater efficiency. Guo et al. (2016) demonstrated, for example, that convolutional neural networks can rival CFD simulations while achieving a computational speedup spanning 2-4 orders of magnitude.

These recent strides in the maturation of ML architectures, and especially with regard to the evolution of deep learning neural networks, suggest that professionals in agricultural design, who may need to be better-versed in CFD, can still harness CFD-generated training data to generate insightful outcomes rapidly. The upshot should be the potential conceptualization of a user-friendly fluid-dynamics-simulation tool—ideally web-deployable—that can be used by non-CFD experts in agricultural and biological realms. Such a tool would empower users to dynamically simulate a myriad of design propositions and operational blueprints through platforms like laptops, electronic tablets, or even mobile phones. By offering this computational

utility, the broader agricultural community—encompassing producers, engineers, researchers, and builders—stands to circumvent the pitfalls of redundant modeling and iterative design errors. Rather than defaulting to a laborious trial-and-error methodology, the envisioned CFD-ML simulator would equip stakeholders with predictive insights. Such a proactive stance would facilitate informed decision-making, potentially addressing queries and challenges before designing large-scale mechanically ventilated barns.

## 1.4. Objectives

In the compendium of research presented in this chapter, a concerted effort was undertaken to harness the capabilities of state-of-the-art sensor networks and sophisticated simulation methodologies. Using these methodologies, the overarching goal was to achieve animal-centric smart dairy barn ventilation and cooling system design and control (Figure 1). In order to attain this goal, an effective animal-based heat stress monitoring and adequate targeted cooling ventilation design need to advance simultaneously and eventually to be integrated together. Accurate heat stress monitoring cannot be effective if the ventilation system is not precisely controllable, and ventilation cannot be operating at full efficiency without appropriate heat stress metric. This is an ambitious goal that requires iterations of interdisciplinary studies to perfect. However, the studies presented in this dissertation aim to provide building blocks and bases for the future studies to come toward the ultimate goal.

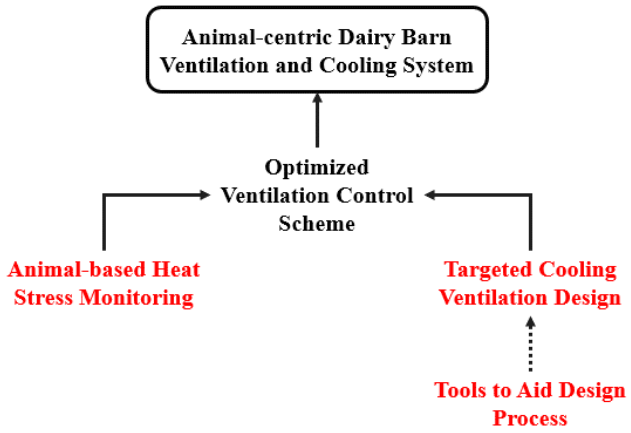


Figure 1. A road to achieving an animal-centric smart dairy barn ventilation and cooling system. This dissertation contains studies that fall under the broad scope of either animal-based heat stress monitoring, targeted cooling ventilation design, or tools to aid design process (red texts).

Chapter Two presents a novel approach for determining the animal-based heat stress index through the measurement of ear base temperature (EBT), which can be interpreted to deduce the core body temperature (CBT) – a direct, quantitative indicator of heat stress, as well as other vital information about dairy cows such as estrus and disease detection. Unlike traditional techniques that measure body temperature, which may not provide real-time data and can be invasive, this study aims to develop and validate an efficient, non-invasive method enabling dairy farmers to monitor their cows' body temperatures using a compact ear tag equipped with a wirelessly rechargeable battery. The device transmits the cow's subcutaneous temperature in real-time through an injectable, passive RFID biosensor. The results demonstrated that the EBT closely mirrors the CBT, exhibiting a similar temperature gradient with an average difference of 0.68 ± 0.35 °C. Regression models indicate that a cow's CBT can be accurately predicted from the EBT, with an average error margin of approximately 0.20 °C, and reduced to 0.11 °C when utilizing a multivariate polynomial regression model factoring in external environmental conditions and the cow's health data, including milk production. The study identified a consistent time lag between changes in microenvironmental conditions and corresponding shifts in a cow's body temperature. These insights empower dairy barn designers to create automated control-loop systems using physiological feedback,

enhancing management practices for timely heat stress detection and mitigation while optimizing energy consumption.

Chapter Three describes the development of CFD-ML as well as its, possibly easy-to-use, application using graphical user interface (GUI). CFD has become one of the leading technology tools for designing and analyzing dairy barn ventilation performance in terms of cooling and ventilation. However, the CFD is not very accessible and user-friendly for producers and other non-CFD users as it requires high end computing hardware to handle large and complex data structure and training and experience to perform meshing and setting boundary conditions. A convolutional neural network (CNN), a representative ML model, allows complex mapping between input barn geometry and the velocity and temperature fields occurring in the barn, resulting in faster prediction time and simpler usage processes. With CNN's ability to proficiently learn complex and voluminous CFD data, the goal of CFD-ML model was to predict velocity and temperature field within the computational domain and predict heat transfer rate in a form of Nusselt Number from cow model surface in given dairy barn models as comparable to normal CFD at fraction of computational cost. As a result, the CFD-ML model can achieve outcomes comparable to those obtained using CFD, with $R^2$ values greater than 0.85, in far less computing time required by CFD. This finding should provide a foundation that could facilitate future CFD-ML advances in dairy science research as well as the development of a user-friendly Graphical User Interface (GUI) that bypasses the complex CFD procedures.

Chapter Four describes the optimization of design and demonstration of cooling performance of a recently explored targeted cooling system called Positive-Pressure Precision Ventilation (PPPV). The proposed benefit of PPPV system improves the ventilation efficiency by relying on a centrally located, pressurized plenum and a series of air-jet nozzles to precisely target each animal. Additionally, it has the potential to provide fresh air by minimizing inlet-to-cow distance. The study delineates a design optimization process, informed by experimentally validated Computational Fluid Dynamics (CFD) simulations, which facilitated the determination of optimal design parameters for the air-jet nozzles. The objective was to integrate design

optimization with CFD simulations to elucidate the advantages of PPPV through various case studies. The performance assessment of these designs, based on specific assumptions and scenarios, showcased the effectiveness of straight air-jets from a medium-sized nozzle (0.1016m diameter) in achieving consistent cooling and optimal pressurization. The case studies revealed that PPPV systems could potentially deliver double the cooling efficiency using only half the mass flow rate compared to traditional methods. Moreover, the system demonstrated scalability, uniform nozzle exhaust, and resilience against drifting ambient air-current at 0.5 m $s^{-1}$. The insights gained from this study are crucial for the successful implementation of PPPV systems and contribute significantly to the evolution of dairy barn ventilation strategies, addressing both economic considerations and animal welfare.

## 1.7. References

Atkins, I., Cook, N.B., Mondaca M.R., & Choi, C.Y. (2018). Continuous respiration rate measurement of heat-stressed dairy cows and relation to environment, body temperature, and lying time. Trans ASABE 2018; 61:1475–85.

Berckmans, D., (2017). General introduction to precision livestock farming. Animal Frontiers, 7(1), 6–11.

Bianca, W., (1968). Thermoregulation. In: Hafez ESE, editor. Adaptation of domestic animals. Philadelphia: Lea & Febiger; p. 97-118.

Brouk, M.J., Smith, J.F., Harner, J.P., Pulkrabek, B.J., McCarty, D.T., & Shirley, J.E. (1999). Performance of lactating dairy cattle housed in a four-row freestall barn equipped with three different cooling systems. Dairy Day 1999. Manhattan, Kansas: Kansas State University,

Bucklin, R.A., Bray, D.R., Martin, J.G., Carlos, L., Carvalho, V. (2009). Environmental Temperatures in Florida Dairy Housing. Applied Engineering in Agriculture. 25, no. 5: 727-735

Chen, J.M., Schütz, K.E., & Tucker., C.B. (2013). Dairy cows use and prefer feed bunks fitted with sprinklers. J. Dairy Sci. 96:5035-5045.

Chen, J.M., Schütz, K.E., & Tucker., C.B. (2016). Cooling cows efficiently with water spray: Behavioral, physiological, and production responses to sprinklers at the feed bunk. J. Dairy Sci. 99.

Chung, H.,Li,J., Kim, Y., Van Os, J.M.C., Brounts, S.H., & Choi, C.Y. (2020). Using implantable biosensors and wearable scanners to monitor dairy cattle's core body temperature in real-time. Computers and Electronics in Agriculture, 174, 105453. https://doi.org/10.1016/j.compag.2020.105453

Cook, N.B., Mentink, R.L., Bennett, T.B., & Burgi, K. (2007). The effect of heat stress and lameness on time budgets of lactating dairy cows. Journal of Dairy Science, 90(4), 1674-1682.

Drewry, J. L., Choi, C. Y., Powell, J. M., & Luck, B. D. (2018). Computational model of methane and ammonia emissions from dairy barns: Development and validation. Computers and electronics in agriculture, 149, 80-89.

Evink, T. L., & Endres, M. I. (2017). Management, operational, animal health, and economic characteristics of large dairy herds in 4 states in the Upper Midwest of the United States. Journal of Dairy Science, 100(11), 9466-9475.

Gebremedhin, K.G., Hillman, P.E., Lee, C.N., Collier, R.J., Willard, S.T., Arthington, J.D., & Brown-Brandl, T.M. (2008). Sweating rates of dairy cows and beef heifers in hot conditions. Trans. ASABE, 51(6), 2167-2178.

Guo, X., Li, W., & Iorio, F. (2016, August). Convolutional neural networks for steady flow approximation. In Proceedings of the 22nd ACM SIGKDD international conference on knowledge discovery and data mining (pp. 481-490).

Holmes. B. (2013). Building Environment. In Dairy Freestall Housing and Equipment (pp. 129 – 148). Ames, IA: MidWest Plan Service (MWPS).

Jara, A.L., Hanson, J.M., Gabbard, J.D., Johnson, S.K., Register, E.T., He, B., & Tompkins, S.M. (2016). Comparison of microchip transponder and noncontact infrared thermometry with rectal thermometry in domestic swine (Sus scrofa domestica). J.Am.Assoc. Lab. Anim. Sci. 55, 588–593

Key, N., Sneeringer, S., & Marquardt, D. (2014). Climate Change, Heat Stress, and US Dairy Production. USDA-ERS Economic Research Report 175.

Marsh, J.R., Gates, R.S., Day, G.B., Aiken, G.E., & Wilkerson, E.G. (2008). Assessment of an injectable RFID temperature sensor for indication of horse well-being. In: ASABE Annual International Meeting - Rhode Island. United States of America Paper Number: 084764.

Mondaca, M. R., & Choi, C. Y. (2016). An evaluation of simplifying assumptions in dairy cow computational fluid dynamics models. Transactions of the ASABE, 59(6), 1575-1584.

Mondaca, M.R. (2019). Ventilation Systems for Adult Dairy Cattle. Veterinary Clinics of North America: Food Anim 35, pp. 139–156

Mondaca, M. R., Choi, C. Y., & Cook, N. B. (2019). Understanding microenvironments within tunnel-ventilated dairy cow freestall facilities: Examination using computational fluid dynamics and experimental validation. Biosystems engineering, 183, 70-84.

Nielsen, P. V. (2015). Fifty years of CFD for room air distribution. Building and Environment, 91, 78-90.

Ortiz, X.A., Smith, J.F., Villar, F., Hall, L., Allen, J., Oddy, A., al-Haddad, A., Lyle, P., & Collier, R.J. (2015). A comparison of 2 evaporative cooling systems on a commercial dairy farm in Saudi Arabia. Journal of dairy science, 98(12), 8710-8722.

Rojano, F., Bournet, P. E., Hassouna, M., Robin, P., Kacira, M., & Choi, C. Y. (2015). Modelling heat and mass transfer of a broiler house using computational fluid dynamics. Biosystems engineering, 136, 25-38.

Rojano, F., Bournet, P. E., Hassouna, M., Robin, P., Kacira, M., & Choi, C. Y. (2016). Computational modelling of thermal and humidity gradients for a naturally ventilated poultry house. Biosystems Engineering, 151, 273-285.

Rong, L., Nielsen, P. V., Bjerg, B., & Zhang, G. (2016). Summary of best guidelines and validation of CFD modeling in livestock buildings to ensure prediction quality. Computers and Electronics in Agriculture, 121, 180-190.

Rosenstock, T., Smukler, S., Cavagnaro, T., 2006. California agricultural landscapes and climate change. Climate Change: Challenges and Solutions for California Agricultural Landscapes. 3-12.

Sellier, N., Guettier, E., & Staub, C. (2014). A Review of Methods to Measure Animal Body Temperature in Precision Farming. American Journal of Agricultural Science and Technology.

Sharpe, K., Heins, B., Reese, M., & Buchanan, E. (2020). Where does the energy go? Hoards Dairyman, May 25, 2020, pp. 323.

Shields, D.A., 2010. Consolidation and Concentration in the U.S. Dairy Industry. Congressional Research Service, 7-5700, www.crs.goc, R41224.

Sørensen, D. N., & Nielsen, P. V. (2003). Quality control of computational fluid dynamics in indoor environments. Indoor air, 13(1), 2-17.

St-Pierre, N.R., Cobanov, B., & Schnitkey, G. (2003). Economic losses from heat stress by US livestock industries. Journal of dairy science, 86, E52-E77.

Tomasello, N., Valenti, F., Cascone, G., & Porto, S. M. (2019). Development of a CFD model to simulate natural ventilation in a semi-open free-stall barn for dairy cows. Buildings, 9(8), 183.

Torrao, N.A., Hetem, R.S., Meyer, L.C.R., & Fick, L.G. (2011). Assessment of the use of temperature-sensitive microchips to determine core body temperature in goats. Vet. Rec. 168 (328).

Tyson, J.T., McFarland, D.F., & Graves, R.E. (2004). Tunnel ventilation for tie stall dairy barns: G-78. University Park, PA: Penn State University.

Van Os, J.M.C. (2019). Considerations for Cooling Dairy Cows with Water. Veterinary Clinics of North America - Food Animal Practice, 35(1), 157–173.

West, J.W. (2003). Effects of Heat-Stress on Production in Dairy Cattle. Journal of Dairy Science, 86(6), 2131–2144.

Wu, W., Zhai, J., Zhang, G., & Nielsen, P. V. (2012). Evaluation of methods for determining air exchange rate in a naturally ventilated dairy cattle building with large openings using computational fluid dynamics (CFD). Atmospheric Environment, 63, 179-188.

Zimbelman, R.B., Collier, R.J., Rhoads, R.P., Rhoads, M.L., Duff, G.C., & Baumgard, L.H. (2009). A re-valuation of the impact of temperature humidity index (THI) and black globe humidity

index (BGHI) on milk production in high producing dairy cows. Proceedings of the 24th Southwest Nutrition and Management conference. Tempe, AZ. pp. 158-168.

Zhou, B., Wang, X., Mondaca, M.R., Rong, L. & Choi, C.Y. (2019). Assessment of optimal airflow baffle locations and angles in mechanically-ventilated dairy houses using computational fluid dynamics. Computers and Electronics in Agriculture, 165, p.104930.

# CHAPTER 2: SUBCUTANEOUS TEMPERATURE MONITORING THROUGH EAR TAG FOR HEAT STRESS DETECTION IN DAIRY COWS

Hanwook Chung, Hien Vu, Younghyun Kim. and Christopher Y. Choi

## 2.1. Abstract

Heat stress remains one of the greatest threats to the economic viability of the dairy industry. The threat becomes even greater during warm and humid conditions, especially for those larger farms seeking to expand their operations. This study sought to develop and test a reliable and timely method that allows dairy farmers to monitor the body temperatures of their animals, using a compact, lightweight ear tag device, including a wirelessly rechargeable battery. The device is also capable of wirelessly transmitting a cow's subcutaneous temperature in real-time by means of an injectable, passive RFID biosensor. The outcomes showed that subcutaneous ear-base temperature (EBT) can synchronously follow the core body temperature (CBT) while also producing a comparable temperature gradient. That is, on average, the difference between a CBT and an EBT is 0.68±0.35 °C. Based on regression models, the CBT of a cow can be accurately predicted based on EBT, with an average error of around 0.20 °C and as low as 0.11 °C by using a

multivariate polynomial regression model, which includes external environmental conditions as well as the cow's health information, including milk production. The outcomes indicate that there is a consistent, predictable time lag between increases in microenvironmental conditions and increases in a cow's body temperature. These findings should enable dairy barn designers to develop and employ automated control-loop systems that utilise physiological feedback to improve management practices aimed at detecting heat stress and mitigating its effects in a timely manner, while minimising energy use.

# Nomenclature

*Roman Letter Symbols*

| | |
|---|---|
| n | Number of Samples |
| RH | Relative Humidity, % |
| t | Time, hr |
| T | Temperature, °C |
| $\Delta T$ | Temperature Difference, °C |
| $T_{db}$ | Average Dry Bulb Temperature, °C |
| $x_i$ | Input Values |
| y | Predicted Values |
| $y_i$ | True Values |
| $\hat{y}i$ | True Values |
| $Z_\alpha$ | Critical Value |

*Acronyms*

| | |
|---|---|
| CBT | Core Body Temperature, °C |
| DCC | Days Carrying Calf, day |
| DIM | Days in Milk, day |
| DMAVG | Daily Milk Average, kg $day^{-1}$ |
| DOY | Day of the Year, day |
| EBT | Ear Base Temperature, °C |

| | |
|---|---|
| IoT | Internet of Things |
| LR | Linear Regression |
| PAR | Parity |
| PR | Polynomial Regression |
| RMSE | Root Mean Square Error |
| THI | Temperature-humidity Index |
| TOD | Time of the Day, hr |

*Greek Letters*

| | |
|---|---|
| $\alpha$ | Type 1 Error |
| $\beta$ | Regression Parameters |
| $\delta$ | Mean Difference |
| $\sigma_a$ | Alternative Standard Deviation |
| $\sigma_0$ | Null Standard Deviation |

## 2.2. Introduction

Traditionally, herd health was monitored by humans and based on observational inspections and experience. However, as the size of dairy operations and the number of animals managed per farmer increased, this monitoring approach became ever more time-consuming and labour-intensive. Therefore, accurately diagnosing the health of individual dairy cows has become an essential aspect of modern dairy barn operation, as animal health status directly impacts the production rate and welfare of a dairy cow. A cow's level of heat stress, for example, can negatively impact the cow's lactation, reproductivity, and mortality, to the extent that the cost of the global dairy industry is expected to rise to a magnitude of billions of dollars (Thornton et al., 2022). Accurate and real-time monitoring of a cow's heat stress can minimise production losses by enabling a dairy farmer to detect such health conditions. It is also essential to achieve effective and efficient use of energy and water with real-time control with timely and optimal cooling methods.

Diary producers have used temperature or thermal indices such as temperature humidity index (THI) as an indirect indication of heat stress. Furthermore, a series of advanced thermal indices, including wind speed

as an important parameter, have been developed and tested to assess the levels of heat stress imposed on cattle. However, individual cow responses vary widely depending on various parameters such as days in milk, parity, days carrying calf, daily milk production, etc. Wang et al. (2018) comprehensively reviewed these cattle-related thermal indices and concluded that each thermal index is distinct to an extent that it should be selected and employed carefully. On the other hand, respiration rates and body temperature are both direct ways to assess how well cows are managing heat stress in real time. Atkins et al. (2018) developed a sensor system to measure the respiration rate of eight lactating Holstein cows. Variation in continuously measured respiration rate corresponded to changes in THI and core body temperature (CBT). However, the development of a miniaturised, real-time, wireless sensor with a rechargeable battery remains to be a challenge.

Recently, many studies have sought to develop automated methods for monitoring various aspects of a dairy cow's health and behaviour. One study, for example, found that a wearable accelerometer sensor in the form of a collar or ear tag could be used to quantify and estimate a cow's feeding and rumination time, and those parameters could be used to detect respiratory diseases and subacute ruminal acidosis (Wolfger et al., 2015). The accelerometer sensor could also be used to monitor the time a cow spent lying down, standing, and walking (Chapa et al., 2020; Nogoy et al., 2022), all of which are key indicators, as time spent lying down is often associated with the wellness of a cow, and the lameness caused by excessive standing significantly affects a cow's productivity (Cook & Nordlund, 2009). Advancing computer vision technologies can be used effectively to monitor these physical behaviours and feeding habits, and postures that indicate lameness (Jorquera-Chavez et al., 2019; Jiang et al., 2022). Also, the respiration rate can be measured by means of a physical pressure sensor mounted on the abdomen of the animal (Atkins et al., 2018) or by using an acoustic sensor (de Carvalho et al., 2020) or a wave radar-based system (Tuan et al., 2022) to count breaths. It should be also noted that Ji et al. (2020) summarized the various measurement options for heat stress indicators related to environmental and/or animal responses, in addition to thermal indices and mitigation strategies.

In addition to these many monitoring parameters that can be used to assess a cow's health, an animal's body-temperature trend can provide much of the vital information associated with heat stress and disease. That is, an adult Holstein dairy cow's body temperature typically ranges from 37.8 to 39.2 °C, and any temperature that exceeds this range will indicate systemic distress (Burfeind et al., 2012; de Andrade Ferrazza et al., 2017; Vitali et al., 2020). Historically, the cow-body temperature has been monitored by inserting a rectal or vaginal temperature device (Andersson et al., 2016; Wang et al., 2020). However, inserting these devices requires significant manual labour, and accessing in real-time the data they collect is difficult.

Advanced sensing technologies have allowed for many different body-temperature-measurement approaches. Although the anatomical site can influence the body-temperature measurement, a cow's body-temperature trend can be determined based on either internal or external measurements (Taylor et al., 2014). An ingestible biosensor, for example, with wireless communication capability, can be placed inside the cow's rumen to enable real-time monitoring of the rumen temperature and detection of the oestrus cycle as well as such diseases as mastitis (Kim et al., 2019; Tao et al., 2019). However, the measurements are inconsistent due to water drinking events. Also, a thermal infrared camera can be used to measure the surface temperature of the udder or eye to determine temperature trend (Yan et al., 2021). In one of the most recent studies focused on how best to measure body temperature, an infrared photodiode thermometer was developed and tested for its ability to monitor a cow's temperature in real-time (Murugeswari et al., 2022). Overall, these readings are far from the core body temperature values using vaginal sensors and sensitive to water spray using soakers and changes in microclimate conditions such as air temperature and wind speed.

A subcutaneous temperature sensor can provide a more stable approach to measuring body temperature as it is less influenced by the environmental conditions during heat waves and certain events such as drinking, spray cooling by soakers, etc.; moreover, the data can be accessed more easily than can data collected by a sensor inserted deep into internal organs. Temperature sensors have already been implanted in various

locations on cows to test for accuracy. Lee and Seo (2015), for one example, surgically inserted thermos-loggers into a cow's neck and around the animal's scapula, and in a more recent study, microchip sensors were implanted near the scutulum of a cow's ear and around the necks of bull calves to monitor body temperature (Setser et al., 2020). Although the functionalities were proven effective, these approaches for monitoring body temperature have predominantly involved either an invasive surgical insertion of an entire physical sensing system or an attachment of a sensor on the skin surface, where the temperature readings can be heavily influenced by microclimate conditions.

As the dairy industry becomes more heavily involved in precision livestock farming — which considers an animal's health status as a key aspect for automatically and efficiently managing animal housing (Schillings et al., 2021; Morrone et al., 2022) — the industry will rely more and more on advancements in the electronics and computing technologies related to the "internet of things" (IoT). As Fig. 1 illustrates, implementing, in place of invasive CBT measurement methods, a real-time, wireless approach to measuring EBT should significantly improve accessibility to each animal's physiological condition and, in return, provide opportunities to develop and improve the methods by which a dairy-barn environment is controlled and managed. That is, the design and system engineers can eventually optimise the operation of cooling fans and soakers based on the real-time monitoring parameters to provide maximum cooling efficiency with minimum energy and water consumption. We are convinced that the EBT data, along with microclimate parameters and other significant factors such as cow's milk yield, can play a significant role in closing the control loop for cooling systems in dairy barns using real-time data analytics. Therefore, the primary objective of the present study is to develop and test an accurate and reliable real-time subcutaneous temperature monitoring system to augment the CBT estimation.

Considering these previous study findings, the present study focuses on developing an ear tag system to minimise the invasiveness while improving data quality. A cow's ear base was deemed an optimal location because of its proximity to the location of the tags that are typically attached to the ears of dairy cows. It should be further noted that Chung et al. (2020) had already demonstrated the viability of using ear-base

temperature (EBT) in place of core body temperature (CBT); however, in place of a neck collar wearable device with a biosensor, this study relied on an ear tag device that was much lighter, more compact, rechargeable, and energy-efficient than the previous devices, and could also collect data for longer periods from the biosensor. With the development of this better device, the primary objectives of this study are: (i) Prove that EBT can adequately represent the CBT and thus be used to monitor levels of heat stress, (ii) Quantify the relationship between body temperature and environmental conditions, and (iii) Provide regression models that use EBT to accurately predict CBT by considering environmental conditions and additional health parameters.

## 2.3. Materials and Method

### 2.3.1. Ear Base Temperature Acquisition

#### 2.3.1.1. Subcutaneous Biosensor Placement

The ear-base, subcutaneous temperature of a dairy cow was measured by injecting a passive RFID temperature biosensor (LifeChip Microchip, Destron Fearing Fort Worth, Texas, USA). The biosensor was inserted using a 12-gauge (2.16 mm inner and 2.77 mm outer diameters) injection needle. The backside of the ear base was chosen as the biosensor location because the area contains copious blood vessels from which a temperature can be recorded and enough muscle fibres to hold the biosensor in place. The injection procedure was performed by a trained veterinary surgeon with appropriate preparation of the injection site, one that involved sterilisations and antiseptics, as well as following proper animal-use protocols and standards. The biosensor and the needle were sterilised using ethylene oxide (EO) gas and Steris Applied Sterilisation Technology (Steris PLC, Mentor, Ohio, USA). The injection site was aseptically prepared before the injection procedure, and 3 mL of lidocaine was injected subcutaneously at the base of each cow's ear to ease injection pain.

#### 2.3.1.2. Wireless Ear Tag Unit and Wireless Data Transmission

With close collaboration, our interdisciplinary team developed a custom wireless ear tag to read EBT from the subcutaneously injected biosensor and transmit the temperature data to a cloud server where users could easily access the data from any internet-connected device in real-time. The primary functions of the wireless ear tag are described in Fig. 2. The ear tag is light and small enough to reside in a cow's ear without causing discomfort. It is circular (11 cm in diameter) and flat in shape and weighs 60 g, and Fig. 3 presents an exploded view of the unit, including all the essential parts. The ear tag was powered by a 150-mAh 3.7-V single-cell Li-ion battery. The assembled tag is waterproof and can reliably read EBT through an RFID from up to approximately 10 cm away which is within range of the implanted biosensor. The ear tag was placed and secured on the top side of cow's ear, which in modern dairy practices is the desirable location for tags other than those used for identification. The ear tag can transmit the EBT data wirelessly to a cloud server by using a combination of LoRa and Wi-Fi communication systems with an additional data relay hub to organise wireless data transmission traffic. Additionally, wireless battery charging was implemented to achieve a lightweight and compact ear-tag design by minimising size and weight, because the battery is usually the heaviest component of any wearable device for its long-term usage.

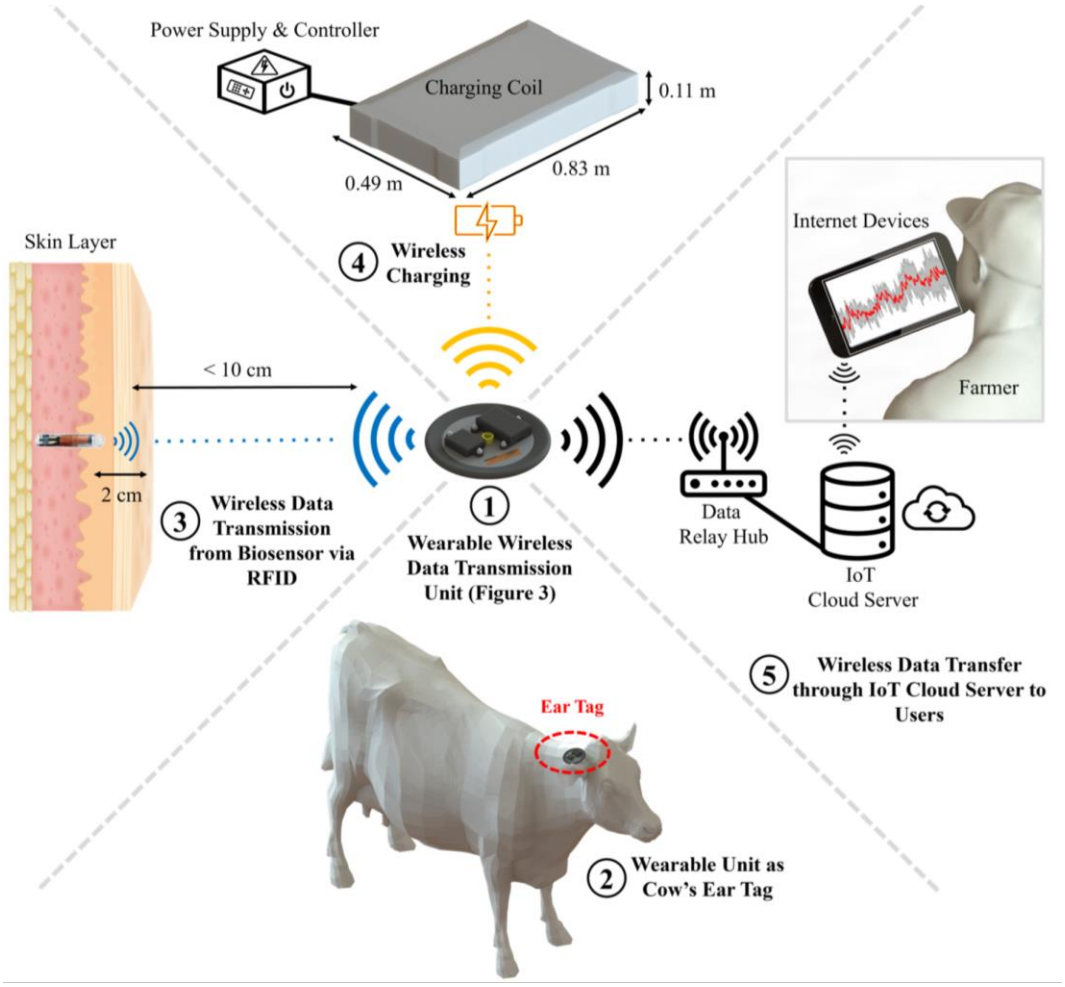


Fig. 2 - Critical elements of the developed ear tag: (1) the ear tag mounted on cow's ear; (2) wireless data transmission from implant sensor via RFID; (3) wireless charging; (4) wireless data transfer through the IoT cloud server to users.

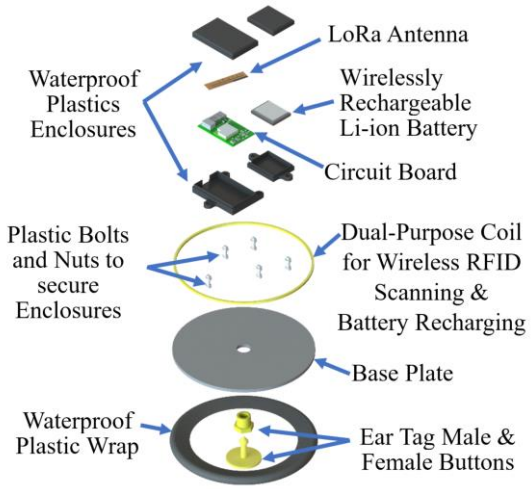


Fig. 3 - An exploded view of the wearable data transmission unit

### 2.3.2. Core Body Temperature Acquisition

The core body temperature (CBT) was measured to compare it with the subcutaneous temperature (i.e., EBT). The CBT of each cow was measured vaginally using a miniature temperature logger (DST centi-T, Star-Oddi, Gardabaer, Iceland), which has an accuracy of ±0.1 °C, and the logger was shrink-wrapped onto a blank (drug-free) controlled internal drug-release (CIDR) insert (Zoetis, Florham Park, New Jersey, USA) with a 30-second sampling interval. Each packaged vaginal temperature sensor and the vaginal area were sterilised and cleaned with a 10% povidone-iodine solution. At the end of the experiment, all the CBTs were collected by retrieving the sensors.

### 2.3.3. Temperature Measurement Recalibration

Before injection, all temperature sensors used to take the CBT and EBT measurements were recalibrated to minimise any reading inconsistency that might be caused by using a different sensor type for each measurement. The sensors were placed in an insulated, constant-temperature water bath. Linear regression was calculated for each sensor against a referencing averaged temperature obtained by means of three

thermocouples (T type, Omega Engineering Inc., Stamford, CT, USA) with the temperature readings ranging from 45 °C to 31 °C (±5 °C typical cow's CBT range).

## 2.3.4. Experimental Setup

### 2.3.4.1. Selection of Dairy Cows

The temperature data collected for this study were taken from seven randomly selected Holstein dairy cows housed at the Dairy Cattle Centre of the University of Wisconsin-Madison. The details concerning each cow, which were recorded at the start of the experiment, can be found in Table 1. Having different 'days in milk' (DIM), parity (PAR), and other reproduction parameters, as expected the cows in the selected group exhibited a wide range of dairy-cow lactation stages, which in total could reasonably represent a typical herd of cows in a commercial dairy barn. DIM refers to the total number of days that the cow is milking from the calving day, and PAR specifies the number of pregnancies that a cow has undergone. Obtaining data from a group of cows with different production characteristics can minimise statistical bias that can occur because of any similarities between cows, if such exist. All seven cows were free of illness or disease at the outset of the experiment.

Table 1. DIM = Days in milk; PAR = Parity; DCC = Days carrying calf; DMAVG = Daily milk average at the beginning of the experiment

| COW [#] | DIM [days] | PAR [-] | DCC [days] | DMAVG [kg day$^{-1}$] |
|---|---|---|---|---|
| 1 | 157 | 5 | 74 | 47.17 |
| 2 | 128 | 3 | 0 | 45.81 |
| 3 | 250 | 3 | 172 | 39.00 |
| 4 | 275 | 4 | 158 | 19.05 |
| 5 | 387 | 2 | 165 | 35.38 |
| 6 | 194 | 2 | 67 | 38.55 |
| 7 | 144 | 3 | 32 | 50.80 |

### 2.3.4.2. Experimental Site

Fig. 4 is a simplified rendering of the indoor experiment facility, including the locations of cows, sensors, and cameras. The experimental facility is a small tie-stall barn within the Dairy Cattle Centre with a highly controlled environment. The enclosed barn is equipped with a negative-pressure ventilation system and evaporative cooling pads, and it can house up to 28 cows. The seven monitored cows were located near the inlets, with three facing south and four facing north, and they were isolated from the rest of the herd with empty stalls immediately adjacent to them. The facility was ventilated by two large (1 m dia.), one medium (0.7 m dia.), and one small (0.5 m dia.) exhaust fans and evaporative cooling pads located at the inlet (1.82 m by 8 m) with wind blowing from west to east.

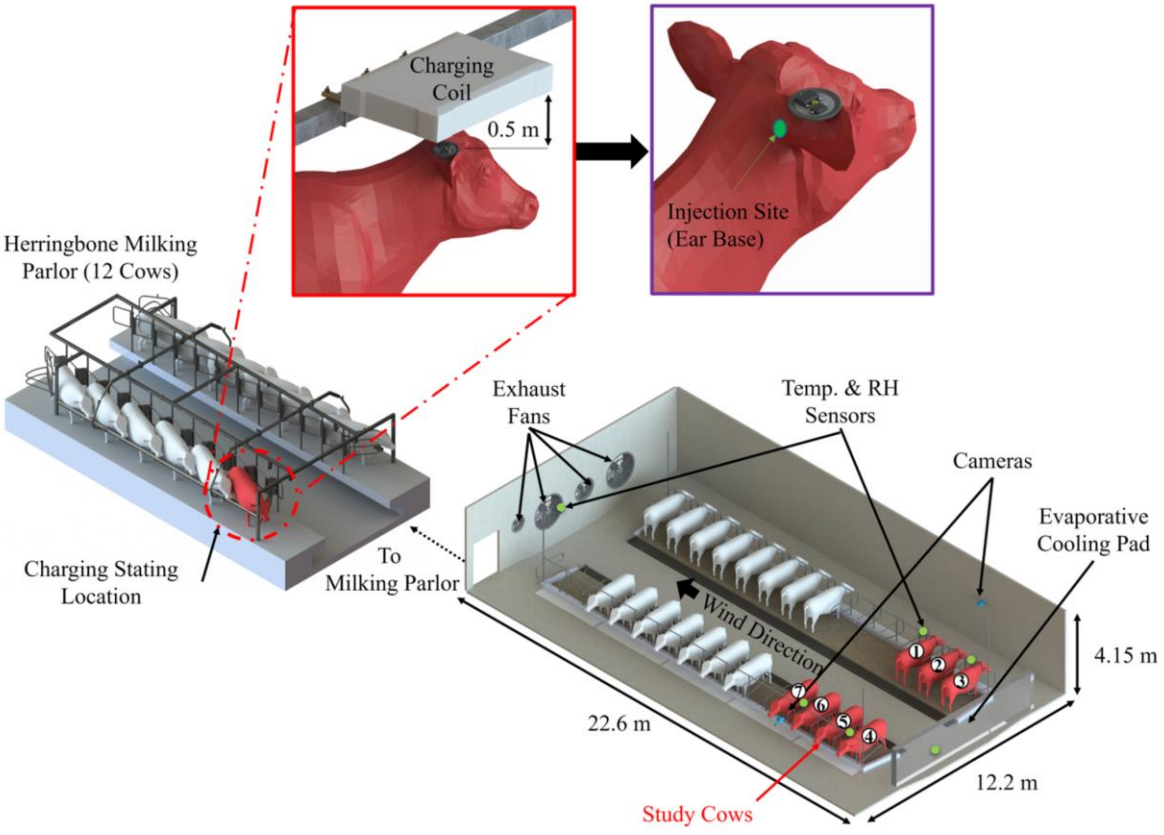


Fig. 4 - Indoor experimental site in the west barn of Dairy Cattle Centre on University of Wisconsin-Madison Campus.

The fans operated constantly throughout the measurement period, yielding a consistent average wind velocity of 0.95 m/s through the middle alley at a 1.5 m height (around 1.21 m/s at the inlet and 3.51 m/s at the exhaust fans). The wind velocity was measured using a hot-wire anemometer (Alnor Velometer AVM440, TSI Inc., Shoreview, Minnesota, USA). The cows were milked twice a day at around 4 AM and 4 PM, during which times the cows were moved to the milking parlour. After each milking session, the cows were released for about 30 minutes to the adjacent yard to expose them to the outdoor environment before returning to their stalls. Six micro-environmental sensors (U23-001 HOBO Pro v2 data loggers, Onset Computer Corp., Bourne, Massachusetts, USA), which can measure dry bulb temperature and relative humidity in 1-minute sampling intervals, were deployed. The sensors were positioned at carefully designated locations within the barn (marked as a green dot in Fig. 4). During the experiment, two internet protocol cameras (Amcrest 4MP Bullet wireless IP camera, Amcrest Technology, Houston, Texas, USA) were mounted on the side walls to monitor all seven cows from the front for behavioural anomaly detection.

#### 2.3.4.2. Weather and Microclimate

The experiment was conducted from the day of the year (DOY) 231 to 244 in 2022. Fig. 5 summarises the outside weather and indoor THI level that occurred during the experiment. The external weather conditions were surveyed at a location near Dane County Regional Airport Station (43.14069°, -89.34521°). THI, the industry's most used environmental indicator, combines ambient air temperature and humidity level to determine a dairy cow's thermal comfort (Dikmen & Hansen, 2009). The THI was calculated using Equation 1, with averaged air temperature and relative humidity as the dependent parameters obtained from six deployed temperature and relative humidity sensors.

$$THI = (1.8 \times T_{db} + 32) - (0.55 - 0.0055 \times RH) \times (1.8 \times T_{db} - 26.8) \quad (1)$$

where

$T_{db}$ = the average dry bulb temperature, °C

$RH$ = the relative humidity, %

Although each cow has a unique tolerance to warm environmental conditions, it has been reported that dairy cows exhibit early signs of heat stress and experience reduced milk production yield at a THI threshold

level of around 68 (Ravagnolo & Misztal, 2002). During the experimental period, the THI level exceeded the pre-determined heat stress threshold of 68 about 58% of the time, as shown in Fig. 5.

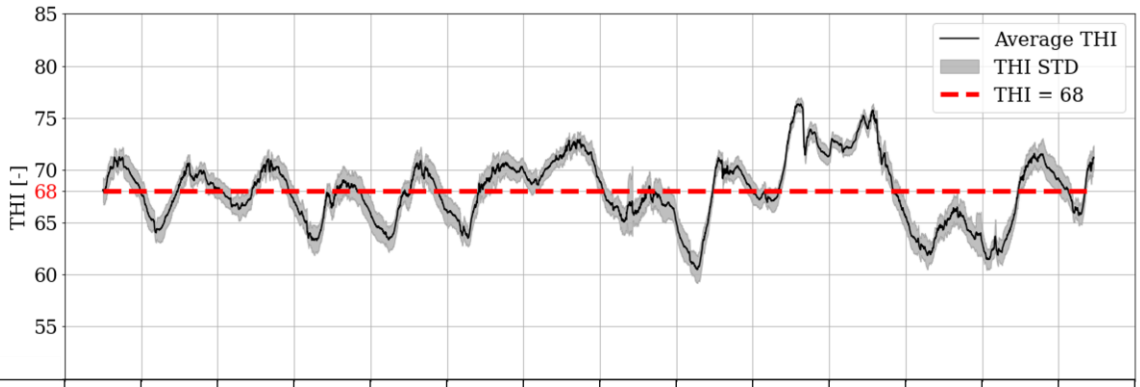


| DOY | 231 | 232 | 233 | 234 | 235 | 236 | 237 | 238 | 239 | 240 | 241 | 242 | 243 | 244 |
|---|---|---|---|---|---|---|---|---|---|---|---|---|---|---|
| T [°C] (HI/LO) | 25/19 | 23/18 | 26/17 | 27/12 | 28/14 | 28/15 | 26/19 | 24/17 | 25/13 | 28/23 | 27/20 | 25/17 | 29/16 | 29/17 |
| Prec. [mm] | 0 | 2.03 | 2.79 | 0 | 0 | 0 | 50.29 | 1.02 | 0 | 11.43 | 1.02 | 0 | 0 | 0 |

Fig. 5 - Summary of outside weather and microclimate conditions. (STD = Standard Deviation; Prec. = Precipitation)

## 2.3.5. Evaluation Methodologies

### 2.3.5.1. Paired T-test

The data sample size of the dairy cows under study was justified by evaluating a statistical power using a paired t-test (Dupont & Plummer, 1990), as presented in Equation 2. Given the significance level and sample size, this power analysis provided the statistical power between two provided sample pools. The higher the power, the more distinction exists between the two compared samples (EBT and CBT in this study), increasing the confidence level of further data analysis.

$$power = \phi\left[\delta\sqrt{n} - \left(\frac{\sigma_0}{\sigma_a}\right)z_{\alpha/2}\right] + \phi\left[-\delta\sqrt{n} - \left(\frac{\sigma_0}{\sigma_a}\right)z_{\alpha/2}\right] \quad (2)$$

where

$\alpha$ = type I error probability for a two-sided test

$\delta$ = mean difference

$\sigma_0$ = null standard deviation

$\sigma_a$ = alternative standard deviation

$z_a$ = the critical value that is exceeds by a standard normal variable with probability α

$n$ = number of samples.

#### 2.3.5.2. Bland-Altmen Plot

A Bland-Altman Plot is a data-plotting method used to investigate the agreement between two datasets and identify potential bias (Altman & Bland, 1983). In this study, the relationship between measured CBT and EBT was represented by the Bland-Altman method, with the difference between CBT and EBT plotted against EBT and THI levels. This method can provide any bias that might be caused by an internal body-temperature level or by external environmental conditions.

#### 2.3.5.3. Temperature Gradient

The temperature gradient was calculated using Equation 3. Each dairy cow produces a unique body temperature profile and physiological response to heat stress. The rate of temperature change can be provided by the temperature profile and its trend agreement between CBT and EBT. In this study, a time length of 12 hours is considered the optimal length of time in which to achieve a meaningful gradient plot due to the diurnal nature of the daily cycle.

$$\Delta T = \frac{dT}{dt} \tag{3}$$

where

$\Delta T$ = temperature difference, °C

$T$ = temperature, °C

$t$ = time, hr

#### 2.3.5.4. Regression Data Fitting

Various regression models and a simple offset approach were tested in order to develop a model that could capture the CBT trend based on the corresponding EBT trend. Because a simple offset approach adds the average difference that exists between a CBT and an EBT to the EBT, a single-variable linear regression (LR) model (Equation 4), as well as single variable polynomial regression (PR) model (Equation 5), were implemented to capture the relationship between CBT and EBT. As presented in Equation 6, a second-order bivariable regression model, a multivariate PR model (Sinha, 2013) was used as a means of considering

variations in temperature and including contextual variables such as THI, Time of the Day (TOD), DIM, PAR, and DMAVG. This study considered 10th-order multivariate PR models because all the calculated RMSE evaluations converged after the 10th order.

$$y = \beta_0 + \beta_1 x \tag{4}$$

$$y = \beta_0 + \beta_1 x + \beta_2 x^2 \tag{5}$$

$$y = \beta_0 + \beta_1 x_1 + \beta_2 x_2 + \beta_{11} x_1^2 + \beta_{22} x_2^2 + \beta_{12} x_1 x_2 \tag{6}$$

where

$y$ = predicted value

$x_i$ = input values

$\beta_i$ = regression parameters

$$Root\ Mean\ Square\ Error = \sqrt{\frac{1}{n}\sum_{i=1}^{n}(y_i - \hat{y}_i)^2} \tag{7}$$

where

$y_i$ = predicted value

$\hat{y}_i$ = true value

$n$ = number of samples.

#### 2.3.5.5. Peak-to-Peak Comparison

Determining whether there is any lag between EBT or body temperature response to environmental changes is important. Accordingly, the daily local maxima for the gradient values of both datasets were identified, and the time differences were compared. The local maxima were determined by a simple comparison of neighbouring values, and a data distance threshold of 12 hours was apparently sufficient for detecting the maxima for each day.

## 2.4. Results and Discussion

### 2.4.1. Temperature Data Summary

Over the course of the two-week experimental period, the ear tag devices collected around 20,000 pairs of CBT and EBT datasets, with the amount of data obtained from each cow ranging from 1,000 to 4,000. The

average temperature readings for CBT and EBT were 38.77 °C and 38.09 °C, respectively, with an average difference of 0.68±0.35 °C (as summarised in Table 2). The temperature spreads recorded at both temperature sources and the standard deviations were slightly higher for the EBT. It should be noted that cows #1, #2, and #7 produced the most milk and recorded higher CBT and EBT averages than did the other cows, reinforcing the observations that higher lactating cows generate more internal body heat and are thus more susceptible to heat stress (Kadzere et al., 2002). Statistical power was calculated for each cow and collectively for all the cows based on the number of collected data. A statistical power of 0.98 was calculated, indicating that the confidence levels concerning the CBT and EBT data obtained from the seven studied cows could be drawn with high confidence.

Table 2. Average body temperature with standard deviation, average difference between CBT and EBT, and statistical power per each cow and in total.

| | Cow #1 | Cow #2 | Cow #3 | Cow #4 | Cow #5 | Cow #6 | Cow #7 | Total |
|---|---|---|---|---|---|---|---|---|
| CBT [°C] | 39.04 ±0.37 | 38.76 ±0.22 | 38.63 ±0.23 | 38.66 ±0.17 | 38.89 ±0.24 | 38.73 ±0.20 | 38.88 ±0.22 | 38.77 ±0.23 |
| EBT [°C] | 38.50 ±0.42 | 37.99 ±0.31 | 38.23 ±0.28 | 37.82 ±0.34 | 37.86 ±0.38 | 37.88 ±0.32 | 38.22 ±0.37 | 38.09 ±0.34 |
| CBT-EBT [°C] | 0.54 ±0.26 | 0.76 ±0.27 | 0.32 ±0.19 | 0.82 ±0.30 | 0.96 ±0.32 | 0.84 ±0.29 | 0.66 ±0.32 | 0.68 ±0.35 |
| Power | 1.00 | 1.00 | 1.00 | 1.00 | 1.00 | 1.00 | 1.00 | 0.98 |

### 2.4.2. CBT vs. EBT

Fig. 6 shows the relationship between the CBT and EBT registered by each cow. The x-axis of each graph tracks the EBT, and the y-axis represents the CBT. The polynomial regression line is also provided on each graph as a red curve. Although the relationship between CBT and EBT is primarily linear and can be captured using a linear regression line (Chung et al. 2020), the polynomial curve was used to capture the trailing end of the data where temperature leaks exist (wide EBT spread on the same CBT levels). This is likely because the ear base is more fully exposed to external conditions and is thus more prone to being cooled by water from drinking troughs and to low THI levels than is the vaginal zone. However, it should

also be noted that temperature leaks were consistently more common at a lower temperature than at a higher CBT, due to vasodilation which would open the blood vessels near the skin surface under heat stress conditions, including the area near the ears. Throughout the experimental period, the average in-barn THI was 68.41, which is over the THI threshold of 68, implying that the summer weather in Wisconsin during the test period was relatively moderate. Given this mild climate, most of the test cows achieved thermal equilibrium through homeostasis. Only Cow #1 (Fig. 6a) experienced detectable heat stress, with her core body temperature climbing to above 40 °C.

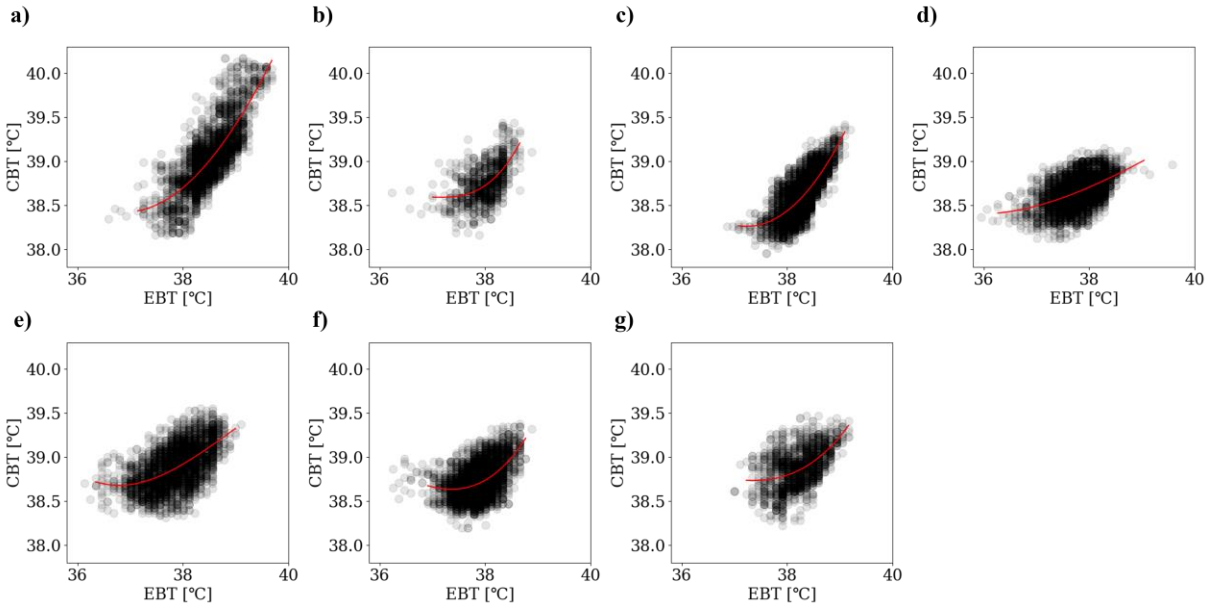


Fig. 6 - XY-plot of CBT and EBT readings with trend line for each cattle. a) to g) is Cow #1 ~ #7, respectively.

While each cow tested during the study was, as stated previously, physically unique, and thus likely to respond at least slightly differently to the same given environmental conditions. Nonetheless, all the cows collectively showed similar overall temperature patterns, and it was therefore crucial to examine the combined data to assess the degree of correlation between CBT and EBT. Fig. 7 shows the Bland-Altman plots of the difference between CBT and EBT against the EBT and THI trends for all data. Against the EBT trend (as indicated in Fig. 7a) the difference between the CBT and EBT diminished and became closer to the average difference, of the higher EBT, an outcome which is similar to the conclusion reached by Chung

et al. (2020). Clearly, the trend indicates the physiological reaction under heat stress due to cutaneous vasodilation that allows for the necessary redirection of blood flow toward the surface of the skin, where the biosensors are located, for heat dissipation. A similar trend can be observed in the Bland-Altman plot based on the THI level. The occurrences of greater differences between EBT and the corresponding CBT are more frequent at the lower THI levels. Again, this indicates that at a higher THI level and a higher CBT, the EBT becomes more fully insulated from the external conditions and thus represents the true value without any temperature leak. This suggests that when using EBT as a tool to represent CBT during periods of heat stress, data collected at temperatures above 37 °C and a THI level of 68 should be more precise and more reliable.

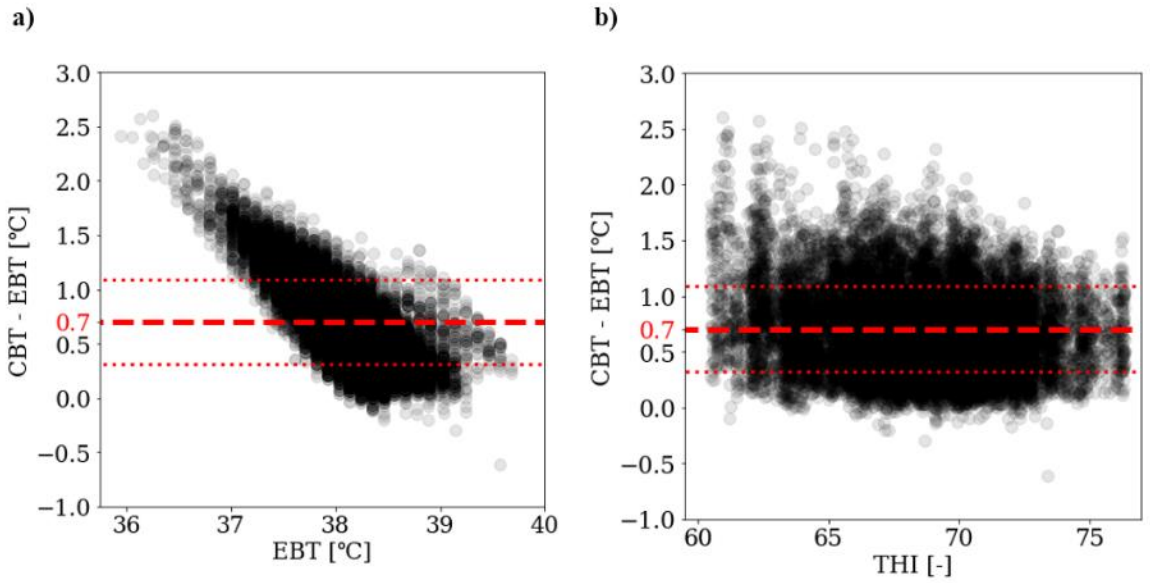


Fig. 7 - Bland-Altman plots: a) the difference between CBT and EBT based on EBT trend; b) the difference between CBT and EBT based on THI trend. Dash lines indicate average difference and dotted lines indicate standard deviations.

### 2.4.3. Average Temperature Trends

Fig. 8a shows the difference between the hourly-averaged CBT and EBT readings throughout the experiment. As can be seen, the EBT follows the same general trend as the CBT. During the experiment, the THI inside the barn was at its highest (rising above the heat threshold of 68) from Day 240 to 242.

Nevertheless, the CBT and EBT readings agreed and rose and fell along with the THI. Although there were occasional and significant spikes in the implant's temperature readings, they consistently occurred during the morning milking time (4 AM). While the THI was not measured when the cows were in the milking parlour or the holding area, the THI would most likely have been much lower throughout the night, when no animals were present and any sudden change in external air conditions would have been likely to impact the EBT. Fig. 8b shows the temperature gradient for CBT and EBT based on time. A 12-hour time window was selected for calculating temperature gradients because, given the diurnal nature of the day and temperature cycle, 12-hour windows produce a smooth curve with gradients for both the CBT and EBT showing comparable trends.

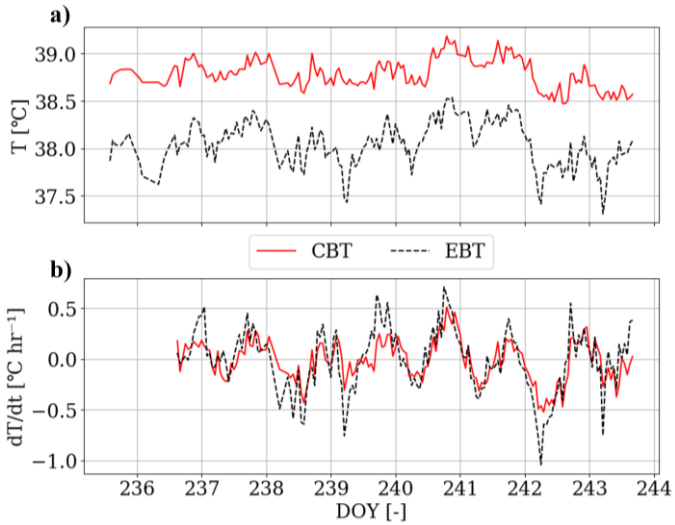


Fig. 8 - Timeseries plot of averaged CBT and EBT trends of all cattle. a) temperature plot; b) temperature gradient plot of 12-hour time window.

Fig. 9 depicts the side-by-side comparison of hourly average EBT and THI. Although THI is a good indicator of body temperature trends, it is not, for the most part, perfect. During the high-THI period, the THI level rose and fell, and the body temperature followed this trend, indicating that a lag time existed between the rise in THI and the cow's physiological response to that rise. Pick-to-pick correlations were analysed with the local maxima for each data trend used to determine the exact degree of lag between the CBT, EBT, and THI readings. This analysis showed that virtually no lag occurred between the two

temperature readings (with nearly 0 hours), while the temperature peaks occurred on average about 3.34 hours after the THI peaks. However, the time lag between the two variables fluctuated from day to day, ranging from 2 to 6+ hours. This finding corresponds with the trend described by Atkins et al. (2018), in which the body temperature of the study's test cows remained elevated despite the decreased THI level in the evening. Using THI to anticipate heat stress level could be a viable option. However, the uncertainty related to the cow's body temperature response delay is far from being precise, especially in larger commercial dairy barns where microclimate conditions are not uniform.

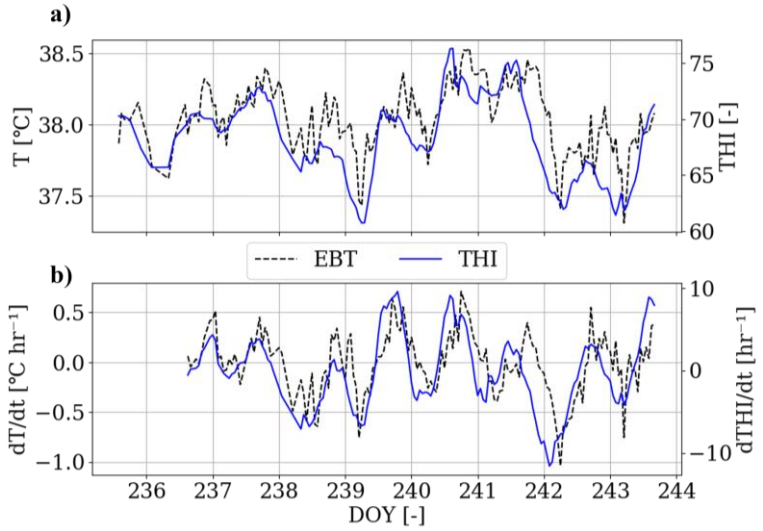


Fig. 9 - Timeseries plot of averaged THI and EBT trends of all cattle: a) absolute values; b) gradient plot of 12-hour time window.

### 2.4.4. Regression Data Fitting

For EBT to stand alone, a regression model that can predict CBT based on EBT should be developed based on the entire dataset. Fig. 10 shows three single-variable regression models capable of capturing accurate CBT levels based on a presented EBT of all seven cows. Overall, the CBT consistently correlated positively with the EBT, and the three models, simple offset based on the average difference (Offset), linear regression (LR), and second-order polynomial regression (PR) captured the CBT with average errors of 0.32, 0.21,

and 0.19, respectively. The PR model works best with a single parameter (EBT), most likely because the EBT behaves with greater accuracy than does the CBT.

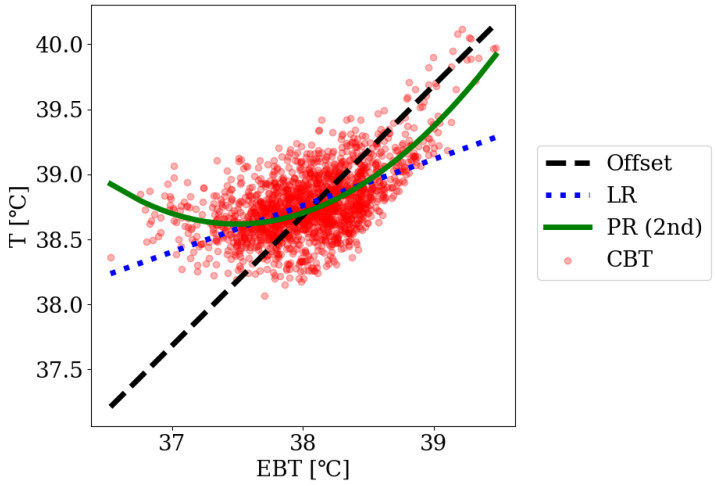


Fig. 10 - CBT vs. simple offset data fitting and single variable regression models. (LR = Linear Regression; PR = Polynomial Regression)

The EBT alone can capture the CBT with a moderately reasonable degree of confidence. However, a cow's body temperature is a complex amalgam of many variables involving the body's interior and external conditions. Consequently, multivariate PR was also used to improve the regression accuracy. Fig. 11 shows the prediction performance of multivariate PR models (which were fitted based on the entire EBT dataset), for predicting, for example, the CBT of Cow #1. In addition to the EBT, the three presented models considered either the THI or TOD as additional variables, or both the THI and TOD. The result showed average errors of 0.19, 0.20, and 0.17, respectively, for those three models. Considering at least one more variable drastically improved the regression model's ability to fit the CBT trends and considering both THI and TOD further improved the accuracy. The overall performance and the individual performances of each cow, as presented by the regression models, are summarised in Table 3.

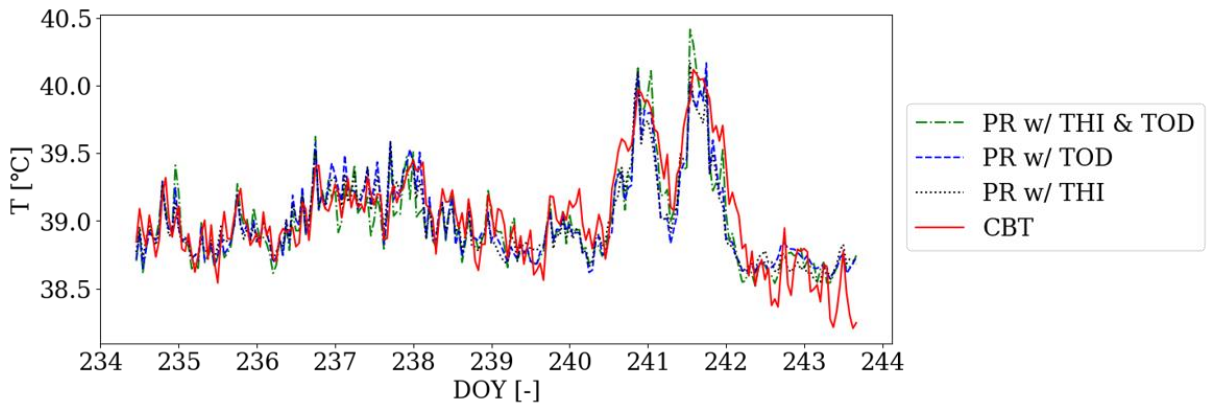


Fig. 11 - Demonstration of multivariate polynomial regression prediction against CBT of Cow #1.

Table 3. RMSE scores for different temperature data fitting models.

| Models [°C] | Cow #1 | Cow #2 | Cow #3 | Cow #4 | Cow #5 | Cow #6 | Cow #7 | Total |
|---|---|---|---|---|---|---|---|---|
| Offset | 0.25 | 0.27 | 0.37 | 0.26 | 0.44 | 0.27 | 0.26 | 0.32 |
| LR | 0.27 | 0.18 | 0.28 | 0.12 | 0.25 | 0.15 | 0.17 | 0.21 |
| PR (2nd) | 0.23 | 0.18 | 0.25 | 0.13 | 0.25 | 0.15 | 0.18 | 0.20 |
| PR w/ THI | 0.19 | 0.19 | 0.24 | 0.13 | 0.24 | 0.16 | 0.18 | 0.19 |
| PR w/ TOD | 0.20 | 0.18 | 0.23 | 0.12 | 0.24 | 0.14 | 0.17 | 0.20 |
| PR w/ THI & TOD | 0.17 | 0.16 | 0.22 | 0.12 | 0.23 | 0.14 | 0.17 | 0.17 |

The CBT, EBT, THI, and TOD are treated as independent variables in this study. Adding certain variables related to a cow's health or production level can potentially further improve the regression model's performance. The lists of RMSE scores shown in Table 4 are derived from a different combination of such additional parameters as DIM, PAR, DCC, and DMAVG. The models that included DMAVG consistently performed the best in predicting the overall CBT (with an average error as low as 0.11 °C). This finding indicated that a meaningful correlation exists between the amount of milk each animal produced and that animal's body temperature trend.

Table 4. The full summary of RMSE scores for multivariate polynomial regression model on top of EBT, THI, and TOD.

| Additional Parameters | Total RMSE [°C] | Additional Parameters | Total RMSE [°C] |
|---|---|---|---|
| DIM | 0.17 | PAR, DCC | 0.13 |
| PAR | 0.17 | PAR, DMAVG | 0.12 |
| DCC | 0.14 | DCC, DMAVG | 0.12 |
| DMAVG | 0.13 | DIM, PAR, DCC | 0.12 |
| DIM, PAR | 0.17 | DIM, PAR, DMAVG | 0.11 |
| DIM, DCC | 0.12 | DIM, DCC, DMAVG | 0.11 |
| DIM, DMAVG | 0.11 | DIM, PAR, DCC, DMAVG | 0.11 |

Regression models offer excellent ways to evaluate the relationship between the two temperature trends (CBT and EBT). By taking a machine learning approach to the multivariate polynomial regression mode, many different variables (even apparently unrelated variables) can be added to provide more information concerning the animals and the environment and thus further improve the regression model's accuracy. The model used in this study considered all the salient temporal (TOD), physiological (CBT and EBT), and production (DIM, PAR, DCC, DMAVG) variables to yield an accurate prediction with a highly acceptable error and two weeks' worth of datasets. With more variables and a larger dataset, the method used in this study could yield even better results, and the EBT could become a crucial component for future heat stress detection systems, dramatically improving the methods dairy farmers use to manage the conditions inside their barns to maintain their animals' well-being.

### 2.4.5. Real-World Application of EBT Readings

For real-world applications and engineering aspects, spaciotemporal data sets are required to provide cool air and/or spray water in real-time to the cows experiencing heat stress. Therefore, a closed-loop system, as presented in Figure 1, is required to determine if fans and soakers should be operated and at what level. In addition to the runtime precision control, the design-time optimization needed to determine the numbers and locations of these cooling methods are also necessary. The system based on physiological (e.g., EBT

or CBT), behavioural (e.g., GPS locations, resting, standing, bunching, and feeding), and environmental (e.g., temperature, humidity, and wind speed) data sets should allow engineers and producers to automate, monitor, and make real-time adjustments by bringing ventilation and cooling into a single decision-making unit. In a unique way, the cloud-based infrastructure, integrated with IoT units, should be capable of controlling variable-frequency-drive (VFD) fans and/or mist and fogging nozzles. In this regard, a few commercial products are already under development and in use in recent years, such as Smartbow® (Zoetis Inc., Parsippany-Troy Hills, NJ, USA) for herd positioning and monitoring and DairyBOS® (VES-Artex, Chippewa Falls, WI, USA) for controlling VFD fans by a real-time, wireless microenvironmental data set. Likewise, the EBT data sets (physiological), along with behavioural and environmental data sets, can be further integrated into a smart decision-making package to improve productivity, welfare, and energy and water efficiency in modern dairy barns.

## 2.5. Conclusions

In lieu of the traditional, more invasive ways of measuring core body temperature, each cow's body temperature was measured by a sensor attached to the animal's ear tag with a biosensor. Results showed that EBT can comparably represent the CBT trends with almost no time lag. On average, the difference between a test cow's EBT and a corresponding CBT was about 0.68±0.35 °C, which is the deviation to be expected when comparing temperatures taken from a location on an animal's core to temperatures taken from the subcutaneous biosensors. The relationship between the EBT and the CBT of each cow tested in this study varied, and therefore, instead of relying on an animal's absolute temperature value, either the rate of temperature change, or the relative temperature difference should be considered when using EBT data to detect the subtle body-temperature increases that signal the onset of heat stress. Data-fitting models can further adjust the recorded EBT readings and accurately predict the CBT within 0.2 °C, given that the body temperature of each cow will invariably differ by at least that much because of variations in physiological parameters and milk yield. As expected, a consistent time lag existed between an increase in the environmental temperature and a subsequent rise in CBT; moreover, the EBT measurements tended to

become increasingly precise as the THI exceeds 68, the heat stress threshold, due to vasodilation. Overall, the outcomes obtained during this study indicate that using an ear-tag sensor to measure EBT could effectively serve as an alternative to the invasive CBT-measurement approach.

The EBT of each animal used in this study was also successfully measured and observed in real-time by means of a custom-designed ear-tag device that can wirelessly transmit EBT to any IoT system. The lightweight and compact design of this ear tag was made possible by recent advancements in wireless battery recharging capabilities and electronics that make power consumption more efficient. Given this study's findings, ear-tag-based body temperature monitoring should become a crucial part of precision livestock agriculture, one that focuses on physiological feedback to manage an animal's environment and health and maximise the animal's well-being as well as productivity more efficiently.

## 2.6. References

Altman, D. G., & Bland, J. M. (1983). Measurement in medicine: the analysis of method comparison studies. The Statistician. 32 (3), 307–317.

Andersson, L. M., Okada, H., Miura, R., Zhang, Y., Yoshioka, K., Aso, H., & Itoh, T. (2016). Wearable wireless estrus detection sensor for cows. Computers and Electronics in Agriculture, 127, 101–108. https://doi.org/10.1016/j.compag.2016.06.007

Atkins, I. K., Cook, N. B., Mondaca, M. R., & Choi, C. Y. (2018). Continuous respiration rate measurement of heat-stressed dairy cows and relation to environment, body temperature, and lying time. In Transactions of the ASABE (Vol. 61, Issue 5, pp. 1475–1485). https://doi.org/10.13031/trans.12451

Bianca, W. (1968) Thermoregulation. In: Hafez ESE, editor. Adaptation of domestic animals. Philadelphia: Lea & Febiger; p. 97–118.

Burnett, T. A., Kaur, M., Polsky, L., & Cerri, R. L. A. (2020). Rumen-Reticular Temperature During Estrus and Ovulation Using Automated Activity Monitors in Dairy Cows. In Frontiers in Veterinary Science (Vol. 7). https://doi.org/10.3389/fvets.2020.597512

Chung, H., Li, J., Kim, Y., Van Os, J. M. C., Brounts, S. H., & Choi, C. Y. (2020). Using implantable biosensors and wearable scanners to monitor dairy cattle's core body temperature in real-time. Computers and Electronics in Agriculture, 174, 105453. https://doi.org/10.1016/j.compag.2020.105453

de Andrade Ferrazza, R., Garcia, H. D. M., Aristizábal, V. H. V., de Souza Nogueira, C., Veríssimo, C. J., Sartori, J. R., ... & Ferreira, J. C. P. (2017). Thermoregulatory responses of Holstein cows exposed to experimentally induced heat stress. Journal of Thermal Biology, 66, 68-80.

da Silva, L. A. F., Gomes, D. F. C., Borges, N. C., Cardoso, J. R., Rabelo, R. E., Mendes, L. A., ... & Qualhato, G. (2017). Auricular pavilion arteriography in cattle. Semina: Ciências Agrárias, 38(5), 3039-3047.

da Silva, R. A. B., Pandorfi, H., de Almeida, G. L. P., & da Silva, M. V. (2020). Exploratory data inference for detecting mastitis in dairy cattle. In Acta Scientiarum - Animal Sciences (Vol. 42, Issue 1). https://doi.org/10.4025/actascianimsci.v42i1.46394

de Carvalho, G. A., Salman, A. K. D., da Cruz, P. G., de Souza, E. C., da Silva, F. R. F., & Schmitt, E. (2020). Technical note: An acoustic method for assessing the respiration rate of free-grazing dairy cattle. Livestock Science, 241, 104270. https://doi.org/10.1016/j.livsci.2020.104270

Dikmen, S., & Hansen, P. J. (2009). Is the temperature-humidity index the best indicator of heat stress in lactating dairy cows in a subtropical environment? In Journal of Dairy Science (Vol. 92, Issue 1, pp. 109–116). https://doi.org/10.3168/jds.2008-1370

Dupont, W. D., & Plummer Jr, W. D. (1990). Power and sample size calculations: a review and computer program. Controlled clinical trials, 11(2), 116-128.

Gaughan, J. B., Mader, T. L., Holt, S. M., & Lisle, A. (2008). A new heat load index for feedlot cattle1. Journal of Animal Science, 86(1), 226–234. https://doi.org/10.2527/jas.2007-0305

Islam, M. A., Lomax, S., Doughty, A., Islam, M. R., Jay, O., Thomson, P., & Clark, C. (2021). Automated Monitoring of Cattle Heat Stress and Its Mitigation. In Frontiers in Animal Science (Vol. 2, Issue October, pp. 1–20). https://www.frontiersin.org/articles/10.3389/fanim.2021.737213/full

Jorquera-Chavez, M., Fuentes, S., Dunshea, F. R., Warner, R. D., Poblete, T., & Jongman, E. C. (2019). Modelling and Validation of Computer Vision Techniques to Assess Heart Rate, Eye Temperature, Ear-Base Temperature and Respiration Rate in Cattle. Animals, 9(12), 1089. https://doi.org/10.3390/ani9121089

Kim, H., Min, Y., & Choi, B. (2019). Real-time temperature monitoring for the early detection of mastitis in dairy cattle: Methods and case researches. Computers and Electronics in Agriculture, 162, 119–125. https://doi.org/10.1016/j.compag.2019.04.004

Lee, M., & Seo, S. (2021). Wearable Wireless Biosensor Technology for Monitoring Cattle: A Review. Animals, 11(10), 2779. https://doi.org/10.3390/ani11102779

Liu, J., Li, L., Chen, X., Lu, Y., & Wang, D. (2019). Effects of heat stress on body temperature, milk production, and reproduction in dairy cows: A novel idea for monitoring and evaluation of heat stress — A review. In Asian-Australasian Journal of Animal Sciences (Vol. 32, Issue 9, pp. 1332–1339). https://doi.org/10.5713/ajas.18.0743

Ludington, D., & Johnson, E. (2003). Dairy farm energy audit summary. Report prepared for FlexTech Services, New York State Energy Research and Development Authority, Albany, NY.

Mader, T. L., Johnson, L. J., & Gaughan, J. B. (2010). A comprehensive index for assessing environmental stress in animals. Journal of Animal Science, 88(6), 2153–2165. https://doi.org/10.2527/jas.2009-2586

Mondaca, M. R., & Cook, N. B. (2019). Modeled construction and operating costs of different ventilation systems for lactating dairy cows. Journal of dairy science, 102(1), 896-908.

Moore, J. A. (1993). Basic Ventilation Considerations for Livestock or Poultry Housing. In Pacific Northwest Extension (Vol. 307, Issue June, pp. 1–6).

Morrone, S., Dimauro, C., Gambella, F., & Cappai, M. G. (2022). Industry 4.0 and Precision Livestock Farming (PLF): An up to Date Overview across Animal Productions. Sensors, 22(12), 4319. https://doi.org/10.3390/s22124319

Ouellet, V., Toledo, I. M., Dado-Senn, B., Dahl, G. E., & Laporta, J. (2021). Critical Temperature-Humidity Index Thresholds for Dry Cows in a Subtropical Climate. Frontiers in Animal Science, 2. https://doi.org/10.3389/fanim.2021.706636

Schillings, J., Bennett, R., & Rose, D. C. (2021). Exploring the Potential of Precision Livestock Farming Technologies to Help Address Farm Animal Welfare. In Frontiers in Animal Science (Vol. 2). https://doi.org/10.3389/fanim.2021.639678

Schüller, L. K., & Heuwieser, W. (2016). Measurement of heat stress conditions at cow level and comparison to climate conditions at stationary locations inside a dairy barn. Journal of Dairy Research, 83(3), 305–311. https://doi.org/10.1017/S0022029916000388

Tao, Y., Ye, S., Jiao, L., Tian, H., & Dong, D. (2019). Design of Bovine Rumen Acid Monitoring Sensor and System. 2019 IEEE 8th Joint International Information Technology and Artificial Intelligence Conference (ITAIC), 926–930. https://doi.org/10.1109/ITAIC.2019.8785853

Thornton, P., Nelson, G., Mayberry, D., & Herrero, M. (2022). Impacts of heat stress on global cattle production during the 21st century: a modelling study. The Lancet Planetary Health, 6(3), e192–e201. https://doi.org/10.1016/S2542-5196(22)00002-X

Tuan, S.-A., Rustia, D. J. A., Hsu, J.-T., & Lin, T.-T. (2022). Frequency modulated continuous wave radar-based system for monitoring dairy cow respiration rate. Computers and Electronics in Agriculture, 196, 106913. https://doi.org/10.1016/j.compag.2022.106913

Van Os, J. M. C. (2019). Considerations for Cooling Dairy Cows with Water. Veterinary Clinics of North America: Food Animal Practice, 35(1), 157–173. https://doi.org/10.1016/j.cvfa.2018.10.009

Wang, F.-K., Shih, J.-Y., Juan, P.-H., Su, Y.-C., & Wang, Y.-C. (2021). Non-Invasive Cattle Body Temperature Measurement Using Infrared Thermography and Auxiliary Sensors. Sensors, 21(7), 2425. https://doi.org/10.3390/s21072425

Wang, S., Zhang, H., Tian, H., Chen, X., Li, S., Lu, Y., Li, L., & Wang, D. (2020). Alterations in vaginal temperature during the estrous cycle in dairy cows detected by a new intravaginal device—a pilot study. Tropical Animal Health and Production, 52(5), 2265–2271. https://doi.org/10.1007/s11250-020-02199-5

Wang, X., Zhang, G., & Choi, C. Y. (2018a). Evaluation of a precision air-supply system in naturally ventilated freestall dairy barns. Biosystems Engineering, 175, 1-15.

Wang, X., Gao, H., Gebremedhin, K. G., Bjerg, B. S., Van Os, J., Tucker, C. B., & Zhang, G. (2018b). A predictive model of equivalent temperature index for dairy cattle (ETIC). Journal of Thermal Biology, 76, 165–170. https://doi.org/10.1016/j.jtherbio.2018.07.013

Yan, G., Li, H., & Shi, Z. (2021). Evaluation of thermal indices as the indicators of heat stress in dairy cows in a temperate climate. In Animals (Vol. 11, Issue 8). https://doi.org/10.3390/ani11082459

# CHAPTER 3: APPLICATION OF MACHINE-LEARNED METADATA-DRIVEN MODEL FOR DAIRY BARN VENTILATION SIMULATION

Hanwook Chung, Xi Zhang, Seunghyeon Jung, Zhou Zhang, and Christopher Y. Choi

## 3.1. Abstract

As US dairy operations consolidate to meet an increasing demand for dairy products, dairy producers have begun to seek more economically efficient dairy-barn designs and ventilation systems to combat the pernicious effects of heat stress. The metabolic changes that heat stress induces not only put the animals at risk of serious illness but also diminish the herd's productivity. Lactation, being a metabolic process, generates a great deal of body heat thereby increasing the risk of heat stress during warm weather, and that risk increases when the animals commingle in an enclosed space. For this reason, predicting heat stress and estimating its severity have taken on special importance. Recently, producers and barn builders have contended with the conditions that promote heat stress by implementing closed mechanical ventilation systems. However, if a proposed ventilation system's performance was not accurately predicted, the system would not work effectively or efficiently. The traditional ways of assessing ventilation performance, which involved either hand-held sensors or stationery sensing monitors, tended to be time-consuming and the larger the barn the more labor-intensive. Additionally, the complex microenvironmental system that exists inside a dairy barn is further complicated by the myriad moving elements, both animals and operational machines. Given these complicating parameters, researchers have lately turned to computation fluid dynamics (CFD) when analyzing such environments because, once properly validated, CFD can accurately predict the heat and mass transfer occurring at any location inside a computer-generated model of a dairy barn. However, operating CFD correctly requires not only an extensive background knowledge and a significant amount of hands-on experience, but also high-end hardware, which is often unavailable to dairy operators and non-CFD--experts. This study proposed CFD-ML, a machine-learning (ML) based "simulator," as a means to achieving computational predictions that are accurate enough to use as a basis for dairy-barn design. A convolutional neural network (CNN), a representative ML model, allows complex mapping between input barn geometry and the velocity and temperature fields occurring in the barn, resulting in faster

prediction time and simpler usage processes. As a result, the CFD-ML model can achieve outcomes comparable to those obtained using CFD, with $R^2$ values greater than 0.85, in far less computing time required by CFD. This finding should provide a foundation that could facilitate future CFD-ML advances in dairy science research as well as the development of a user-friendly Graphical User Interface (GUI) that bypasses the complex CFD procedures.

## 3.2. Introduction

The demand for more efficiency and economic viability, a demand driven by an ongoing increase in dairy-product consumption, has forced U.S. dairy producers to seek new ways to increase production and build larger operations. In the Upper Midwest, for instance, farms milking more than 500 head increased their production more than threefold from 2000 to 2012, and in Wisconsin in particular, these larger farms' contribution to the state's total milk production grew from 9.0 to 38.1% (Evink and Endres, 2017). Moreover, while the largest operations surveyed (those milking more than 2,500 cows) only comprised 0.2% of the total number of dairy farms in the region, they proved to be responsible for more than 11% of the Midwestern region's total milk production. It seems likely, too, that the economic advantages achieved by larger farms over the past two decades will likely lead to further operational consolidation within the dairy industry. And while these producers are meeting demand with considerably fewer cows and a much-reduced carbon footprint (Rotz et al., 2010), operations of such scale create a significant dilemma: to produce more milk, each cow must generate more internal body heat, and when hundreds of cows commingle in a confined facility, each cow's risk of suffering from heat stress rises and along with it the risk of serious health, wellbeing, and social issues that ultimately cost the U.S. dairy industry roughly a billion dollars annually (Chung et al., 2020). Thus far, producers have responded to this challenge by installing closed mechanical ventilation systems that rely on electric fans to create currents of fast-moving air; they also routinely employ soaker systems to assist in cooling the cows, especially in barns designed to house more than 500 animals at a time (Van Os, 2019). These systems can require a significant amount of energy during the warmer months (for example, in central and northern New York as much as 22% of a farm's annual energy consumption will be spent on ventilation (Mondaca and Cook, 2019). As a result, estimating and predicting the rate of heat and mass transfer occurring inside animal houses has become ever more important to the economic viability of modern dairy operations because an inaccurate estimation of the energy transfer occurring

within the barn can lead to either insufficient heat removal or overcompensation for higher operating costs. Traditionally, a ventilation system's performance has been evaluated by deploying an array of physical sensors (either hand-held or stationary). However, modern large-scale dairy facilities wherein many animals and machines are frequently in motion, physical data collection can be extremely time-consuming and labor-intensive, making objective assessment difficult. Additionally, many of the stationary sensing monitors used to control ventilation systems will not be placed in an ideal location within the animal occupied zone (AOZ). Given these shortcomings, it would seem that a way to accurately evaluate and predict the performance of a dairy barn's ventilation system could significantly help producers wishing to optimize the dairy's operational efficiency.

For this reason, Computational Fluid Dynamics (CFD) has become an important tool among scientists engaged in dairy-barn ventilation-system research due to its ability to virtually evaluate the performance of existing systems and also future designs, either to improve the system via retrofitting or to test the proposed system before actual construction begins. CFD serves as a reliable tool, one that can solve the variations that occur in the Navier-Stokes equation and compute solutions for partial-differential equations. Moreover, CFD is widely used to simulate flow fields as well as to model the patterns of heat and mass transport taking place in a defined computational domain. CFD has been applied in a variety of fields in agricultural and biosystems engineering. Owing to its advantages, CFD has already taken on a crucial role in animal housing ventilation studies, and Table 5 summarizes recent publications specifically relevant to dairy barns. Figure 12 shows the steamline outcomes obtained from an evaluation of the overall flow patterns occurring in a large-volume dairy barn and also the impact of air baffles. Such an evaluation would have been nearly impossible to achieve without the aid of CFD.

Table 5: Summary of recent dairy housing ventilation studies using CFD

| Authors | Technical Contents |
|---|---|
| Mondaca and Choi (2016a) | An evaluation of a newly proposed mechanical cooling method called perforated polyethylene tube ventilation. |
| Drewry et al. (2018) | A modeling of gas and heat generation occurring in the holding area of a large-scale dairy barn and also the efficiency of the barn's ventilation system. |
| Zhou et al. (2019) | An assessment of the impact that air baffles installed at various locations in a large-scale cross-ventilated dairy barn have on airflow, cow cooling, and energy consumption. |
| Mondaca et al. (2019) | An analysis identifying flow patterns occurring in a large-scale tunnel-ventilated study. |
| Saha et al. (2020) | An analysis of the effects produced by sidewall curtain openings with respect to airflow patterns and airflow rates occurring in a naturally ventilated dairy barn. |
| Doumbia et al. (2021) | A modelling of an animal occupied zone using an anisotropic porous medium model with resistance parameters that depend on velocity. |
| Pakari and Ghani (2021) | A comparison of three structurally identical dairy barns with different mechanical ventilation systems with varying number of fans and locations. |
| Tomasello et al. (2021) | An optimization of the barn's structural layout accomplished by evaluating varying structural configurations. |
| Cao et al. (2022) | An evaluation of air jet cooling from a perforated air ducting systems to remove heat from cows in free stalls |

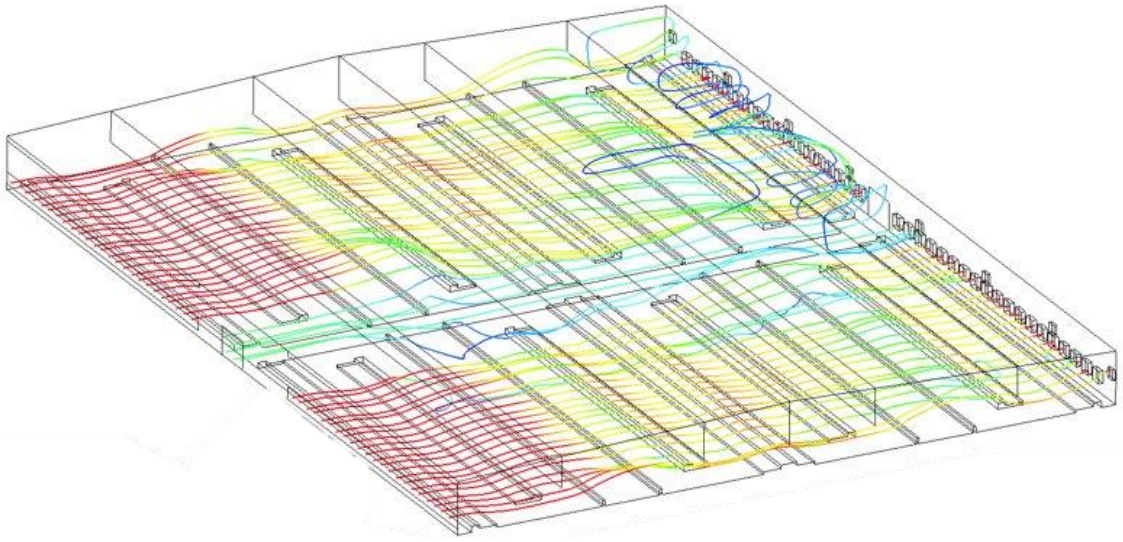

Figure 12. An example of a large-scale and complex dairy barn ventilation simulation with streamline visualization (Jung, 2021).

Despite these successes, achieving reliable outcomes with the aid of CFD depends to a great extent on the background knowledge, skills, and experience of the user. CFD analysis typically requires the following steps: (i) modeling a computational domain, (ii) meshing, (iii) setting up boundary conditions, (iv) establishing user-defined functions (UDF) for specific physical phenomena, (v) selecting an appropriate numerical scheme, and (vi) conducting post-data-analysis. Each task, to be completed correctly, depends on the extent of the user's theoretical background in the numerical method and fluid mechanics associated with heat and mass transfer and also an in-depth understanding of certain iterative convergence criteria that can only be managed by high-level CFD experts who have access to high-performance computing facilities. Because it relies heavily on the numerical method and large data arrays of discretized cells, the CFD process takes an excessively long time to obtain converged solutions, and the computing time increases significantly when the process involves the meshing and calculation inherent when large dairy structures become the subject of the simulation. In some studies, to simplify the model, the complex cow geometry is represented by corresponding porous block models that reduce computational costs (Mondaca and Choi, 2016b). Consequently, CFD has thus far been used primarily to conduct research but rarely to evaluate the commercial system designs and corresponding day-to-day operations.

Deep learning (DL), a branch of Machine Learning (ML), has become widely used in studies that involve complex, and large-volume data structures due to its ability to handle non-linearity by means of a multi-layer learning process. Deep learning (DL) can handle such non-linearity by means of a multi-layer learning process. Given that CFD can be computationally expensive (due to high CPU, RAM, and GPU usages), especially when it comes to simulating a full-scale dairy barn as shown in Figure 1, it is not a feasible approach for non-CFD-experts; however, several research groups comprised of members drawn from various fields of study have recently been considering a data-driven approach, one based on the CFD simulation outcomes that use DL (which is a subfield of ML) and by relying on CFD-based metadata, this deep learning technique has the potential to produce comparable outcomes much more quickly and efficiently than can CFD simulations. Table 6 shows a list of recent and relevant studies regarding various ML approaches used to aid CFD with different applications. These recent advancements in the development of ML models, and in particular the development of deep learning neural networks, strongly suggest that non-CFD-experts working in the relevant agricultural design fields could use the training data (generated and stored by CFD simulations) to quickly produce highly interactive outcomes. Consequently, it may now be viable to develop a practical fluid dynamics simulation tool, one that, ideally, could be deployed via the Internet and used by non-CFD-experts working in agricultural and biological systems. Mobile devices such as laptop computers, tables, or even mobile phones would enable end-users to instantly simulate a series of proposed designs and potential operation scenarios. Such a practical computer modeling tool could thus help producers, engineers, researchers, and builders avoid redundant and time-consuming modeling efforts and repeating design mistakes perpetuated by trial and error, as the CFD-ML simulator would enable the end-users to ask questions that would otherwise be difficult or impossible to answer before an actual agricultural facility was built.

Table 6: Relevant CFD-ML studies.

| ML Algorithm | Application | Performance |
|---|---|---|
| Gradient Descent | Predicting Force Distribution on Horizontal Axis Wind Turbine (Bagalkot et al., 2021) | A variance score of up to 0.933 was achieved showing good agreement between the CFD and ML obtained force distribution on the wind turbine. |
| Support Vector Machine and ResNet | Predicting particle properties in plasma spraying (Bobzin et al., 2021) | The ResNet and SVM were able to replicate the average particle properties with high accuracy to CFD. ML approaches take between 0.01 and 4.2 seconds to predict while CFD simulation takes about 3 hours to complete. |
| Decision Tree, Random Forest, NN, and Symbolic Regression | Estimation of clarification basin performance (Li and Sansalone, 2021) | Trained ML models could predict CFD simulations of total particulate matter separation within +/- 15%. |
| Long Short-Term Memory | Predicting unsteady aerodynamics of different airfoils (Li et al., 2021) | Aerodynamic responses by geometric variations of airfoils could be accurately captured by the ML method with the computational efficiency improved at least one order of magnitude when compared to CFD simulations. |
| Artificial Neural Network | Predicting turbine wake (Ti et al., 2020) | The result shows that ANN is capable of wake prediction with a favorable accuracy of within 5% to CFD simulations. |
| Deep Neural Network | Predicting steady and unsteady flow (Bhushan et al., 2020) | ML model performed significantly better than unsteady Reynolds Averaged Navier-Stokes prediction (URANS) model and compared with 85 of the Direct Numerical Simulation (DNS) on unsteady boundary layer flow prediction. |
| Fully Connected Neural Network | Predicting aerodynamic flow around distributed structures (Zhang and Zhao, 2021) | ML model predicted the wind farm velocity with an average root-mean-square error of 2% with significantly reduced computational processing time when compared to high-fidelity simulation. |
| Convolutional Neural Network | Approximation of steady flow (Guo et al., 2016) | ML model was able to a produce comparable result to CFD simulation with 2-4 orders of magnitude speedup. |

This study intends to build the foundation on which a CFD-ML simulator (Figure 13) could be developed, one that would enable non-CFD-expert users to simulate, and more fully visualize, the real-world ventilation problems that occur routinely in the areas of animal housing. Additionally, this study devised a novel method for extracting geometrical features from CFD simulations, one that can capture the dynamic quantities and locations of multiple cows within the computational domain. In so doing, the proposed work

aimed to develop an ML model based on a Convolutional Neural Network (CNN) algorithm, which is a class of DL networks that can predict the flow and heat and mass transfer that would occur inside a simplified dairy barn model that included both solid and porous model cows randomly located. Along with the development of the CNN models, a user-friendly Graphical User Interface (GUI) also be developed. The outcomes from this study should provide a CFD-ML platform that could develop into a user-friendly, low-computational-cost "CFD" application with which a full-scale large barn airflow visualization could be accomplished even using mobile devices.

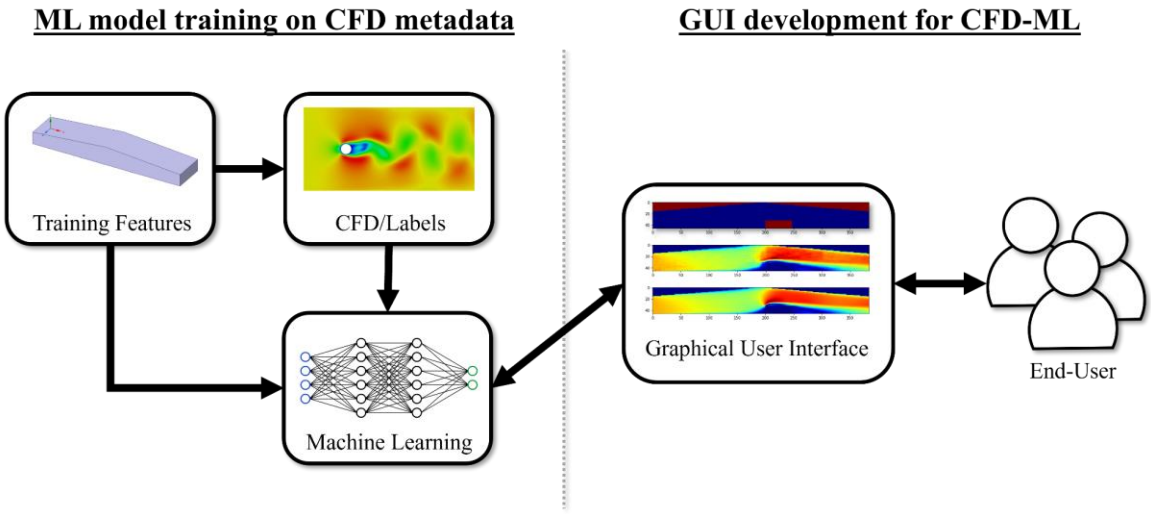


Figure 13. The overall concept of CFD-ML.

## 3.3. Methodology and Materials

The overall experimental workflow required for the CFD-ML model is shown in Figure 14. The CFD related metadata were produced through a scripted loop that automatically created randomized geometry, generated meshing, and ran the CFD simulation based on given boundary conditions. The metadata consisted of a 2D and a 3D barn geometry that included randomized cow locations and varying cow body types (solid and porous). Two different CNN models were developed: CNN1, which was used to predict velocity and temperature fields, and CNN2, which was used to predict the surface Nusselt number. Due to the differences in training- and testing-data dimensions, generating the field data and surface data required

separate models. CNN1 was trained based on the Directional Distance Function (DDF) as an input feature and velocity and temperature fields of the whole computational domain as training labels. CNN2 was trained based on smaller velocity and temperature fields around the cow body as input features and surface Nusselt number as training labels. With respect to CNN2, the workflow path was only applicable in those cases involving barns that included solid cow bodies. The detail of each element is described in the rest of this section.

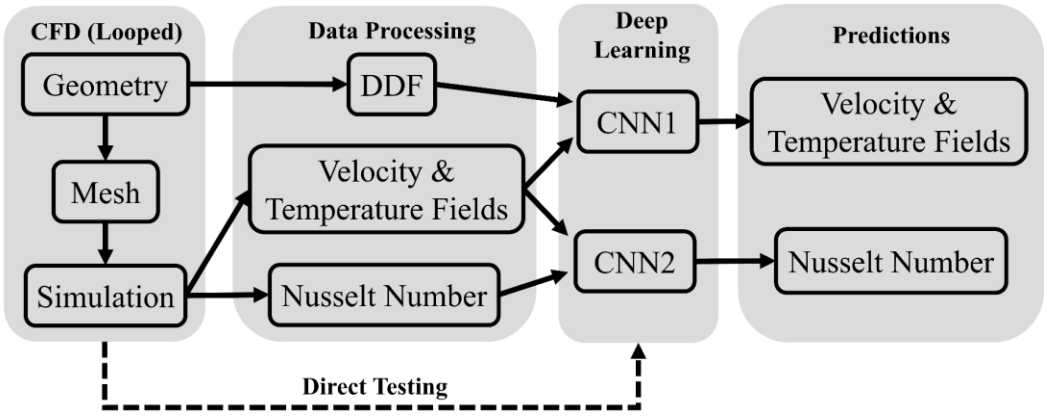


Figure 14. The overview of the experimental setup. Four main parts in this study: CFD metadata generation, data preprocessing for ML, constructing ML models, and evaluating predictions.

### 3.3.1 Barn Geometry

The example depicting a 2D barn geometry that included one cow body is shown in Figure 15. The 19.2 m long dairy barn with 1.6 m inlet openings and a 1:12 ratio pitched roof was considered the simplified template geometry for demonstration purposes. In a barn domain, a model cow block (0.7 m in height and 2.4 m in length) represented an AOZ of dairy cow in the lying posture. The dimensions of the barn depicted in 3D were identical except the width of the barn was 2.0 m. The location of the cow body was assigned randomly using a uniformly distributed random-number generator. To represent the conventional locations of freestalls near the inlet and outlet walls in an actual barn, the location of the cow body was limited to between 1.0 m away from the inlet and outlet walls, and a minimum of 0.1 m distance between two cow

bodies was assigned to reflect an actual situation involving multiple cows. Additionally, to generate the 3D cow body a 0.2 m minimum gap was chosen as the distance from the sidewall of the barn and the side of the cow body.

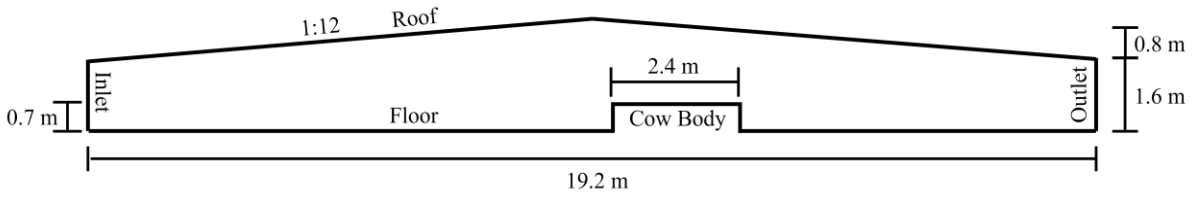


Figure 15. Dimensions of an example 2D barn with one cow body present. In case involving 3D models, the geometry was extruded 2.0 m into the page.

### 3.3.2 CFD Metadata Generation

The labels used to train the model were generated using the finite-volume method that is based on CFD (Ansys version 2021 R2; Canonsburg, PA, USA). The randomized geometry was produced using SpaceClaim 3D solid-modeling software; the computational meshing was generated by Mesh; and the simulation was completed using Fluent. That is, the whole process was completed within the Workbench environment using Ansys journal scripting. Two different types of cow-body representations were considered. One had a solid surface and a constant surface temperature boundary condition, and the other was a porous medium with constant heat generation to match the total energy transfer of the counter-part solid cow body. To demonstrate the CFD-ML learning in 3D space, a single 3D case involving a solid cow body was also studied. As indicated in Table 7, five total cases were developed during the course of this study.

Table 7. All the generated data case types for this study.

| Dimensions | Cow Body Type | No. of Cow Bodies |
|---|---|---|
| 2D | Solid | 1 |
| 2D | Solid | 2 |
| 2D | Porous | 1 |
| 2D | Porous | 2 |
| 3D | Solid | 1 |

All the surfaces other than those of the inlet, the outlet, and the cow body, in both the 2D and 3D cases, were set as no-slip wall-boundary conditions and with an adiabatic condition. The velocity-inlet was set as 2.0 m $s^{-1}$ with air properties at 298 K, and the solid cow body was set as 308 K based on the observations made by Hillman et al. (2003) and Gebremedhin et al. (2008). The heat generation associated with the porous cow body in 2D cases was set as 205 W $m^{-2}$. The applied heat generation was calculated to produce an overall heat transfer equal to the solid cow body with an equivalent constant surface temperature. The outlet-side of the computational domain was set as an out-flow condition. To represent cow bodies inside a dairy barn, a non-Darcy flow model was adopted, and inertial resistance was not considered when creating the porous cow-body model (Mondaca and Choi, 2016b). The viscous resistances of the porous medium were set as 50,000 $m^2$ and 15,000 $m^2$ in front flow (x-direction) and top flow (y-direction). The viscous resistance values of the porous medium used in this study were set based on preliminary simulations as well as in reference to the values set by Drewry et al. (2018).

For all CFD simulations, the realizable k-e turbulence model was used in conjunction with enhanced wall condition. In accordance with the suggestion made by Rong et al. (2016), the realizable k-e model proved effective in predicting air movement occurring inside buildings. The steady-state Reynolds-Averaged method (RANS) was used to solve the Navier-Stokes equation, and the SIMPLE (Semi-Implicit Method for Pressure-Linked Equations) numerical scheme and the second-order upwind differencing scheme were

used. The pseudo-transient steady-state model was applied in those cases involving the porous cow-body zones (ANSYS, 2013). All simulation calculations were carried out until the convergence of these criteria: continuity, velocities, k, and e. Additionally, to ensure the stability of energy transfer, area-weighted averages of the heat transfer occurring on the cow-body surfaces were also considered a key convergence criterion. The maximum mesh cell size was set as smaller than the data grid to ensure the correct data conversion. Pressure-velocity coupling with second-order spatial discretization was applied.

For all generated CFD metadata, the mesh for each simulation case was automatically generated with the constraint that each mesh cell element would be 0.05 m in size at the maximum. The maximum cell size was defined and limited based on the cell size of the input geometry for the neural network. The mesh was generated as a mix of tetrahedron and triangular cells. As a result, 16,000 cells were generated in the 2D cases and 1,700,000 cells in the 3D cases. The size of the meshing was deemed appropriate for the purpose of this study. All CFD simulations were solved by means of double-precision and parallel CPU solver processes, and they were iterated until the following simulation residuals had converged: continuity, x-velocity, y-velocity, z-velocity (in 3D cases only), energy, kinetic energy, turbulent dissipation rate, and mass-flow in and mass-flow out. Also, x-velocity, y-velocity, z-velocity (in 3D cases only), temperature, and surface local Nusselt number (in solid cow-body cases only) were exported directly from the CFD simulations.

All the data obtained from the CFD simulations were converted into unidirectional arrays before being used to train the CNN models. This step was necessary because, unlike the Lattice-Boltzmann method presented by Guo et al. (2016), which mostly relies on a fixed lattice structure as its computational domain, the Navier-Stokes equation-based CFD relies on a more dynamic and flexible triangular and tetrahedral meshing within the computational domain. As a result, the automatically produced mesh cells were not uniformly distributed. In the 2D cases, a data shape of 24 by 192 was adequate for representing the slanted roofs of a typical cross-ventilated dairy barn in a matrix grid. A data shape of 24 by 192 by 20 was appropriate in the 3D cases. Each converted grid represented a square with a 0.1 m side length, and any cell centers located

within the square were averaged. With regard to the zone where CFD data were not available (beyond the roof surface and inside the cow body used in the solid cow-body cases), the data array was filled with 0. Figure 16 shows the conversion obtained from the CFD data from the mesh into the grids for the CNN model.

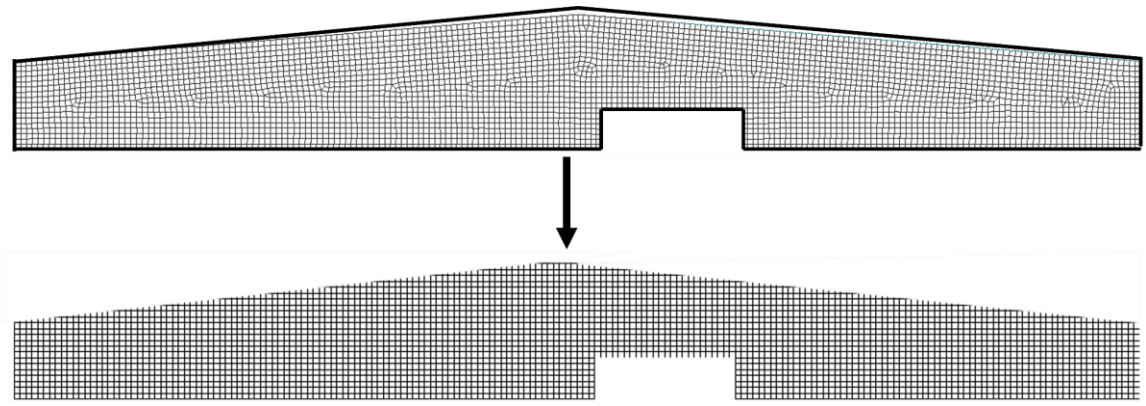

Figure 16. An exemplary conversion case of the CFD data into the grids for the CNN model.

### 3.3.3. Directional Distance Function

To extract from the CFD simulations the geometric features needed for CNN model training, this study developed a modified version of the Signed Distance Function (SDF) that was commonly used in the related studies. The new version, named the Directional Distance function (DDF), was able to generalize the referencing location, which was needed to calculate the distance. Unlike the SDF described in Guo et al. (2016), which was used to calculate the distance from a target object and each point within a grid containing a single distance value, the DDF uses an information grid wherein each point location contains multiple distance values, with each value calculated based on the direction that must be taken from the point to reach a solid surface (see Figure 17 for an example, the black block representing the cow body). With the DDF, a CNN model can be trained using data that contains a varying number of cow bodies because each location is independent of the number of cows present.

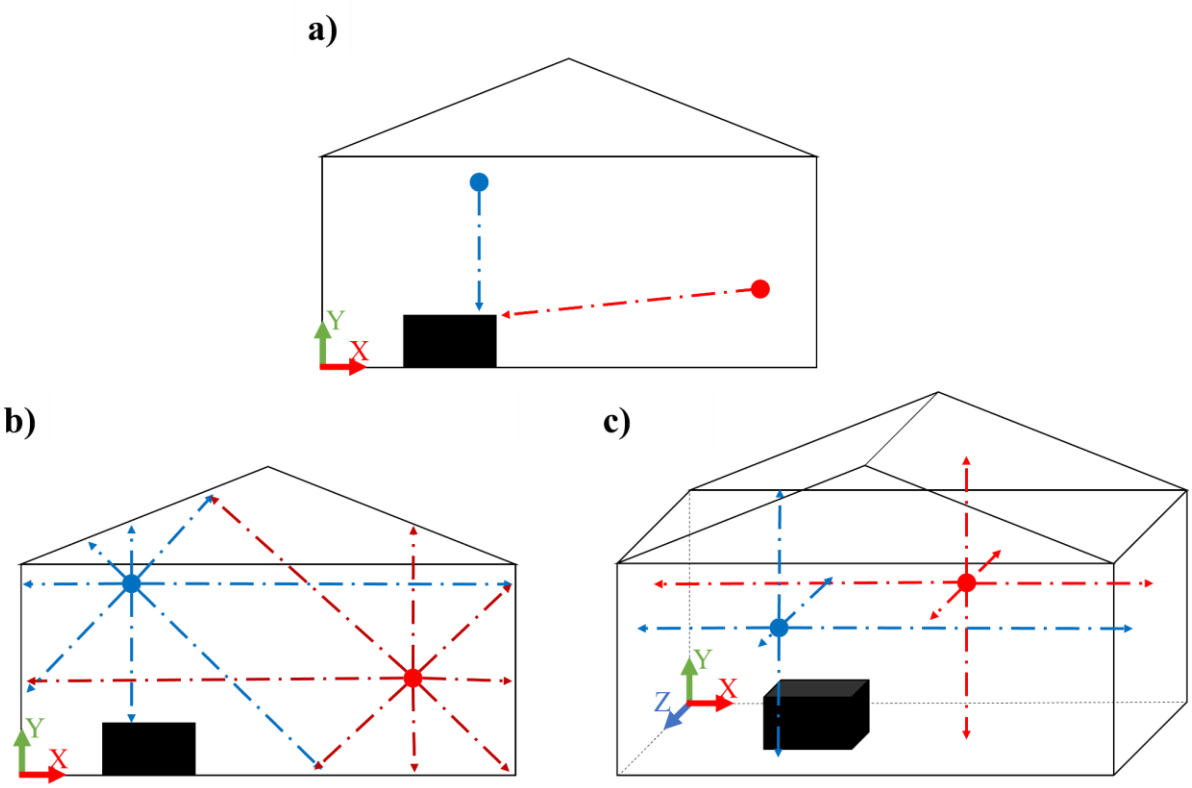


Figure 17. Comparison between a) SDF 2D, b) DDF 2D, and c) DDF 3D with two example points in each domain. The black block represents the cow body. In SDF, each point has only one value, and that is the closest distance to the target object. In DDF, each point is associated with multiple distance values based on the fixed, uniformly distributed directions.

Figure 18 shows one 2D example involving eight directional ways (0, 45, 90, 135, 180, 225, 270, and 315 degrees clockwise from the vertically up direction). The color of each pixel represents how far it is from the solid surface in its respective direction. The pixel is blue if the distance is zero to the surface. While there are many different angles to choose from, in this study, 36 and 27 equiangular directions were used in the 2D and 3D cases, respectively, to ensure that the training features would provide sufficient information without exponentially increasing the computational time (by increasing the number of directions).

To train the CNN model to predict the local Nusselt number associated with the cow-body surface, flow and temperature fields around the cow body were used as input data (instead of using spatial information as the training features). The smaller flow and temperature fields that were within 0.4 m of the cow-body

surface were extracted from the CFD results. A distance of 0.4 m was deemed appropriate after several iterations of the preliminary tests had been completed. In the 2D cases, the extracted data was stored in an array measuring 10 by 32 by 3, and in the 3D cases, the array measured 10 by 32 by 14 by 4.

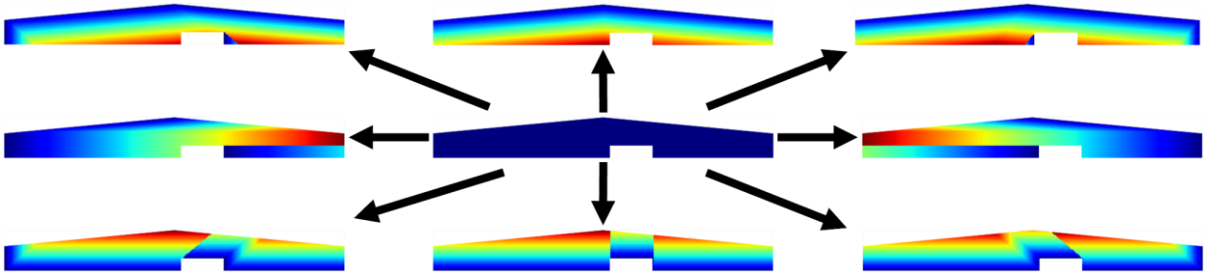

Figure 18. Visualization of DDF outputs when the directions are 45-degree (interval equiangular).

### 3.3.4. CNN Model Training and Input Data

All the data manipulation and programming required for ML were accomplished in Google Colaboratory environment (version Pro+), with Python (version 3.6) as the main programming language, and NVIDIA V100 Tensor Core GPU. From the CFD simulations, a total of 600 training and testing datasets were obtained with each scenario based on the parameters: 2D or 3D, solid or porous, and one or two cow bodies listed in Table 7. Accordingly, a total of 5 scenarios were simulated (only the single solid-cow-body case was considered in 3D), resulting in a total of 3000 CFD metadata. 600 datasets were generated to provide enough information to ensure that the 3D cases would provide reliable outcomes while minimizing the amount of data needed for computational processing. In each case, 480 datasets were retained to serve as a training set, while the remaining 120 datasets were used as a testing set. In every 2D case where both a single cow body and two cow bodies were available, the training and testing datasets were combined and used to test whether the input feature could capture different numbers of cow bodies present within the barn geometry. Figure 19 shows the generalized CNN structures. Specifically, two CNN models were developed to predict the velocity and temperature fields (CNN1) and the Nusselt number (CNN2), for each 2D and 3D scenario. The model structures used in the 2D and 3D cases are the same except for the dimensionality in each layer. In the models that predicted velocity and temperature fields (CNN1s), convolutional, fully-

connected, and deconvolutional layers were used, whereas in the models that predicted the Nusselt number (CNN2s), only convolutional and fully-connected layers were used. In the CNN1s, the convolution and deconvolution sizing trends were symmetrical, and no padding was applied in any of the layers. The stride of convolution and deconvolution was set equal to the kernel size. After the convolutional layer, the kernels were flattened into the fully connected layers and were reshaped into the deconvolutional layers. Details pertaining to the models are provided in Appendix A.

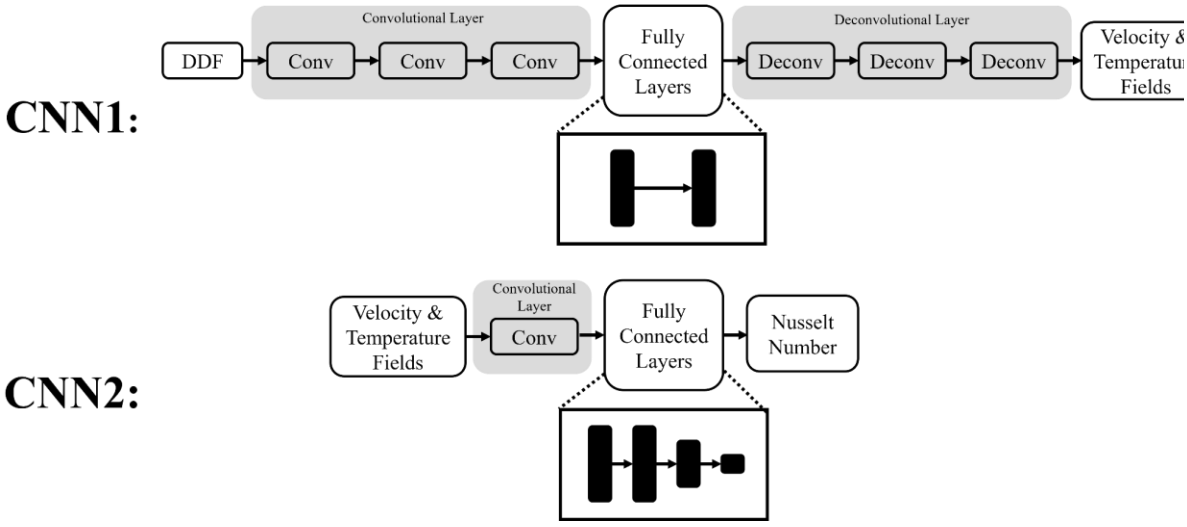


Figure 19. The architecture of the developed CNN models. CNN1 predicts velocity and temperature fields, and CNN2 predicts Nusselt numbers.

Table 8 provides more detailed summaries of the CNN models used in both the 2D and 3D cases as well as the number of training samples extracted from the CFD metadata for each scenario. Regarding the 2D CNN1, the one-cow and two-cow datasets were merged so that the CNN1 models could train not only based on shifting cow locations but also changes in the number of cows present within the domain, the resulting being a total of 1200 data for the 2D case. Because only the one-cow scenario was considered, the dataset for 3D CNN1 remained at 600. Because the CNN2 model considered the temperature and velocity fields around the cow-body surface as input features, it obtained a total of 1800 (600 *1 cow + 600* 2 cows) data for 2D CNN2 while 3D CNN2 remained at 600 datasets.

Table 8. Summary of the CNN: Input and output data types (with dimensions) are shown. Types of NN layers integrated into the model are also described.

| | Cow Model Type | Training Samples | Input Data | Output Data | Layer Structure | Testing Samples |
|---|---|---|---|---|---|---|
| 2D CNN1 | Solid and Porous | 960 | DDF (24, 192, 36) | x-velocity, y-velocity, and Temperature fields (24, 192, 3) | 1. Convolutional Layers<br>2. Fully-connected Layers<br>3. Deconvolutional Layers | 240 |
| 2D CNN2 | Solid | 1440 | Trimmed x-velocity, y-velocity, and Temperature fields (10, 32, 3) | Nusselt Number (36,1) | 1. Convolutional Layers<br>2. Fully-connected Layers | 360 |
| 3D CNN1 | Solid | 480 | DDF (24, 192, 20, 27) | x-velocity, y-velocity, z-velocity, and Temperature fields (24, 192, 20, 4) | 1. Convolutional Layers<br>2. Fully-connected Layers<br>3. Deconvolutional Layers | 120 |
| 3D CNN2 | Solid | 480 | Trimmed x-velocity, y-velocity, z-velocity, and Temperature fields (10, 32, 14, 4) | Nusselt Number (648,1) | 1. Convolutional Layers<br>2. Fully-connected Layers | 120 |

In a manner similar to that used by Guo et al. (2017), The CNN models were implemented using the open-source ML software library (TensorFlow 2.7) Both the CNN1 and CNN2 models were trained in a way that minimized the Mean Square Error (MSE). Adaptive moment estimation (Kingma and Ba, 2015), also known as "Adam," was used as an optimizer, with 0.001, 0.9, 0.999, 1e-7 used for learning rate, beta1, beta2, and epsilon, respectively. The rectified linear unit ("ReLu") was used as the activation function except in the output layer into which a linear function was applied (Agarap, 2018). A data batch size of 5 was propagated into the networks. The convergence of MSE was monitored throughout all training

processes. Within the given Google Colaboratory environment, training 80 GB 2D and 120 GB 3D datasets took approximately 1 hour and 2 hours, to train the models with 2000 and 3000 epochs, respectively.

### 3.3.5. Normalization and Nondimensionalization

Data preprocessing is an important part of the machine learning process because it directly affects the model's ability to learn. The DDT outputs were scaled down by multiplying 0.01 in a manner similar to Guo et al. (2016). The velocity and temperature parameters were nondimensionalized using Equations 8 and 9:

$$u^* = \frac{u}{U_{ref}}, v^* = \frac{v}{U_{ref}}, w^* = \frac{w}{U_{ref}}, U^* = \sqrt{u^{*2} + v^{*2} + w^{*2}} \quad (8)$$

$$\theta = \frac{T - T_\infty}{T_{sur} - T_\infty} \quad (9)$$

Where $u^*$, $v^*$, $w^*$, $U^*$, and $\theta$ are nondimensionalized x, y, z velocities, velocity magnitude, and temperature, $U_{ref}$ is the reference velocity (inlet velocity), $T_\infty$ is the reference bulk-air temperature of the flow, and $T_{sur}$ is a reference cow body surface temperature.

### 3.3.6. CNN Performance Evaluation

The trained CNN model is used primarily to predict the flow field and heat transfer components in each computational domain that involves the varying locations of the cow bodies, and it does so in a way similar to that used by a CFD simulation but at a lower error rate and a lower computational cost. In this study, several different elements of the CFD and CNN predictions were compared regarding the identical given geometry and boundary conditions. In the solid cow-body cases, the velocity flow field, temperature field, and surface Nusselt number were compared. In the porous cases, the velocity flow field, temperature field, and temperature profile were compared. The compared parameters were all nondimensionalized.

To evaluate the CNN prediction performance, the mean, minimum, maximum, and median absolute errors were measured. An absolute error was used instead of the percentage error due to a dead zone (no flow),

which resulted in unreliable infinite values. Additionally, $R^2$ (Equation 10) and root mean square error (Equation 11) were also calculated to further evaluate the prediction accuracy in a manner similar to Ma et al. (2021).

$$R^2 = 1 - \frac{\sum_{i=1}^{n}(y_i - \hat{y}_i)^2}{\sum_{i=1}^{n}(y_i - \bar{y}_i)^2} \tag{10}$$

$$RMSE = \sqrt{\frac{1}{n}\sum_{i=1}^{n}(y_i - \hat{y}_i)^2} \tag{11}$$

Where $y_i$, $\hat{y}_i$, and $\bar{y}_i$ are CFD, CNN, and averaged CNN predictions, respectively, and n is the number of testing data samples.

To compare the difference between CFD and CNN in computing costs with respect to fluid flow prediction, computing time was also compared in both the 2D and 3D cases. A single CFD process includes meshing and simulation in a scripted loop. In each case, 120 testing geometries were analyzed and averaged. The two processes were tested on hardware with identical specifications: two Intel Xeon E5-2623 v3 processors with 3 GHz and 124 GB of RAM. For all cases, the total computing time was calculated. With respect to CNN, the time needed for DDF feature generation and CNN prediction processes were measured. For CFD, generating and loading the CAD Geometry, meshing, and simulations were measured.

## 3.4. Results and Discussion

To minimize the number of pixelated representations, bilinear interpolation was applied to all visual outcomes presented in this study. All the visual outcomes are representative results of a single testing case out of 120 setting datasets.

### 3.4.1. Results for Solid Cow Body in 2D

Table 9 shows the averaged maximum, mean, median, and minimum absolute errors that occurred during the 120 case tests in regard to predicting the flow and temperature fields that would occur in the single solid

cow body and in the two solid cow body cases. Also, with regard to the single solid body and the two solid body cases, the average absolute errors that occurred in predicting the flow fields were 0.0030 and 0.0063, respectively. The maximum errors were relatively higher in the two-body cases than in the one-body cases. However, the median values were relatively close to each other because of the airflow passing through areas farther away from the cow bodies was less agitated and the flow patterns therefore more easily recognized by the CNN models. Additionally, the absolute errors that occurred in temperature prediction were smaller than those that occurred in flow prediction, possibly because the global value range was smaller. To conduct an additional performance analysis, the $R^2$ and RMSE values were also calculated. Between the cases, the relative estimated error trends were similar to the trend followed by the absolute error values, and $R^2$ shows acceptable values of more than 0.95 and the $R^2$ values (which were greater than 0.95) were deemed acceptable.

Table 9. Averaged maximum, mean, median, and minimum absolute errors that occurred in predictions of the flow and temperature fields in the 120 tests of the single solid-body and two solid-body cases.

| | Maximum | Mean | Median | Minimum | $R^2$ | RMSE |
|---|---|---|---|---|---|---|
| Flow, One Solid Cow Body | 0.0652 | 0.0030 | 0.0019 | 0.0000 | 0.9999 | 0.0047 |
| Temperature, One Solid Cow Body | 0.0725 | 0.0013 | 0.0007 | 0.0000 | 0.9818 | 0.0030 |
| Flow, Two Solid Cow Bodies | 0.1478 | 0.0063 | 0.0033 | 0.0000 | 0.9994 | 0.0114 |
| Temperature, Two Solid Cow Bodies | 0.1681 | 0.0024 | 0.0024 | 0.0000 | 0.9543 | 0.0073 |

Figure 20 provides representations of the flow and the temperature predicted by the CFD and CNN models. The original input geometry, the CFD predictions, the CNN predictions, and absolute error data are also provided. Overall, the CNN models were able to predict airflow patterns and temperature distributions to a degree of accuracy that was comparable to that of its CFD counterpart. During flow simulations, most of the errors occurred at the front of the bodies, where the flow area within the computation domain changed abruptly. In the temperature field simulations, most of the significant errors occurred in the flow's dead

zones, where the lower downstream corners of the body came in contact with the floor. Nevertheless, the CNN was able to adequately simulate the trailing temperature trends.

Figure 21 provides the predicted Nusselt number at the surface of the solid bodies. Figure 9a provides a visual representation of the one-body case, while Figure 9b provides a representation of the two-body case. The blue line represents the CNN's prediction, and the orange line represents the CFD's simulation outcome. As can be seen, the Nusselt numbers are ranged along the y axis, while the x-axis shows the surface locations ranging from the corner of the body in front to the back corner in a clockwise direction. In the two-body cases, the Nusselt number values that correspond to the front and rear end of the bodies are connected. The calculated average absolute error, $R^2$, and RMSE were 0.0089, 0.9752, and 0.0099. These results show that the CNN model can predict (in the form of a Nusselt number) the surface-heat transfer that will occur and do so as reliably as can the CFD model.

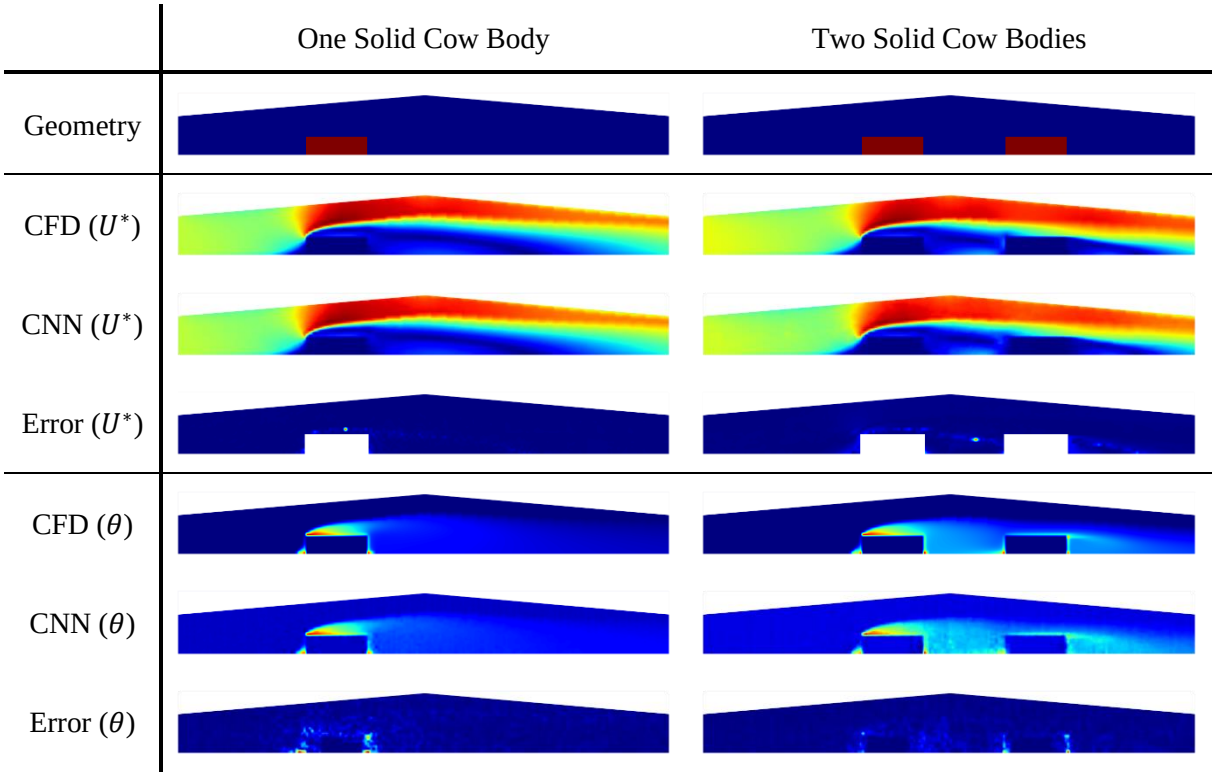


Figure 20. Outcomes of the predicted flow field as the air passed over solid bodies. The first column corresponds to a single-body case, and the second column corresponds to the two cow body cases. The first row corresponds to the geometry with the case involving randomized body locations; the second row shows the CFD prediction regarding the given geometry; the third row shows the CNN prediction of the given geometry; the fifth and sixth rows show CFD and CNN predictions of temperature field, respectively; the fourth and seventh rows show the absolute error between CFD and CNN predictions for velocity and temperature fields respectively.

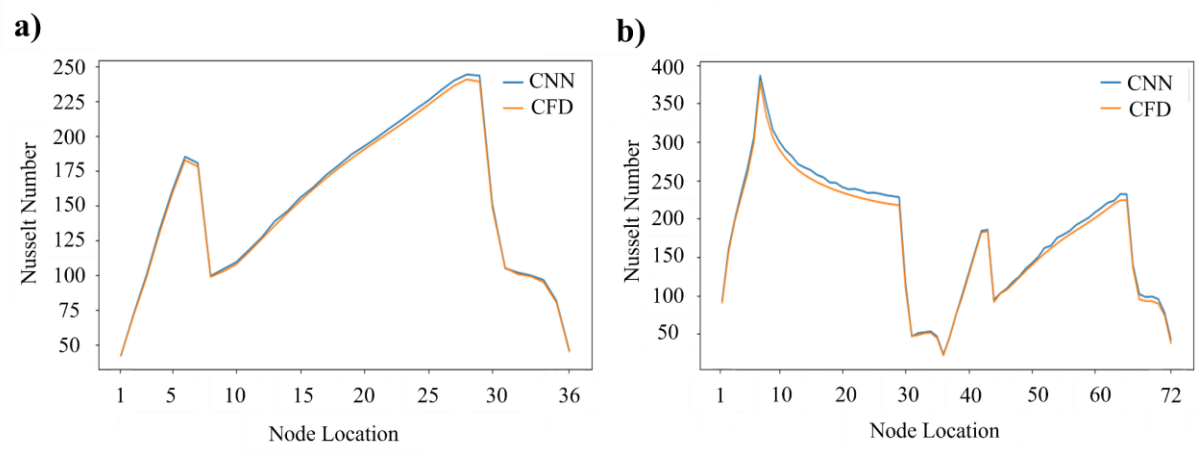


Figure 21. Nusselt number predictions at solid-body surfaces. a) Prediction obtained from a single body surface, and b) prediction obtained from two solid-body surfaces. The x-axis values are surface locations ranging from the front corner of the body to the back corner in a clockwise direction.

### 3.4.2. Results Obtained using the Porous Cow Body in 2D

Table 10 shows the averaged maximum, mean, median, and minimum absolute errors that occurred in predicting the flow and temperature fields over 120 case tests (one case involving a porous-body and one case involving two porous bodies). In this model, the averaged mean absolute error in each flow prediction, with regard to both the one-body case and the two-body case, were 0.0235 and 0.0361, respectively. The CNN models' solid-body geometries were able to predict flow and temperature fields at error rates that were significantly lower than those associated with the CNN models' porous-body geometries. This is likely because the less solid geometries served as obstacles, inducing a more abrupt change in flow pattern as the air passed over the body. Furthermore, as in the solid-body cases, the error rates associated with the temperature-field predictions were lower than those associated with the flow-field predictions. The calculated $R^2$ and RMSE values were slightly below those values associated with the solid cases. Regardless, these values were acceptable.

Table 10. Averaged maximum, mean, median, and minimum absolute errors that occurred in predictions of flow and temperature fields in 120 tests of the one porous-body and two porous-body cases.

| | Maximum | Mean | Median | Minimum | $R^2$ | RMSE |
|---|---|---|---|---|---|---|
| Flow, One Porous Cow Body | 0.7870 | 0.0235 | 0.0030 | 0.0000 | 0.9066 | 0.1085 |
| Temperature, One Porous Cow Body | 0.0027 | 0.0027 | 0.0005 | 0.0000 | 0.9953 | 0.0007 |
| Flow, Two Porous Cow Bodies | 0.7862 | 0.0361 | 0.0032 | 0.0000 | 0.8925 | 0.1272 |
| Temperature, Two Porous Cow Bodies | 0.0040 | 0.0007 | 0.0006 | 0.0000 | 0.9983 | 0.0008 |

Figure 22 provides a visual representation of the CNN model's performance with regard to predicting the flow field and temperature field associated with the porous cow bodies. The figure shows the original input geometries, CFD simulation outputs, and CNN predictions, as well as the difference in absolute error by the two methods. As shown, the CNN models can predict outcomes similar to those predicted by the CFD simulations with respect to both flow field and temperature field. Unlike the predictions associated with the solid-body cases, these errors were not concentrated in sharp corners; rather, the errors were spread relatively evenly across the field, thereby reducing the overall errors, and especially the maximum prediction error.

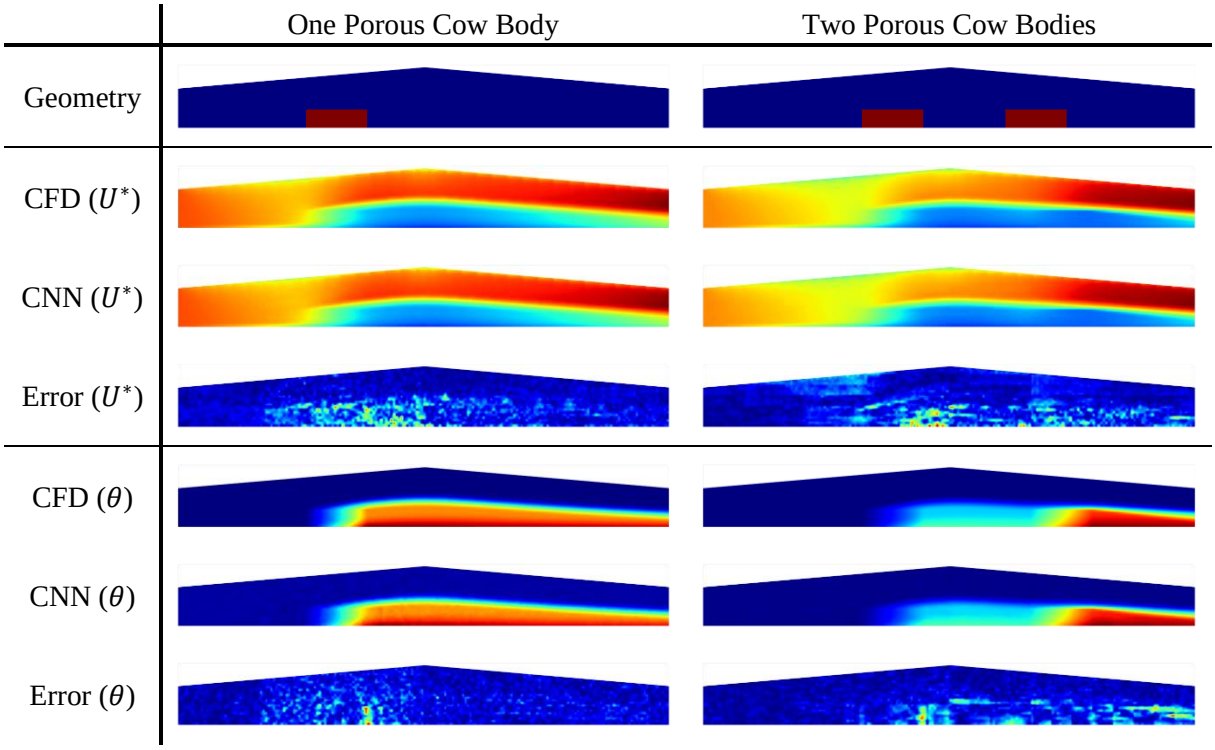


Figure 22. Visual outcomes of the temperature field prediction through porous bodies. The first column is a single cow body case, and the second body is two cow body cases. The first row is geometry with randomized body locations; the second row shows the CFD prediction regarding the given geometry; the third row shows the CNN prediction of the given geometry; the fifth and sixth rows show CFD and CNN predictions of temperature field, respectively; the fourth and seventh rows show the absolute error between CFD and CNN predictions for velocity and temperature fields respectively.

Figure 23 shows a comparison of the temperature profiles generated by the CNN models and the CFD simulation, with the porous cow bodies. The solid lines represent the outcomes obtained from the CFD simulations, and the dotted line shows the outcomes obtained from the CNN models. This figure demonstrates the CNN model's accuracy in predicting the temperature field in comparison with the outcomes obtained by the CFD simulations. In the two porous-body cases, the temperature predictions corresponding to the body toward the rear achieved a lower error when compared to that corresponding to the body in front.

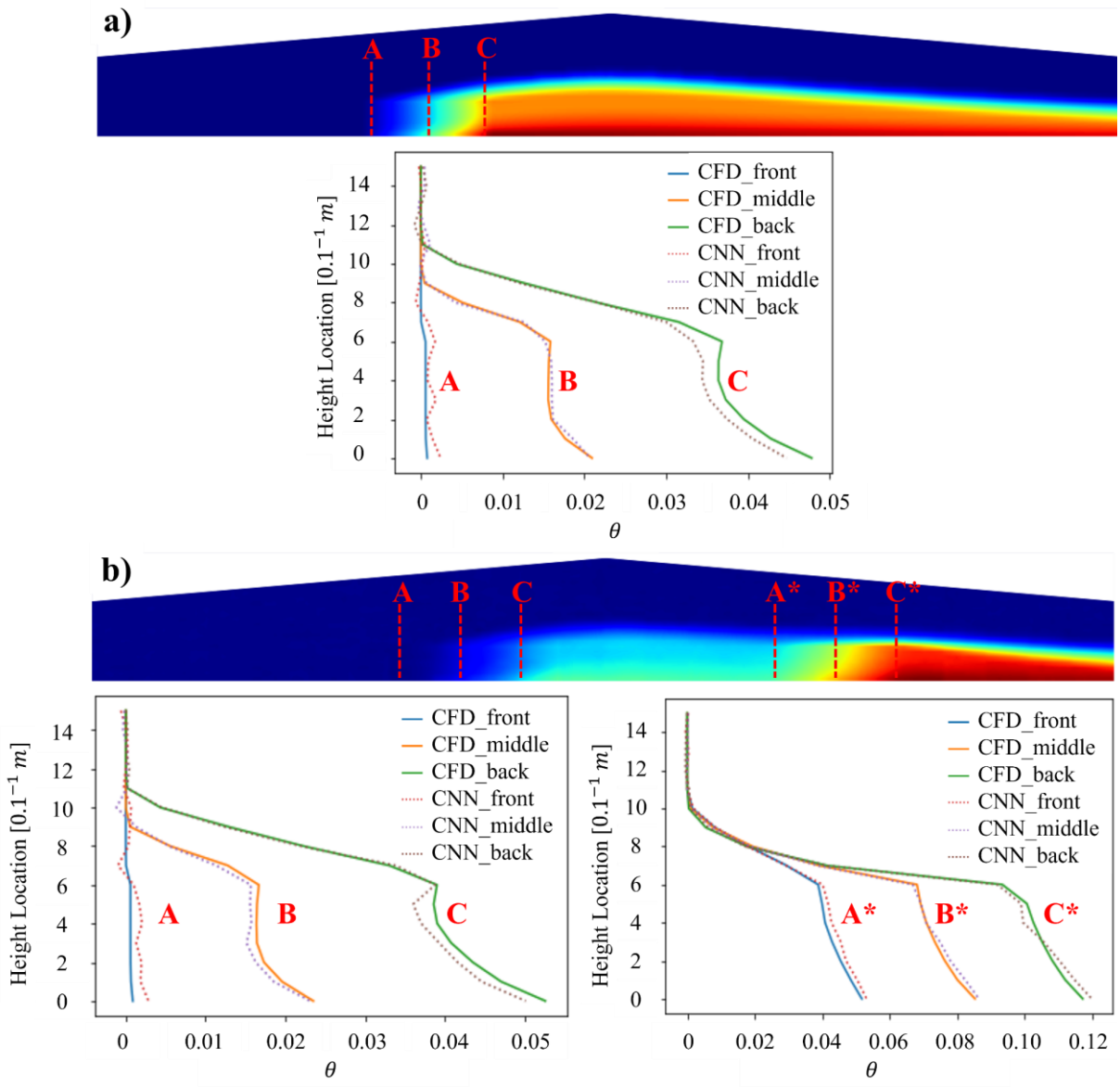


Figure 23. Dimensionless temperature profile comparison between CFD and CNN through porous cow bodies.

### 3.4.3. Results Obtained from the Solid Cow Body in 3D

Figure 24 presents the flow- and temperature-field predictions that correspond to a 3D solid cow-body case. The three contour axial planes intersecting at the center of the solid body represent the data generated in 3D. Even though the field array was almost 20 times larger than that associated with the 2D cases, achieved

with fewer training data nodes and fewer angular variations for DDF, similar prediction results were obtained. Medium absolute errors of 0.0076 and 0.0022 for velocity and temperature-field predictions were calculated. The calculated $R^2$ and RMSE values that corresponded to each velocity and temperature prediction were 0.9948, 0.02372, 0.8433, and 0.0059. respectively. However, unlike in the 2D cases, the $R^2$ corresponding to velocity prediction was better than those of the temperature predictions. Most of the significant errors associated with the velocity field predictions achieved by the CNN models occurred along the front edges of the solid body whereas most of the errors in temperature-field predictions occurred on the back surface of the body. The location of this body, having been randomly generated, was not at the center of the computational domain; nevertheless, the CNN was able to predict the skewed downstream flow extending outward behind the body.

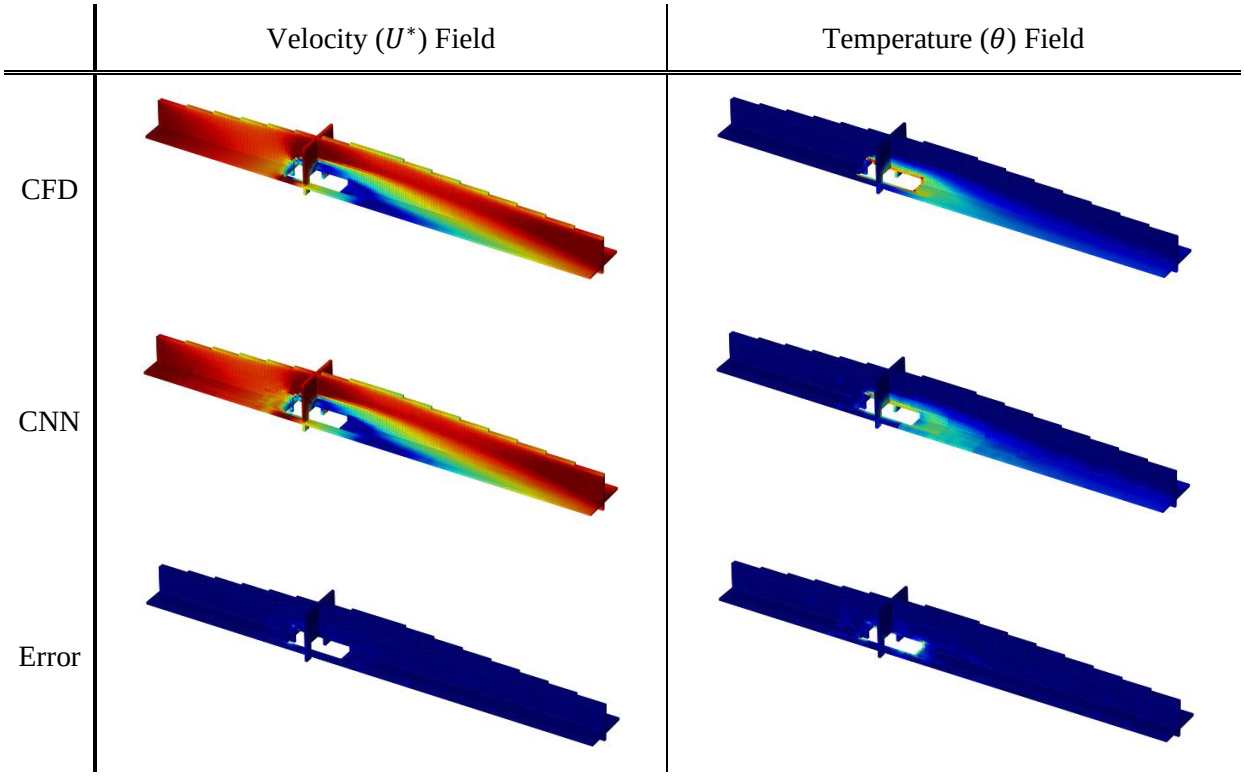


Figure 24. Visual representations of the velocity and temperature field predictions associated with the solid bodies in 3D. First column shows the velocity fields, and the second shows the temperature fields.

Figure 25 is a visual representation of the Nusselt-number that correspond to the front, top, and back surfaces of the solid body. The CNN model was able to capture the key locations where a higher heat

transfer rate had occurred at corners and edges and where a lower heat transfer rate had occurred on the back surface. The calculated average absolute error, $R^2$, and RMSE were 0.1526, 0.8913, and 0.2674. Most of the notable errors occurred on the front and the rear surfaces of the body. This is likely due to the abrupt differences in heat flux caused by the stagnation and separation of air flow. Finally, Figure 13c demonstrates a plot comparing the two predictions of the averaged values Nusselt number of the entire cross-section along the x-direction.

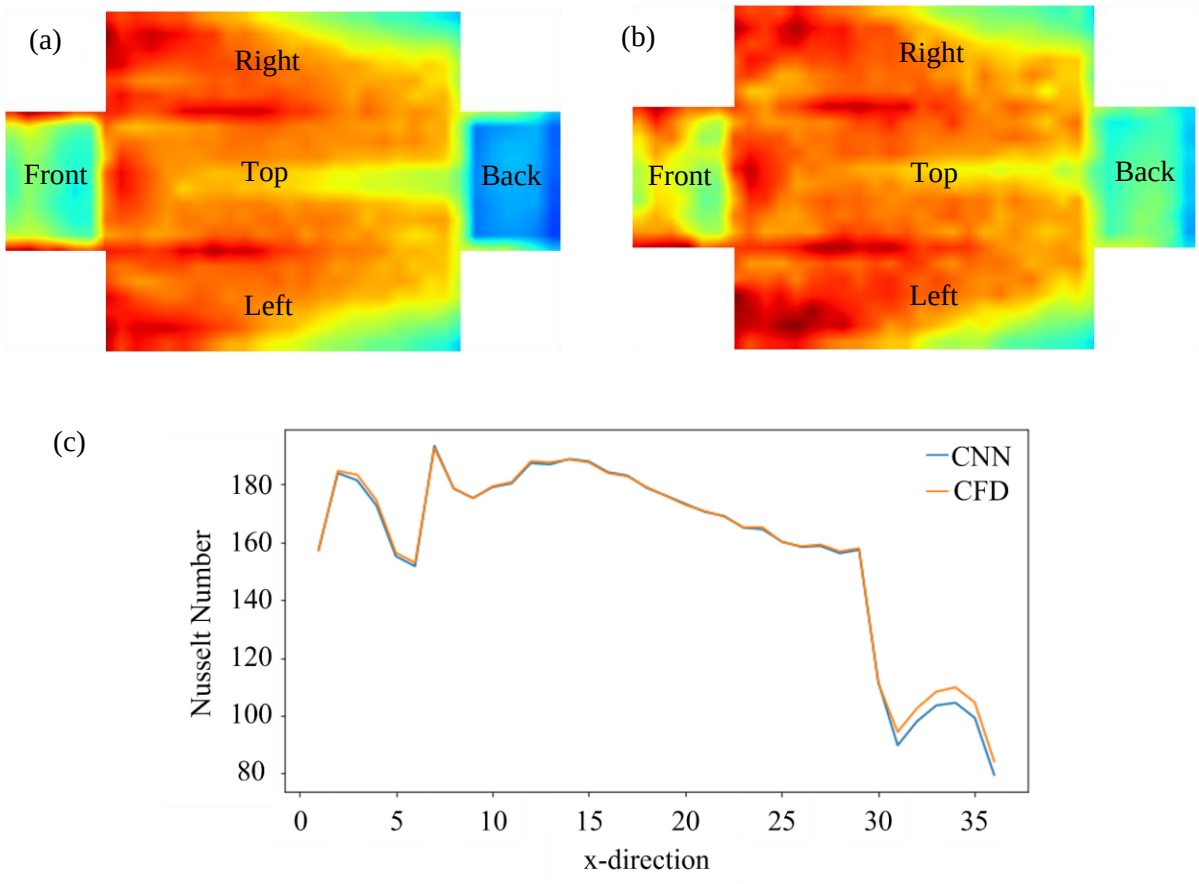


Figure 25. A comparison of the local Nusselt-number outcomes on an unfolded view of the body surfaces obtained by (a) CFD, (b) CNN, and (c) the average Nusselt number on the YZ-plane along x-axis.

### 3.4.4. Computing Cost Analysis

Table 11 shows a comparison of the computing times required by the CFD and CNN (with respect to velocity and temperature field predictions) in both the 2D and 3D cases that involved solid cow bodies. The total computing times for the CNN models (2D), CFD (2D), CNN (3D) and the CFD (3D) simulations were 31.37, 336.54, 400.57, and 6309.71 seconds respectively. A similar trend was observed with respect to the cases with the porous body. In the 2D cases, the CNN was about 10-fold faster than was the CFD, and it was 15-fold faster in the 3D cases. In the CNN, DDF generation took most of the time while the actual CNN prediction time with respect to a given feature was minimal. When CFD was used, meshing and simulation each took approximately the same amount of time. Overall, the CNN proved to be more time efficient than the CFD. As the size of the simulation-generated dataset increases, the difference will become even more pronounced. Moreover, the script needed to generate the DDF features will always be able to accommodate more optimization, while the presented time for the CFD was acquired from automated scripting. Thus, in most CFD processes wherein the user must manually interact with each process to set parameters (i.e., geometry modeling, meshing, pre-processing, and post-processing), the whole processing time would most likely be even longer than the aforementioned computing time.

Table 11. A comparison of the average computing times required by the CFD and CNN1 models when predicting 120 testing datasets.

| Unit: Seconds | Total | CAD Geometry | Meshing | CFD | DDF | CNN |
|---|---|---|---|---|---|---|
| CNN (2D) | 31.37 | - | - | - | 31.19 | 0.18 |
| CFD (2D) | 336.54 | 0.74 | 181.77 | 154.03 | - | - |
| CNN (3D) | 400.57 | - | - | - | 400.04 | 0.53 |
| CFD (3D) | 6309.71 | 3.58 | 454.82 | 5851.31 | - | - |

### 3.4.5. Graphical User Interface

Figure 26 provides a simple example of the GUI integrating the work of this study. For the purpose of demonstration, only the predictions of velocity and temperature fields occurring in the 2D barn containing solid cow bodies were considered. There are many ways to develop a GUI; however, in this study, Python web framework and Flask, along with a combination of JavaScript and HTML codes, were used to build a foundation that could be efficiently integrated with the CNN models developed in this study, and one easy to deploy on the internet as a web application. Developed CNN models can be exported in a ".h5" file format that already trained models can be loaded into the Flask Web Framework. The web interface, wherein users interact, was developed in an HTML format in which JavaScript was utilized to power the drag-and-drop interactivity occurring within the HTML page. Through the developed GUI, end-users can simply place cow bodies within the computational domain and achieve velocity and temperature-field results in seconds, whereas in when CFD is used, achieving comparable outcomes would require significantly more time.

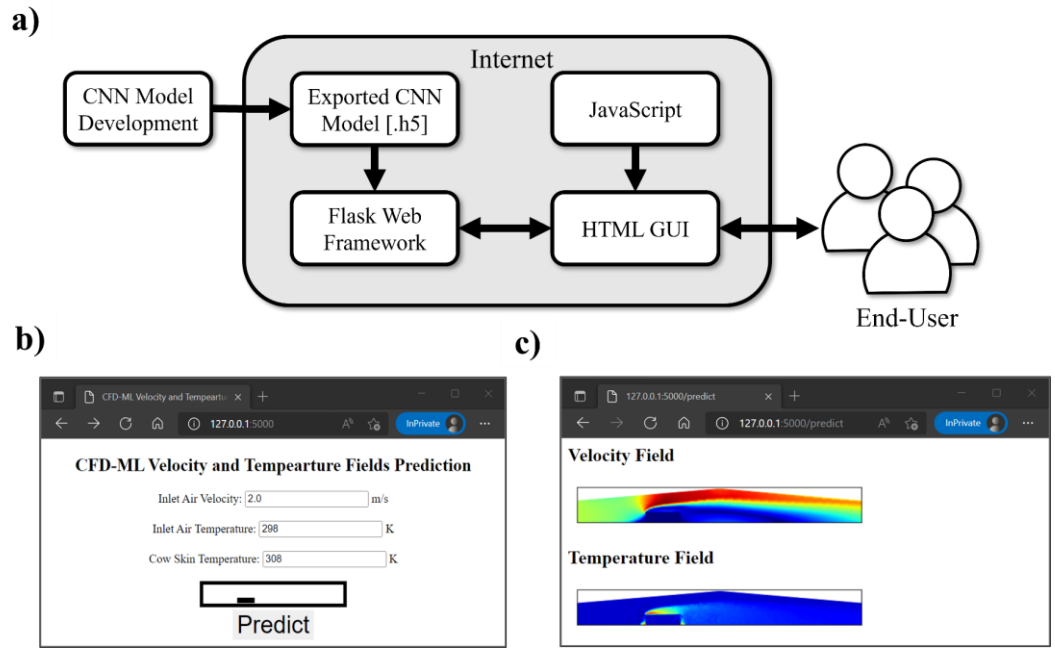


Figure 26. a) The web-based GUI developed for a demonstration of the CFD-ML models. b) The web interface wherein a user can drag-and-drop 'cows' to any location within the domain. c) The results page (presenting the field data generated when a user presses the "Predict" button).

## 3.5. Conclusion

The CNN model trained with the CFD metadata could efficiently predict the flow field and heat flux occurring inside a dairy barn with an accuracy comparable to the predictions achieved by both the 2D and the 3D CFD simulations. Overall, the calculated $R^2$ values for both flow and thermal energy field predictions were higher than 0.85 overall and higher than 0.90 for 2D cases. In a comparison of the CNN and, CFD outcomes, the Nusselt-number predictions obtained by the CNN2 model of the solid cow-body surfaces also indicate an acceptable level of error for the practical use. When CNN is used, a prediction can be obtained in less than 1/10th of the time that would be required if the CFD procedure were used. The outcomes of this work suggest that the CFD-ML approach has great potential for studies seeking ways to mitigate heat stress and optimize dairy-barn ventilation and building design. Although the models developed in this study are specific to the provided dairy barn template geometries, further development of

generalized training features, such as DDF, could allow for a model capable of predicting CFD outcomes even from “unlearned” barn scenarios.

Given that large-scale dairy barns will become more common as the U.S. dairy industry expands to meet increasing demand, the outcomes obtained during the course of this study should be taken seriously, their implication being that the applications of the CNN can improve the process of generating CFD simulations, producing comparable predictions and yet significantly reducing the required commutating time and user-interface complexity. Moreover, when the CNN is applied to the conventional CFD simulations, not only can a much more affordable and user-friendly GUI setup on the Internet be used to obtain similar results but also the user need not be an expert at in the CFD modeling, which requires extensive pre-processing and knowledge of computational methods. More efficient NN algorithms in the future will also advance the technology, and if so, then the application of CNN in CFD will become extremely relevant, especially in the field of large-scale dairy barn design and operation where computational simulations are critical.

## 3.6. References

Agarap, A.F., 2018. Deep learning using rectified linear units (relu). ArXiv Preprint ArXiv:1803.08375.

ANSYS, 2013. Section 20.6.1.: Automatic Pseudo Transient Time Step. In Ansys Fleunt Theory Guide, Release 15.0. Canonsburg, PA: ANSYS

Bagalkot, N., Keprate, A., Orderløkken, R, 2021. Combining Computational Fluid Dynamics and Gradient Boosting Regressor for Predicting Force Distribution on Horizontal Axis Wind Turbine. Vibration, 4(1), 248–262.

Bhushan, S., Burgreen, G.W., Bowman, J.L., Dettwiller, I.D., Brewer, W., 2020. Predictions of steady and unsteady flows using machine-learned surrogate models. Proceedings of 2020 IEEE/ACM Workshop on Machine Learning in High Performance Computing Environments, MLHPC 2020 and Workshop on Artificial Intelligence and Machine Learning for Scientific Applications, AI4S 2020 - Held in Conjunction with SC 2020: The International Conference for High Performance Computing, Networking, Storage and Analysis, 80–87.

Bobzin, K., Wietheger, W., Heinemann, H., Dokhanchi, S.R., Rom, M., Visconti, G., 2021. Prediction of Particle Properties in Plasma Spraying Based on Machine Learning. Journal of Thermal Spray Technology, 30(7), 1751–1764.

Cao, M., Rong, L., Choi, C.Y., Wang, K., Wang, X., 2022, Computational evaluation of air jet cooling from a perforated air ducting system to mitigate heat stress of cows in free stalls. Computers and Electronics in Agriculture, 199, 107198.

Chung, H., Li, J., Kim, Y., Van Os, J.M.C., Brounts, S. H., Choi, C.Y., 2020. Using implantable biosensors and wearable scanners to monitor dairy cattle's core body temperature in real-time. Computers and Electronics in Agriculture, 174, 105453.

Doumbia, E.M., Janke, D., Yi, Q., Amon, T., Kriegel, M., Hempel, S., 2021. CFD modelling of an animal occupied zone using an anisotropic porous medium model with velocity depended resistance parameters. Computers and Electronics in Agriculture, 181.

Drewry, J.L., Choi, C.Y., Powell, J.M., Luck, B.D., 2018. Computational model of methane and ammonia emissions from dairy barns: Development and validation. Computers and Electronics in Agriculture, 149, 80–89.

Evink, T.L., Endres, M.I., 2017. Management, operational, animal health, and economic characteristics of large dairy herds in 4 states in the Upper Midwest of the United States. Journal of Dairy Science, 100(11), 9466–9475.

Gebremedhin, K.G., Hillman, P.E., Lee, C.N., Collier, R.J., Willard, S.T., Arthington, J.D., Brown-Brandl, T.M., 2008. Sweating Rates of Dairy Cows and Beef Heifers in Hot Conditions. Transactions of the ASABE, 51(6), 2167–2178.

Guo, X., Li, W., Iorio, I., 2016. Convolutional Neural Networks for Steady Flow Approximation. Proceedings: ACM SIGKDD Conference on Knowledge Discovery and Data Mining. San Francisco, CA, USA.

Hillman, P.E., Willard, S.T., Lee, C.N., Kennedy, S.D., 2003. Efficacy of a vaginal temperature logger to record body temperatures of dairy cows. ASAE Paper No. 034011.

Jung, S., 2021, Innovative Mechanically Ventilated Dairy Barn Designs using Computational Fluid Dynamics, PhD Dissertation, University of Wisconsin-Madison, Madison, Wisconsin, USA.

Kingma, D.P., Ba, J.L., 2015. Adam: A method for stochastic optimization. 3rd International Conference on Learning Representations, ICLR 2015 - Conference Track Proceedings, 1–15.

Li, H., Sansalone, J., 2021. A CFD-ML augmented alternative to residence time for clarification basin scaling and design. Water Research, 209(December 2021), 117965.

Li, K., Kou, J., Zhang, W., 2021. Unsteady aerodynamic reduced-order modeling based on machine learning across multiple airfoils. Aerospace Science and Technology, 119, 107173.

Ma, Y., Zhang, Z., Kang, Y., Özdoğan, M., 2021. Corn yield prediction and uncertainty analysis based on remotely sensed variables using a Bayesian neural network approach. Remote Sensing of Environment, 259(March).

Mondaca, M.R., Choi, C.Y., 2016a. A computational fluid dynamics model of a perforated polyethylene tube ventilation system for dairy operations. Transactions of the ASABE, 59(6), 1585–1564.

Mondaca, M.R., Choi, C.Y., 2016b. An evaluation of simplifying assumptions in dairy cow computational fluid dynamics models. Transactions of the ASABE, 59(6), 1575–1584.

Mondaca, M.R., Choi, C.Y., Cook, N.B., 2019. Understanding microenvironments within tunnel-ventilated dairy cow freestall facilities: Examination using computational fluid dynamics and experimental validation. Biosystems Engineering, 183, 70–84

Mondaca, M.R., Cook, N.B., 2019. Modeled construction and operating costs of different ventilation systems for lactating dairy cows. Journal of Dairy Science, 102(1), 896–908.

Pakari, A., Ghani, S., 2021. Comparison of different mechanical ventilation systems for dairy cow barns: CFD simulations and field measurements. Computers and Electronics in Agriculture, 186(May).

Rong, L., Nielsen, P.V., Bjerg, B., Zhang, G., 2016. Summary of best guidelines and validation of CFD modeling in livestock buildings to ensure prediction quality. Computers and Electronics in Agriculture, 121, 180–190.

Rotz, C.A., Montes, F., Chianese, D.S., 2010. The carbon footprint of dairy production systems through partial life cycle assessment. Journal of Dairy Science, 93(3), 1266–1282.

Saha, C.K., Yi, Q., Janke, D., Hempel, S., Amon, B., Amon, T., 2020. Opening size effects on airflow pattern and airflow rate of a naturally ventilated dairy building-A CFD study. Applied Sciences (Switzerland), 10(17).

Ti, Z., Deng, X.W., Yang, H., 2020. Wake modeling of wind turbines using machine learning. Applied Energy, 257 (July 2019), 114025.

Tomasello, N., Valenti, F., Cascone, G., Porto, S.M.C., 2021. Improving natural ventilation in renovated free-stall barns for dairy cows: Optimized building solutions by using a validated computational fluid dynamics model. Journal of Agricultural Engineering, 52(1).

Van Os, J.M.C., 2019. Considerations for Cooling Dairy Cows with Water. Veterinary Clinics of North America - Food Animal Practice, 35(1), 157–173.

Zhang, J., Zhao, X., 2021. Machine-learning-based surrogate modeling of aerodynamic flow around distributed structures. AIAA Journal, 59(3), 868–879.

Zhou, B., Wang, X., Mondaca, M.R., Rong, L., Choi, C.Y., 2019. Assessment of optimal airflow baffle locations and angles in mechanically-ventilated dairy houses using computational fluid dynamics. Computers and Electronics in Agriculture, 165, 104930.

# CHAPTER 4: EVALUATION AND OPTIMIZATION OF A POSITIVE-PRESSURE PRECISION VENTILATION SYSTEM TO PREVENT HEAT STRESS FOR DAIRY CATTLE

Hanwook Chung, Dimuth Panditharatne, Kenneth V. Nordlund, and Christopher Choi

## 4.1. Abstract

A dairy barn's ventilation system is essential to any effort aimed at preventing heat stress, and for this reason, its performance directly affects both the farm's economic viability and the animal's welfare. One type of system, Positive-Pressure Precision Ventilation (PPPV), has emerged as an innovative design solution because it overcomes the most prevalent limitations of traditional mechanical ventilation schemes and improves the ventilation efficiency by relying on a centrally located, pressurized plenum and a series of air-jet nozzles to precisely target each animal. This study describes a design optimization procedure involving a series of experimentally validated Computational Fluid Dynamics (CFD) simulations that provided the study's authors with insights that enabled them to establish ideal design parameters for the system's air-jet nozzles. To assess system performance, these designs were tested according to specified assumptions and scenarios and in conjunction with computational case studies. The outcomes demonstrated the efficacy of using straight air-jets emitted through a medium-sized nozzle opening (0.1016m in diameter) to achieve balanced cooling performance and the most efficient operational pressurization level. The case studies showed that PPPV systems could double the cooling efficiency at half the required mass flow rate employed by traditional systems and demonstrated the system's scalability, uniformity with respect to nozzle exhaust, and resilience when subjected to a drifting ambient air-current of 0.5 m $s^{-1}$. This study's approach and resultant insights should be considered instrumental when installing a PPPV system and could play a significant role in the evolution of dairy barn ventilation systems aimed at addressing economic and animal welfare concerns.

## 4.2. Introduction

### 4.2.1. Dairy Heat Stress

Heat stress is a widespread threat for both dairy cows and producers in the U.S., especially during hot and humid conditions that, if allowed to persist unabated, will continue to concern animal wellbeing while causing significant economic losses. When producing milk, a dairy cow undertakes a highly metabolic, heat-generative process that produces a significant amount of heat (Tao et al., 2020). Moreover, when excessive external heat is added to the lactating cow's body heat, the cow will overheat and begin to suffer from heat stress, which will negatively affect not only her milk production but also the quality of milk, fertility, and overall health, and the drive to increase milk production has only worsened the problem. For instance, a cow in the U.S. today produces 270% more milk than in 1967 (USDA-NASS, 2017). This escalating milk yield necessitates an increased feed intake, which imposes an even greater heat load on the cow and leads to negative feedback of inefficiency.

When confronted with heat stress, a dairy cow undergoes both physiological and behavioral changes. She will, for example, consume less feed, which will result in decreased milk production and, consequently, less income for the producer (Bohmanova et al., 2007; Liu et al., 2019). The stress also diminishes estrus activity and fertility, thereby increasing costs related to breeding services (Polsky & von Keyserlingk, 2017). A heat-stressed cow also tends to stand longer to maximize convective heat loss (Cook et al., 2007). This prolonged standing, however, puts the cow at a heightened risk of lameness, which can lead to her being culled. Furthermore, the milk quality will be degraded (characterized by reduced percentages of milk fat and protein, the essential components for dairy product processing and value). Altogether, these ramifications produce losses exceeding a billion dollars annually for the U.S. dairy industry (St-Pierre et al., 2003; Key et al., 2014). With the continuous pursuit of greater milk production rates and with the ongoing effects of climate change to longer and hotter summers, the problems associated with heat stress

will most likely intensify. This growing challenge underscores the pressing need for the dairy industry to devise more efficient and effective cooling solutions for cows.

### 4.2.2. Cooling and Ventilation

Ensuring the thermal comfort of a dairy cow is crucial to her welfare and production efficiency. To this end, the U.S. dairy industry employs various ventilation systems, mainly categorized into natural and mechanical ventilation (Mondaca, 2019). Smaller barns often rely on natural ventilation, which leverages natural breezes, while larger facilities most often resort to mechanical systems that can draw air through the barn using large fans. Tunnel-ventilation and cross-ventilation are the two most common system design configurations. In tunnel-ventilated barns, air moves from one end of the barn to the other in parallel with the roof ridge. In contrast, air passing through cross-ventilated barns moves from one side to the other, across the width of the barn, and perpendicular to the roof ridge. With the growth of the dairy industry and the enlargement of barn sizes, structural design and cooling strategies revolving around dairy mechanical ventilation systems have evolved to provide optimal and uniform conditions for cows, especially during hotter seasons.

On top of the installation of fans, some large barns in hot and dry regions enhance their cooling performance by incorporating water sources such as sprinklers or misters to increase the cooling effect (Van Os, 2019). When the addition of water cooling is not appropriate (in humid regions), additional fans are strategically installed to increase the air speed for the cows. Some even carry out structural modifications, such as adding air baffles that redirect the airflow, to passively improve the cooling in the pen (Zhou et al., 2019). With these strategies, the mechanical ventilation system with crosswind direction can provide an effective means to control the overall flow rate into the barn with easy integration to additional cooling methodologies like air baffle and water cooling to help the cow cooling in large facilities. However, the crosswind system has some limitations in controlling airflow behavior in animal-occupied zones (AOZ) and their microclimate zones (zones that describe where cows are actually influenced by airflow and air conditions within a barn), which is the critical zone when evaluating the cooling performances by the overall ventilation systems, that,

at the worst case scenarios, up to 80% of the airflow produced by the ventilation system can be wasted (not cooling the cows) due to air traveling predominantly along the barn's paths of least resistance and bypassing essential AOZ (Mondaca et al., 2019).

The risk of heat stress continues to increase because, as many smaller barns consolidate to form larger dairy barns for economic and operational benefits, more cows are housed per facility that push the airflow even further away from AOZ due to higher animal density. Across the U.S., larger operations are increasingly responsible for more of the total milk production. In the Upper Midwest alone, the percentage of milk produced by farms milking more than 500 cows has increased by more than threefold from 2000 to 2012, growing from 9.0% to 38.1% in Wisconsin, for example (Evink & Endres, 2017).

### 4.2.3. Positive-Pressure Precision Ventilation

The positively pressured precision ventilation (PPPV) system was specifically designed to uniformly distribute to cooling target air-jets to each cow inside the barn using pressurized plenum, and by having a shorter inlet-to-cow distance, the PPPV system can potentially allow all cows to have fresh air access (Jung et al., 2023). The concept of targeted cooling for adult dairy cows, such as polytube ventilation methods (Mondaca & Choi, 2016a), can suggest better control over the cooling airflow right in the cow-occupied zones, providing uniform air distribution as well as an opportunity to significantly decrease the required volumetric flow rate, fan energy, of the ventilation system. In a previous study, Jung et al. (2023) combined both experimental data and computational simulation, such as computational fluid dynamics (CFD), to validate the PPPV system. Their findings not only revealed that pressurization was consistent throughout the plenum but also indicated that the jet of air produced the minimal air speed of 2 m $s^{-1}$ that Mondaca recommended (2019). In its general design and purpose, the PPPV system resembles certain previous systems (Mondaca & Choi, 2016a; Wang et al., 2018) but delivers a more precisely targeted cooling in large-scale barns. Thus, although its design has only been evaluated in one specific configuration, it promises enhanced scalability and precision. Historically, the problems associated with targeted cooling (typically delivered via perforated circular air ducts) involved the difficulty of controlling the air-jet's

direction and minimizing ambient air-current influences. Yet, as demonstrated by Mondaca and Choi (2016a), innovative solutions, such as air-jet deflectors or the specific perforation shapes tested by Cao et al. (2023), have been devised. The rigid extruded nozzle design of the PPPV system could potentially further lessen the air-current influence on the targeted air-jets with precise targeting and higher flow rate. Thus different nozzle design parameters, such as diameter, length, and location, should be carefully explored for their influence on air-jet pattern.

### 4.2.4. Computational Fluid Dynamics and Design Optimization

Computational fluid dynamics (CFD) has emerged as a pivotal instrument in the design optimization of fluid flow models chiefly because it can provide dependable simulation results, which in turn can inform and justify specific design decisions. Using CFD, engineers can streamline fluid flow designs virtually, resulting in significant savings in time, cost, and other resources that would otherwise be spent on tangible experiments. Integrating CFD with optimization techniques has proven instrumental in solving many flow design problems. For instance, Calautit et al. (2015) harnessed CFD-based optimization to pinpoint an ideal spacing for heat transfer devices to achieve optimal cooling of air in HVAC systems. Similarly, He et al. (2018) leveraged CFD simulations to refine greenhouse temperature distribution by adjusting the back-wall vent dimensions. Abeykoon (2020) further illustrated how CFD outcomes could be pivotal in dissecting fluid flow dynamics in heat exchanger designs (doing so by focusing on elements like baffles and tubes). Furthermore, CFD-driven design optimization need not be limited to direct scenario comparisons; it can also model sophisticated optimization techniques involving response surface models, radial basis functions, and even artificial intelligence, as described by Li et al. (2018). The optimization approach should be chosen carefully, considering the nature of available variables/data (whether linear or nonlinear) and the specific parameter being optimized.

To facilitate our research, we optimized the design parameters of the PPPV system's key design parameters (nozzle size, length, position, and angle) with a primary focus on enhancing the system's cooling performance. These parameters were evaluated against the efficacy of the system's overarching cooling

effects on cow models (mainly expressed in terms of the Nusselt number. To ensure the accuracy of our CFD simulations, a tangible prototype was constructed in such a way that it could serve both as a tool for validating the CFD results and as a means of fine-tuning the simulation configurations (most notably the meshing). With the suggested optimized design, we embarked on additional case studies to test the following postulations:

1. The PPPV system is scalable.
2. The PPPV system is adept at generating potent air-jets that are minimally affected by the surrounding conditions.
3. The PPPV system can significantly reduce the amount of fan energy for inlet air while providing sufficient cooling airflow for each cow.

## 4.3. Materials and Method

### 4.3.1. PPPV Parameters

The main principles of the PPPV system are illustrated in Figure 27a. The system's performance should be defined essentially on its ability to cool the cows by means of targeted air jets and the uniform distribution of fresh air through a positively pressurized chamber. In this study, a simple cylindrical nozzle shape was considered. The cooling performance of the PPPV system, when operating under the same flow rate from each nozzle and set at a fixed ceiling height, depends on nozzle diameter, length, angle, and position (Figure 27b). Any variation in these four parameters will affect the throw distance and area coverage of the jet when it strikes a cow's body surface. The efficiency of the air distribution via a collection of these nozzles may be influenced by the differences in airflow resistance and the choke points formed because of these parameters.

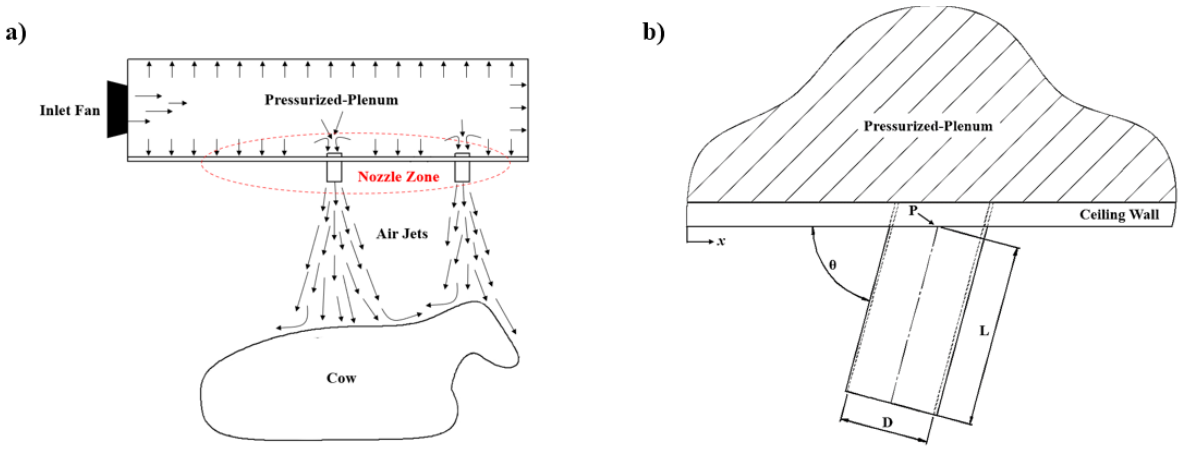


Figure 27. a) The principles of PPPV system; b) Nozzle parameters: D = Diameter of the nozzle; L = Length of the nozzle; θ = Angle of the nozzle P = Position on the nozzle.

Table 12 shows the lists of values considered for each parameter (values were carefully selected to minimize the optimizing process). The nozzle diameters chosen were based on commercially available PVC pipe sizes. The only limitation to the length of the nozzle was that the nozzle exit should be high enough that a cow could not reach it. In this study, two nozzles were considered with regard to their ability to provide two air jets to each cow. The nozzle positions (P1 and P2) were determined in accordance with the length of the typical cow's body (2.0 m and with the tail end considered to be 0 m), and one nozzle could not be positioned closer than 0.2 m from the other. Only a couple of nozzle angles were considered because, in a head-to-head stall configuration, a nozzle set at an angle greater than 30 degrees would produce an impinging zone that would overlap with the target area produced by an adjacent nozzle. With these values selected, there is a total possible parametric scenario of more than 1,440 combinations.

Table 21. Different PPPV design nozzle parameters with their range and selected values.

| Parameter | Value Range | Selected Values |
|---|---|---|
| Nozzle Diameter [cm], D | 7.61 – 15.24 | 7.61, 10.16, 12.7, 15.24 |
| Nozzle Length [cm], L | 6.36 – 38.1 | 6.36, 12.7, 19.05, 25.4, 31.75, 38.1 |
| Nozzle Position 1 [m], P1 | 0 – 2 | 0.2 increments |
| Nozzle Position 2 [m], P2 | 0 – 2 | 0.2 increments |
| Nozzle Angle [˚], θ | 0 – 30 | 0, 30 |

### 4.3.2. CFD Simulation and Validation

#### 4.3.2.1. Computational Model

A computational model of the experimental PPPV system was constructed in order to facilitate the virtual testing of diverse design parameters. The dimensions of the pressurized plenum and the computational domain located beneath it (depicted in Figure 28a) were derived from the two-cow model described by Jung et al. (2023). A gray box labeled “Nozzle Zone” highlights the area featuring the various nozzle configurations. The positioning of the reclining cow geometry conforms to a standard head-to-head stall arrangement. The simplified cow geometry was adapted (and subsequently modified) from the work by Wang et al. (2018), with the modifications influenced by more recent publications. As proposed by Mondaca and Choi (2016b), this simpler cow geometry yields results in flow and heat transfer patterns that are nearly equivalent to those yielded by a more detailed cow model while providing the benefit of markedly reduced computational costs. The surface area of the reclining cow was designated as 4.30 m2, per Le Cozler et al. (2019).

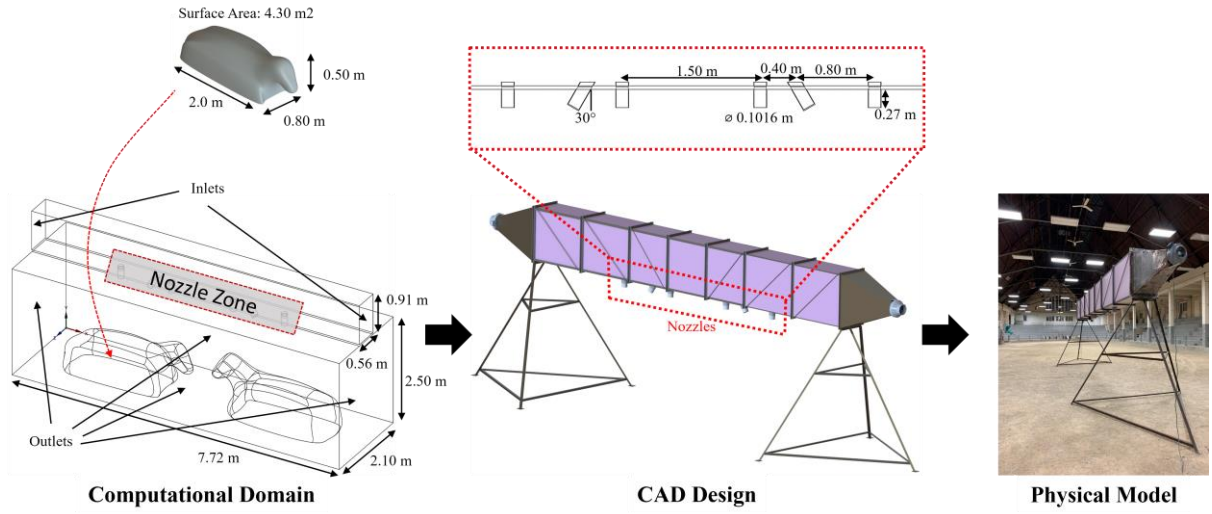


Figure 28. The computational domain and physical domain of the PPPV system.

The heat transfer occurring on the surface of the cow will significantly affect the optimization process's outcomes. Thus, the temperature-dependent surface heat flux model was defined as a cow surface-boundary

condition, which called for Equations 12 and 13 (Li et al., 2021). A constant temperature model would have sufficed when comparing the relative average differences in the cooling performances of different airflow models. However, to optimize the cooling performance based on rapidly dissipating air jets (such as the throw distance and the air jet coverage), it is necessary to eliminate false global maximum and minimum due to the uncapped heat transfer rate from the cow surface. The surface temperature will vary depending on the location of the cow's body surface. Nonetheless, to stabilize the simulation, the maximum allowed $T_{surface}$ was set as $T_{core}$ (311.15 K).

$$q" = \frac{\rho C_p(T_{core} - T_{surface})}{R_{skin}} \tag{12}$$

$$R_{skin} = \max(-5.44(T_{surface} - 273.15) + 225, 29) \tag{13}$$

where

q" = Skin Surface Heat Flux, W $m^{-2}$

$\rho C_p$ = Volumetric heat capacity of air, J $m^{-3}$ $K^{-1}$

$T_{core}$ = Core Temperature, K

$T_{surface}$ = Skin Surface Temperature, K

$R_{skin}$ = Skin Thermal Resistance, $m^2$ K $W^{-1}$

Several energy transfer variables and dimensionless numbers were chosen to serve as optimizing target parameters. As shown in Equations 14, 15, 17, and 18, the surface-area-averaged heat-flux Nusselt number (and their respective standard deviation) and Reynolds number were calculated. Considering standard deviation is critical to assess the uniformity of heat transfer performance throughout the cow's geometry instead of the overall average, which may not capture regions of high and low heat transfer and their differences.

$$\bar{q"} = \frac{1}{A_{cow}} \int q" dA_{cow} \tag{14}$$

$$\sigma_{q"} = \sqrt{\frac{\sum_{i=1}^{n} (\bar{q"} - q"_i)^2}{n}} \tag{15}$$

$$Nu = 2.0 + 0.6Re0.5Pr^{0.333} \tag{16}$$

$$\overline{Nu} = \frac{1}{A_{cow}} \int Nu dA_{cow} \tag{17}$$

$$\sigma_{Nu} = \sqrt{\frac{\sum_{i=1}^{n} (\overline{Nu} - Nu_i)^2}{n}} \tag{18}$$

where

$q$" = heat flux at each cow geometry surface facet, W m$^{-2}$

$\overline{q}$" = area-weight average of heat flux, W m$^{-2}$

$\overline{Nu}$ = area-weight average of Nusselt number

$A_{cow}$ = cow geometry surface area, m$^2$

$Pr$ = Prandtl Number (assumed 0.71 for air)

$n$ = a number of geometry surface facets

$Re$ = Reynold's Number

This study adheres to the validated CFD simulation setup described by Jung et al. (2022). The CFD simulations undertaken in this study utilize the steady-state Reynolds-Averaged Navier-Stokes (RANS) method for addressing the Navier-Stokes equations. To decipher the RANS model, the Semi-Implicit Method for Pressure-Linked Equations (SIMPLE) numerical scheme and the second-order upwind differencing scheme (UDS) were employed. This model, which has been widely used in studies aimed at simulating microclimates inside livestock buildings, has achieved good agreement with experimental data (Norton et al., 2010; Wu et al., 2012). For all simulations, the standard k-ε turbulence model was applied in tandem with the enhanced wall-treatment function used on wall surfaces, and double precision variables were consistently used in all the simulation calculations.

Due to the intricate geometry of both the cows and the nozzles, most of the computational domain was discretized using an unstructured tetrahedral mesh. A more refined mesh was formulated at nozzle zones, and structured prism layers were incorporated on the cow surface. A computational model featuring an angled nozzle configuration, reclining model cows, and high pressurization served as the basis for mesh-independence testing. Various meshing parameters, such as global size, the number of prism layers, and growth rates, were modulated for mesh testing. To guarantee stable heat transfer results, this study

considered five convergence criteria on the cow surface: total heat transfer rate, wall y+, total surface heat flux, wall y*, and wall shear stress. As cell discretization become finer with a mesh setup encompassing approximately 1.5 million elements, all five parameters began converging and thus satisfied the acceptable y+ range for k–ε turbulence models ($y+ < 5$ or $30 < y+ < 300$), as per Rong et al. (2016). This mesh setup was consistently applied to all the other CFD models.

#### 4.3.2.2. Physical Validation Model

Using field data to validate the computational model is crucial to substantiating the utility of a CFD simulation. Two scenarios, illustrated in Figure 28b and 28c, were chosen from several possible parameter combinations and used as reference models. The chosen model incorporated six nozzles, and this permitted two distinct cases, one featuring two straight nozzles and the other a combination of straight and 30° angled nozzles designated for each cow located beneath the pressurized plenum. Each emitter was fitted with a nozzle 0.127 in length and 0.1016 in diameter. These six nozzles were integrated into the pre-existing, angle-iron welded structure delineated in Jung et al. (2023).

The inner pair of nozzles was oriented in such a way as to target the head area, and two operational configurations that focused on the entire body (one straight and the other angled) were considered. The transition between nozzle configurations was achieved by sealing the unnecessary nozzle using a pipe cap fastened on with stainless steel clamps. As depicted in Figure 27, a rectangular plenum with inner dimensions of 0.56 m by 0.91 m by 8 m was located 2.5 m above the floor of the barn and supported by two iron tripod structures. Flanking the plenum were two in-line duct fans (0.2032 m diameter, Vortex Powerfans, Terrebonne, QC, Canada), connected to the plenum by 1.15 m long diffuser units housing multiple honeycomb cores (3.81 cm thick with a 2.54 cm cell size, McMaster-Carr, Elmhurst, IL, USA), which acted as flow straighteners. The fan speeds, which were modifiable by means of potentiometers, were well suited to both maximum (summer) and minimum (winter) capacity scenarios. The physical chamber, which was strategically positioned indoors at the multifunctional Stock Pavilion on the UW-Madison campus, stood over 10 m away from the adjacent walls.

Considering different fan capacities and nozzle configurations, plenum pressurization was gauged using a micromanometer (Fluke 622, TSI, Shoreview, MN, USA) (refer to Table 13). For each scenario, three distinct points at each nozzle location were assessed, resulting in a total of 15 measurement points. Uniform pressurization, with minimal deviations, was observed at all 15 points regardless of the fan capacity. Despite angled cases exhibiting some deviations, the differences between the configurations were deemed negligible. These pressure values were pivotal in determining the CFD inlet conditions.

Table 13. Plenum inner averaged field measured pressure at two different fan settings at straight and angled nozzle configurations.

| | HIGH [Pa] | LOW [Pa] |
|---|---|---|
| Straight Nozzle Config. | 126.42 ± 0.49 | 46.66 ± 0.47 |
| Angled Nozzle Config. | 126.25 ± 0.72 | 46.25 ± 1.01 |

To validate the CFD model, velocities beneath the nozzles within the animal-occupied zone were meticulously measured. Two distinct measurement heights, 0.5 m and 1.5 m, were assumed to correspond to the elevations of an average cow (one standing, the other reclining). Given the symmetrical nature of the experimental setup at its midpoint, measurements were taken within the first half of the chamber. To correspond with heights (1.5 m and 0.5 m), a total of 35 and 40 respective measurement points were chosen at 5 cm increments along the center axis of the chamber. The number of measurements taken at 0.5 m was increased in order to encompass a larger area due to the angled nozzle; locations directly beneath the angled nozzle were omitted. To gauge velocity, an ultrasonic anemometer (model 81000, R.M. Young, Traverse City, MI, USA) was mounted securely on a heavy-duty metal tripod (to maintain sensor stability). The exact locations of the measurement points were meticulously determined using a plumb bob (in reference to the chamber's floor surface). For each measurement point, 30 seconds of data, encompassing 10 samples per second, were accumulated using a data logger (CR3000 Series, Campbell Scientific, Logan, UT, USA) with the entire measurement process being replicated three times. Despite the experimental site being relatively shielded from external conditions, a subtle passive natural air drift (below 0.3 m $s^{-1}$ and attributable to the building’s HVAC system) was consistently present throughout the experimentation phase.

### 4.3.3. Design Optimization Approach

Given the nonlinear nature of this problem (due to such parameters as nozzle angle and location), developing a universal method for processing and optimizing all data concurrently would have posed significant challenges, and the result would have been far from straightforward. Therefore, to fine-tune the nozzle parameters, an approach comprising a series of steps underpinned by known assumptions was employed. Figure 29 provides a schematic representation of the optimization steps and presents a series of case studies that illustrate the finalized design. Initially, the feasibility of the angled nozzle orientation was ascertained, aligning with the physical model and corresponding CFD outcomes. The head-to-head stall orientation inherently imposed significant limitations on the permissible degree of nozzle angle and location. Subsequently, to pinpoint the optimal nozzle location, pressurization data derived from the physical validation test were referenced. Given the nonlinear nature of the problem, a direct comparison of outcomes was undertaken to determine the viable locations. Finally, once the nozzle locations were determined, variations in nozzle dimensions were explored with respect to their impact on the static pressure occurring within the pressurized plenum and their cooling performance. In this phase, Sequential Least Squares Programming (SLSQP) (Kraft, 1988) and trust-region constrained optimization (Friedlander et al., 1994) algorithms were deployed to identify the optimal nozzle dimensions. These algorithms facilitated the integration of parameter constraints. The results and following discussions should elucidate the simplifying assumptions employed to identify the ideal nozzle dimensions.

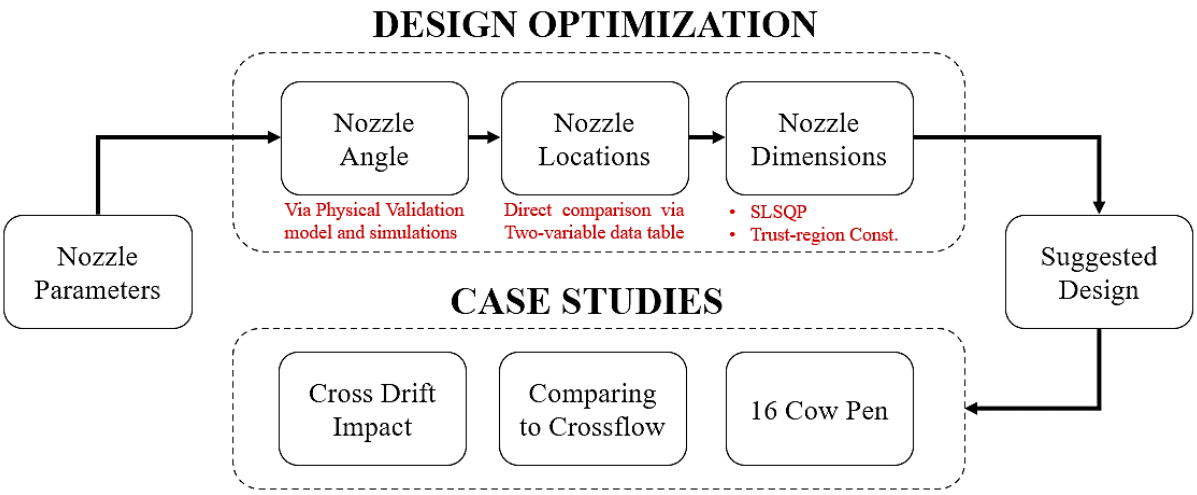


Figure 29. Design Optimization Flow Diagram.

### 4.3.4. Case Studies

Three distinctive simulation cases were explored to elaborate on the performance features of the PPPV system, each using the nozzle design parameters proposed in the optimization steps. First, simulation parameters were set to assess the heat-transfer performance of the model cow to compare the relative performance differences. An idealized cross-ventilation prototype (Figure 30a) was designed to represent a segment of the proposed system's cooling-performance enhancement in comparison to the mechanically ventilated system (wherein air traverses horizontally). This model was deemed ideal as a commercial barn would likely have a larger cross-sectional area of airflow rather than a flat, low-rise ceiling wall. All boundary conditions paralleled those of the PPPV cases, except that the outlet was set at 2 m $s^{-1}$ to provide the recommended ideal wind speed (Mondaca, 2019). Second, a scaled-up PPPV model (Figure 30b) capable of covering 16 cows (typically the number in one pen) was designed to assess the system's scalability. The gap between each row of cows was established at 1.33 m. To maintain mass flowrate consistency, the same pressurization value used in the validation case was employed as the inlet boundary conditions. Three different sets of inlets were selected in order to pressurize the plenum and determine how different inlet locations and in-flow directions might affect the pressurization (and influence the uniformity of air distribution). However, the locations, numbers, and sizes of the inlets can be altered depending on

the structure in which the PPPV is to be installed. Both high and low pressurization values were applied to determine the correlation between cooling performance and pressurization and to analyze their respective uniformity as it related to the resulting air jets. Last, as a primary consideration regarding targeted cooling, the impact of drift was evaluated (as this drift can deflect the direction of the air jet). Drift velocities of 0.25 to 2.00 m $s^{-1}$ at 0.25 m $s^{-1}$ were introduced to the PPPV system, as shown in Figure 30c. A symmetrical wall condition was applied to the side wall instead of to a pressure outlet.

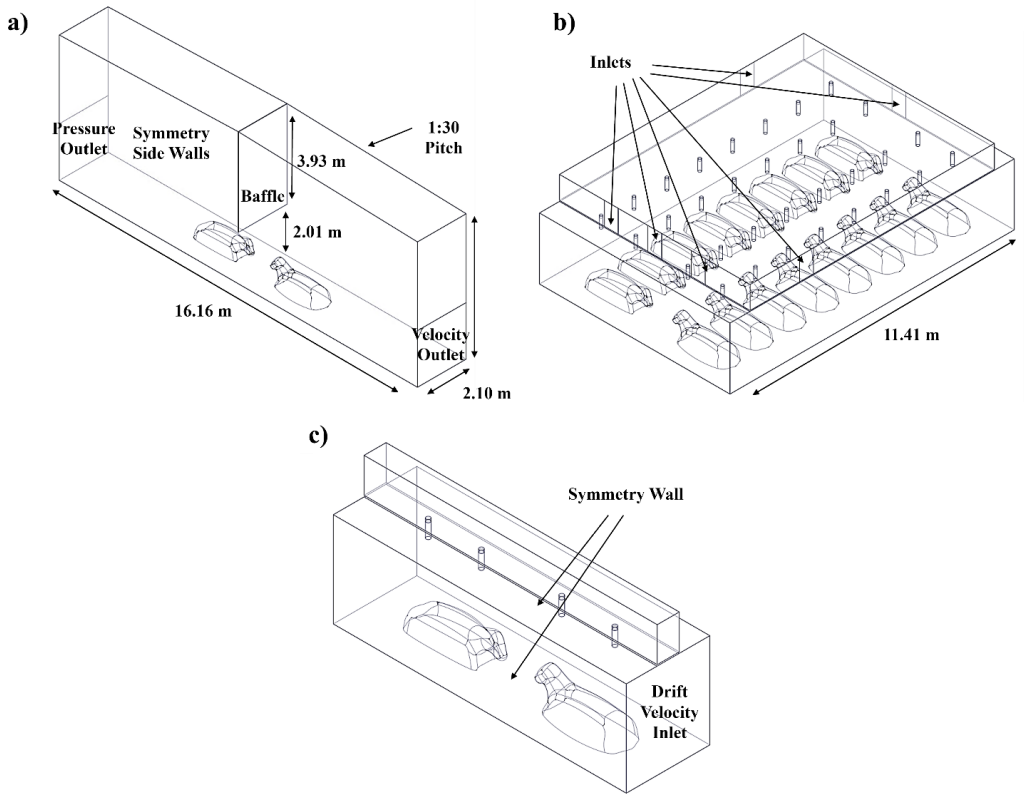


Figure 30 Two models for case studies: a) Idealized crosswind model; b) scaled up 16 cow pen model; c) 2-cow PPPV model incorporated with drift inlet.

## 4.4. Result and Discussion

### 4.4.1. CFD Model Validation

The velocity measurements obtained experimentally were juxtaposed directly with the velocity magnitudes obtained at the corresponding coordinates in the computational PPPV model (which did not include the

cow models). Figure 31, which depicts the four distinct comparisons made for validation purposes, illustrates scenarios involving high and low pressurization at heights of 1.5 m and 0.5 m. Here, the positional nodes are placed at 5 cm intervals. As anticipated, the air jet's cross-sectional area (coverage) broadens in relation to its distance from the nozzle, exhibiting diameters of approximately 0.5 m and 0.8 m at the 1.5 m and 0.5 m heights, respectively. The field velocity measurements at 1.5 m height follow a coherent bell-shaped trend, while those at 0.5 m exhibit readings that vary more widely. This greater variability can be attributed to the 0.5 m height being more susceptible to the inherent drift associated with the experimental site and to the turbulence of the air that was rebounding from the uneven sand floor. Nonetheless, the measurement trends aligned broadly with the CFD results (despite the idealized assumptions inherent in the CFD simulation setup). Regarding the low-pressure comparisons associated with the 0.5 m height, all peak discrepancies found to exist between the experimental measurements and CFD outcomes were subsumed within 0.5 m $s^{-1}$. Moreover, field measurements found an airflow speed of about 0.5 m $s^{-1}$ occurring between the target areas (i.e., between the stalls), in contrast to the near-zero speed recorded in the CFD simulation.

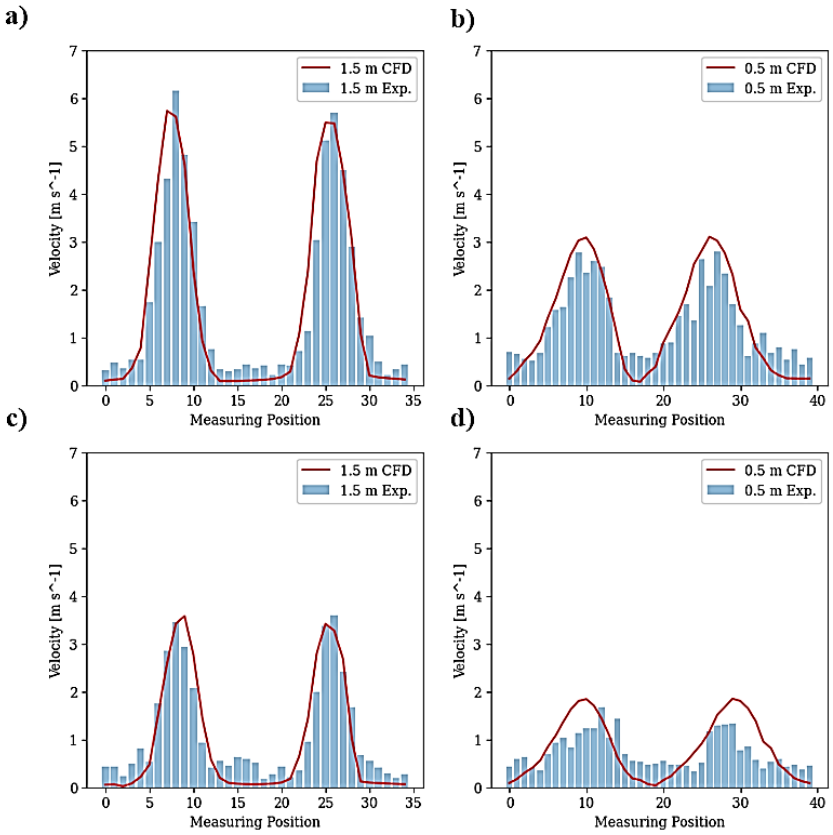


Figure 31. Comparison between CFD and field measurement: a) high pressurization at 1.5 m; high pressurization at 0.5 m; low pressurization at 1.5 m; low pressurization at 0.5 m.

## 4.4.2. Cow Cooling Performance: Optimization

### 4.4.2.1. Straight vs. Angled Nozzle Performance on Cooling

Figure 32 shows the results obtained from a comparative analysis of the velocity contours (derived from the two distinct nozzle-set scenarios that were simulated based on the physical model's setup). The average Nusselt Number per cow registered a 230.02 for the straight nozzle scenario. In contrast, the number was approximately 10% lower (registering at 207.28) in the mixed-nozzle scenario (which involved the same fan input setup). This trend remained consistent even under reduced fan capacity. It should be noted that a decline in overall heat transfer was observed despite the augmented air-jet coverage produced by the angled nozzles. This phenomenon implies that in the context of targeted cooling, heat transfer may be more positively correlated with air-jet speed than with area coverage.

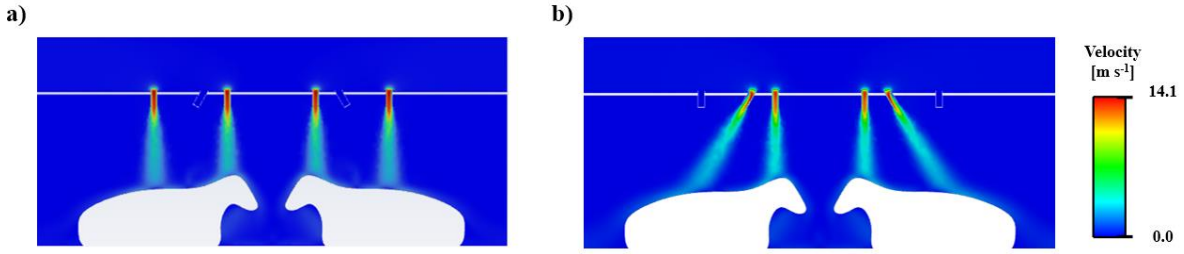


Figure 32. Velocity contour of the CFD outcomes based on the physical validation model setup as high fan capacity. a) straight nozzles only; b) a mix of straight and angled nozzles.

#### 4.4.2.2. Ideal Nozzle Locations per Cow

A total of 45 nozzle scenarios were assessed, with two nozzles directed at each cow. The heat transfer outcomes associated with each scenario (each involving one cow) are shown in Table 14. These outcomes were achieved by the predetermined nozzle dimensions (which corresponded to the physical model dimensions) with a known pressure of 126.42 Pa inside the plenum. The results do not indicate a distinct optimal arrangement. However, the four most efficient arrangements (0.4-1.4, 0.6-1.2, 0.6-1.4, and 0.8-1.0) corresponded to P1-P2 locations. Conversely, the 0.2-0.2 and 0.2-0.4 arrangements (both nozzles aimed at the lower back/tail area of the cow) were among the least effective. Subsequent simulations involving all four top nozzle arrangements were conducted to evaluate the sensitivity of the heat transfer outcomes. These simulations aimed to discern variations in outcomes and to establish whether the observed efficacies were consistent across different simulations.

Table 14. Grid table showing area-weighted heat flux from cow's surface at each nozzle location combination. Color scheme is based on the flux value where green tiles shows higher flux values.

Nozzle 1 Location (P1) [m]

| Nozzle 2 Location (P2) [m] / [W m$^{-2}$] | 0.2 | 0.4 | 0.6 | 0.8 | 1.0 | 1.2 | 1.4 | 1.6 | 1.8 |
|---|---|---|---|---|---|---|---|---|---|
| 0.2 | 498.1 | 560.6 | 609.7 | 639.5 | 643.6 | 632.6 | 612.7 | 597.9 | 581.7 |
| 0.4 | 499.8 | 550.3 | 587.5 | 604.0 | 602.0 | 587.1 | 584.1 | 540.8 | |
| 0.6 | 534.9 | 579.4 | 602.1 | 614.4 | 615.9 | 615.2 | 595.2 | | |
| 0.8 | 575.2 | 610.1 | 624.1 | 633.3 | 647.9 | 631.6 | | | |
| 1 | 603.1 | 625.7 | 644.9 | 677.4 | 648.1 | | | | |
| 1.2 | 616.4 | 640.9 | 673.5 | 652.7 | | | | | |
| 1.4 | 626.9 | 677.4 | 673.3 | | | | | | |
| 1.6 | 642.6 | 658.1 | | | | | | | |
| 1.8 | 626.5 | | | | | | | | |

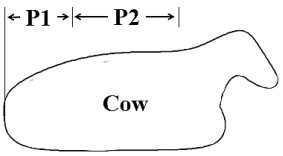


#### 4.4.2.3. Nozzle Dimensions vs. Static Pressure & Nusselt Number

To evaluate the optimal nozzle placement, a comprehensive study involving 24 cases was conducted with a special focus on nozzle-dimension variations, including diameter and length. The cases involving the 0.4-1.4 scenario are depicted in Figure 34, along with the (similar) outcomes observed in the other three P1-P2 scenarios. Figure 33a illustrates the correlation between the plenum's static pressure and the various nozzle diameters and lengths (while maintaining a consistent flow rate). As anticipated, a diminutive nozzle diameter correlates with an augmented static pressure within the plenum, with the augmentation exhibiting an exponential rather than linear trend. For instance, diameter transitions from 0.1524 m to 0.127 m and from 0.127 m to 0.1016 m resulted in pressure increases of 216% and 244%, respectively, whereas a further reduction to 0.0762 m increased the static pressure by 322%. Notably, changes in the nozzle's length had a negligible impact on the overall pressure. Nonetheless, pressurization should be considered carefully in order to ensure that an appropriate mass (or volume rate) is delivered throughout the barn, as the static pressure under which the fans function will influence the selection, operational cost, efficiency, and capacity of the fans and the system at large.

Figure 33b highlights the relationship between the average Nusselt Number on the cow's body surface and the nozzle's diameter and length when subjected to a uniform mass flow rate. Contrary to pressure levels, changes in heat-transfer performance correlated linearly with a diminishing nozzle diameter, indicating an increased exit velocity. Again, the length of the nozzle has an insignificant influence. The standard deviation of the Nusselt Number for each scenario demonstrates that static pressure and overall heat transfer do not significantly affect the uniformity of the cooling effect occurring across the cow's body surface. This can likely be attributed to the air-jet's dispersion upon impact on the body surface. Similar trends were observed in heat flux and their standard deviations. Smaller nozzle sizes were found to be the most effective (with respect to heat transfer). However, given the static pressure buildup that occurs and the compromise that must be made between heat transfer efficiency and system efficiency, determining the optimal nozzle parameters should be accomplished carefully.

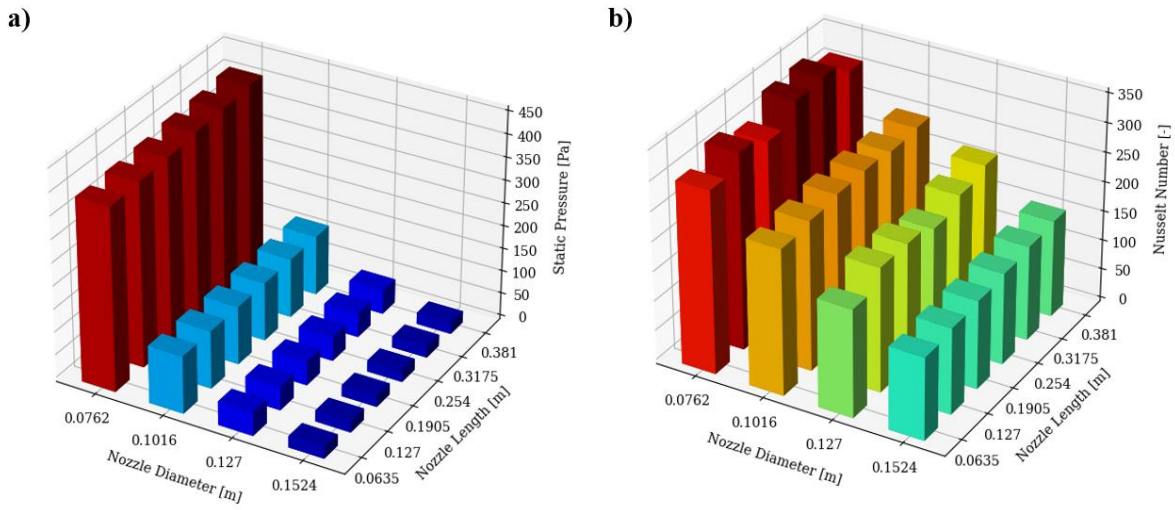


Figure 33. These graphs show the resulting static pressure within the plenum and Nusselt Number on the cow's body surface based on the varying nozzle diameter and length. a) Static Pressure; b) Nusselt Number. The color is based on the value of the bar, and red means a higher value.

#### 4.4.2.4. Optimizing Nozzle Dimensions

A response surface optimization model was constructed and resolved by leveraging preceding results that depicted the relationship between nozzle dimension, static pressure, and the Nusselt Number. Given the

negligible impact that nozzle length had on the outcomes, values were averaged for each nozzle diameter. To combine the two objectives (minimizing pressurization and maximizing heat transfer), an optimization objective, complemented by constraints, was formulated as expressed by Equation 19:

$$minmize: 9.783e4 * x^2 - 2.9308e4 * x + 1426 \quad (19)$$
$$subject\ to: 0.08 \leq x \leq 0.15$$

Here, x represents the nozzle diameter, with the underlying assumption being the equal weighting of static pressure and heat transfer in terms of importance. The optimal nozzle diameters, derived using SLSQP and trust region constrained algorithms, were 0.1 m and 0.115 m, respectively. The deduced values aligned reasonably well with the prevailing simplifying assumptions. However, variations of different importance weight on each variable and constraints could lead to different outcomes depending on external conditions (such as different incoming air temperatures and introducing humidity) and model selection (such as cow surface heat generation and pressurization inlet models) that were not considered when the current objective was established for simplicity. Despite this, subsequent case study models employed 0.1016 m as the default diameter, which aligned closely with the optimized results and served as one of the initial selections. All the following study cases involved 0.4-1.4 nozzle positions, a straight configuration, and 0.1016 m in diameter and 0.381 m in length.

### 4.4.3. Case Studies Outcomes

#### 4.4.3.1. Comparison to Idealized Crossflow Model

The efficiency of the PPPV system was evaluated in conjunction with the conventional crosswind model to ensure a balanced comparison focused on the sensible heat loss from identical cow models and total volumetric flow rate. The velocity contours with airflow vectors in both instances are depicted in Figure 34a and 34c. The velocity contour of the sectional cross-ventilated barn with baffle reasonable match well with the contour depicted in Jung et al. (2023). The Nusselt Number surface contour on cows for each ventilation design are shown in Figure 34b and 34d. Crosswind simulation setup with 1.25 m $s^{-1}$ velocity

outlet boundary condition with a given cross-sectional area yielded a volumetric flow rate of 5.78 $m^3 s^{-1}$, a rate that indicates an area-weighted average Nusselt Number of 111.16 and 180.21 per each pressure inlet side and velocity outlet side cow, respectively. Within the confines of the simulation setup, the model only accommodates two cows. However, in actuality, a flow rate of 5.78 $m^3 s^{-1}$ should adequately serve 8 to 12 cows aligned in the direction of the flow as volumetric flow rates between 0.47 to 0.71 $m^3 s^{-1}$ per cow is recommended in a crosswind setup for adequate heat removal (Mondaca & Cook, 2019). Conversely, the PPPV system delivered an area-weighted average Nusselt Number of 263.3 per cow, achieving approximately 0.17 $m^3 s^{-1}$ with respect to the two-cow model. If scaled up to accommodate 8 to 12 cows, the PPPV system must generate an airflow of only around 1.36 to 2.04 $m^3 s^{-1}$. These results suggest that PPPV system has a potential to improve convective cow cooling while significantly reducing the operational volumetric flow rate.

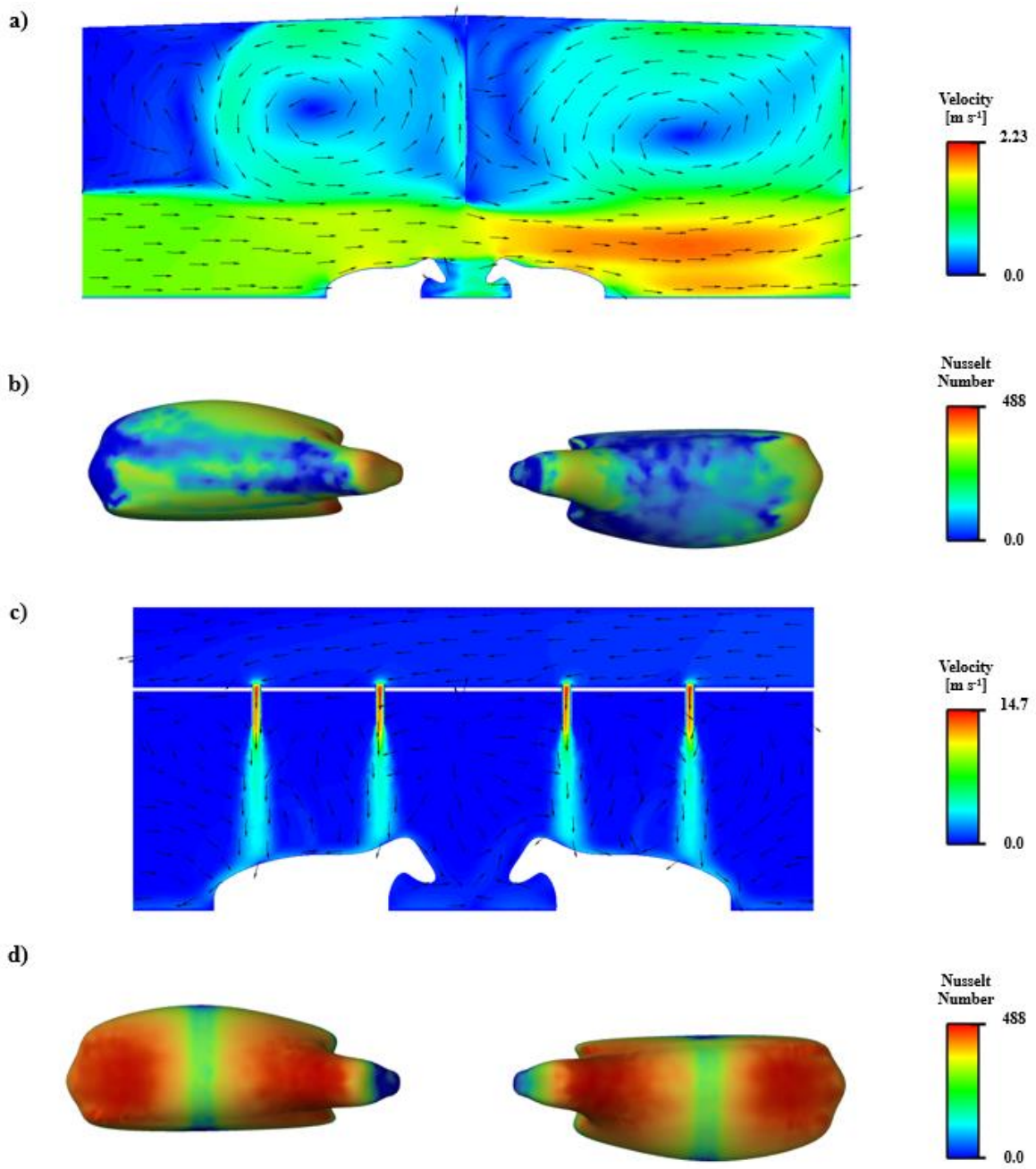


Figure 34. a) crosswind velocity contour and vector; b) Nusselt Number surface contour for cross-ventilation cows; c) PPPV system velocity contour; b) Nusselt Number surface contour for PPPV cows.

#### 4.4.3.2. PPPV vs. Air Drift

This study investigated the heat transfer performance of the PPPV system under various constant air-current conditions. For each air-current velocity evaluated (0.25, 0.50, 0.75, 1.0, 1.25, 1.50, 1.75, and 2.00 m $s^{-1}$), the area-weighted average Nusselt Number was computed for each cow body surface both upwind, cow #2, and downwind, cow #1, from the current (fig. 35c). The results showed that, for an air-current velocity of up to 0.5 m $s^{-1}$, the Nusselt number underwent only a minor reduction of 3.2%. Beyond this point, a performance decline occurred, one that aligned with trends observed by Cao et al. (2022) in their study of targeted cooling. However, once the air-current exceeded 1 m $s^{-1}$ (fig. 35a), an interesting phenomenon occurred: the system's performance started to improve, suggesting that high air-current velocities were beginning to emulate the effects produced by crosswind ventilation cooling. The variation in performance associated with the upwind as opposed to downwind cows is understandable, given that, due to the air-current, the airflow produced by the nozzle targeting the upwind cow could still affect the downwind cow. Crucially, and despite the air-current's impact on the PPPV system's efficiency, the resulting performance still surpassed that of an idealized crosswind ventilation setup with a Nusselt number of 130.2. Moreover, it should be kept in mind that the ambient air-current, simulated as a constant bulk airflow, represents a scenario unlikely to occur in a typical mechanically ventilated barn equipped with curtains. Even if wind gusts were to penetrate a barn, they would likely be transient. Additionally, subtle pressurization at the pen area due to air-jets coming down should buffer incoming wind coming in from outside.

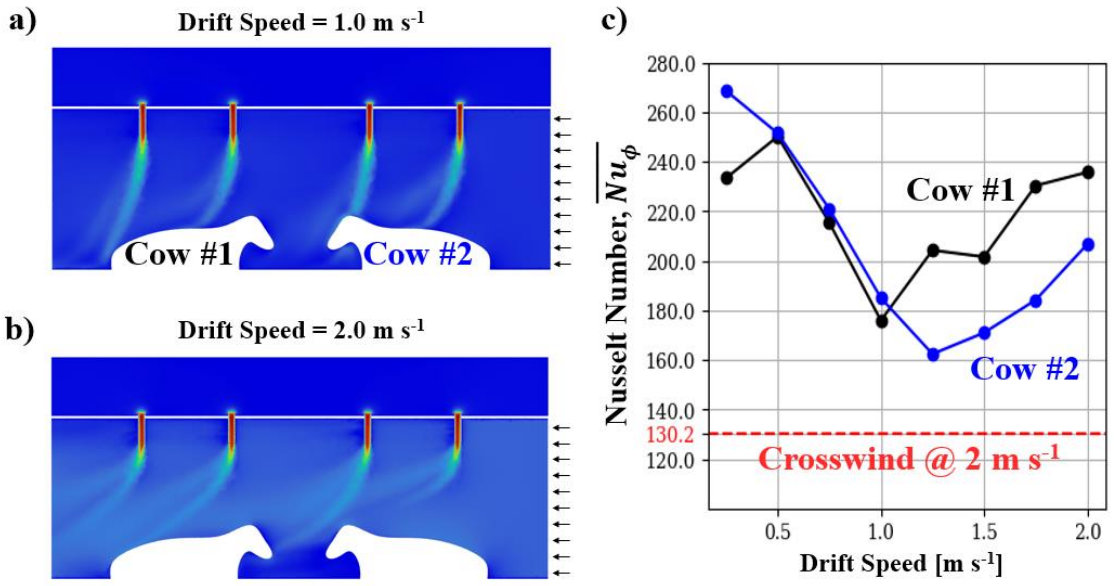


Figure 35. Ambient air-current influence on PPPV air-jets with varying air-current speed. a) velocity contour at 1.0 m $s^{-1}$ air-current; b) velocity contour at 2.0 m $s^{-1}$ air-current; c) air-current speed vs. Nusselt Number at air-current speeds from 0.25 to 2.0 m $s^{-1}$.

#### 4.4.3.3. Pen Size Scalability Test

Figure 36 presents an exploded 3D view of the volumetric contour projections depicting velocity, pressure, and surface Nusselt Number across different model sections. The position of the plenum pressurization inlets significantly influenced the internal pressure and velocity profiles. Despite their differences, none of the configurations produced more than a minimal variation between their high- and low-pressure areas. Remarkably, all three scenarios produced consistent air jets in the pen area, resulting in closely matched average area-weighted Nusselt numbers: 190.42±17.01, 190.28±16.75, and 191.133±16.04 per cow. The estimated volumetric flow rate for each case stood at 2.45 $m^3$ $s^{-1}$. A similar trend was found to occur at an average Nusselt number of 111.41±7.44 under a 46.66 Pa plenum pressurization. The efficiency (in terms of the heat transfer rates achieved by these configurations) was slightly less than those predicted by the two-cow model. This discrepancy is primarily a result of the two-cow model's idealized isolation assumption. In the 16-cow scenarios, the cows' physical interactions come into play more prominently. Notably, cows on the outer rows exhibited an enhanced heat-transfer performance compared to their

counterparts in the central formation. This difference can be attributed to their proximity to the outlet and to the decelerated air movement that occurred at the row's center. However, even as the system's scale and design introduced variables that could influence cooling efficiency, the consistency of the air jet flowing from each nozzle remained reliably uniform.

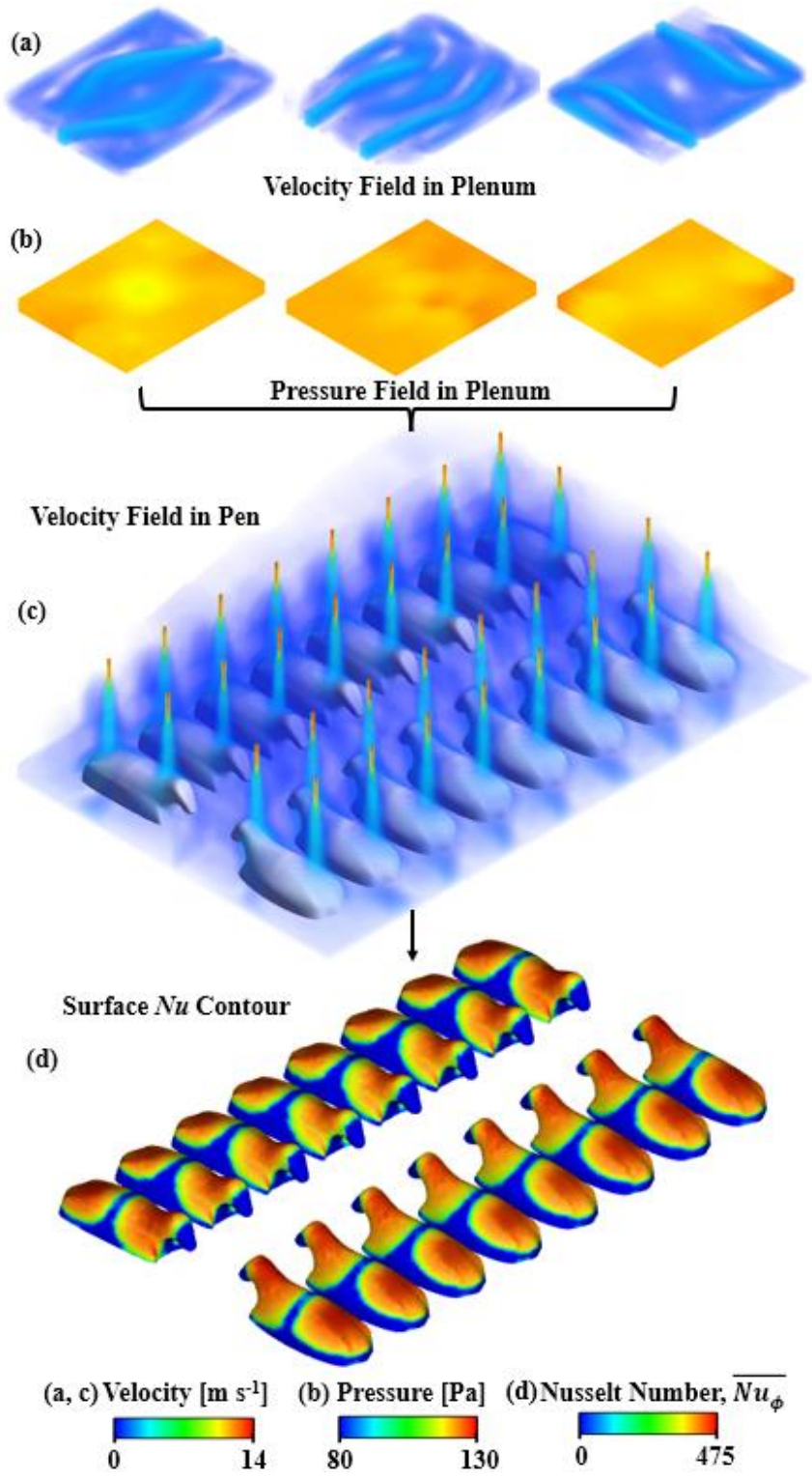


Figure 36. An exploded view of 3D volumetric contour projections, depicting velocity, pressure, and surface Nusselt Number across different model sections.

## 4.5. Conclusion

In this study, a computational analysis using experimentally validated CFD simulations was conducted to optimize and evaluate the PPPV system's design in regard to its cooling performance. In designing a PPPV system, the nozzle's specifications (especially its opening diameter, length, angle, and location) significantly affect the system's cooling performance and efficiency. This study demonstrated, that for each cow, an optimal nozzle design could be determined by means of a direct statistical comparison and linear programming with carefully selected parameter boundaries and simplified assumptions. It was noted that the angle of the targeted cooling air jet increases the rate at which heat is transferred away from a cow's body, but only a little (<5%), and that the velocity of the air jet is more significant than the area it covers. Additionally, the diameter of the nozzle's opening exponentially and positively influences the pressure occurring inside the plenum: the larger the opening, the higher the operation and equipment costs. Consequently, when determining the best design, both cooling performance and required power should be considered.

To evaluate the performance of PPPV, we created, computationally, a few case studies (using the suggested design parameters and an experimental model). Compared to traditional crosswind cooling systems, the PPPV system was found to produce as much as twice the cooling performance and could reduce the air supply requirement by half. Next, the scalability of the PPPV system was tested using a model of the barn occupied by 16 model cows. The simulation results showed that even with a plenum large enough to serve 16 cows, the pressurization was sufficiently uniform and could deliver constant air jets at each nozzle exit. This finding indicates that the cooling performance occurring at the center row of stalls would be less than that which would occur at the outer rows. Finally, the impact of perpendicular bulk air movement on the air jet was evaluated by introducing a relatively light crossflow in addition to the flow produced by the PPPV system. At a crossflow of 0.5 m $s^{-1}$, the overall cooling performance of the PPPV system decreased by about 3.9%.

The series of simulations we created showed that the PPPV system we evaluated can effectively and uniformly provide cooling air jets to each cow in the barn and do so at a more cost-effectively than can traditional cross- and tunnel-ventilation systems. By applying design-optimization techniques and with the aid of CFD simulation methods, we were able to accurately predict an optimal design and a ventilation strategy and thus avoid using the traditional, and far more costly, physical trial-and-error approach.

## 4.6. References

Abeykoon, C. (2020). Compact heat exchangers–Design and optimization with CFD. International Journal of Heat and Mass Transfer, 146, 118766.

Bohmanova, J., Misztal, I., & Cole, J. B. (2007). Temperature-humidity indices as indicators of milk production losses due to heat stress. Journal of dairy science, 90(4), 1947-1956.

Calautit, J. K., O'Connor, D., Sofotasiou, P., & Hughes, B. R. (2014). CFD simulation and optimisation of a low energy ventilation and cooling system. Computation, 3(2), 128-149.

Cao, M., Rong, L., Choi, C. Y., Wang, K., & Wang, X. (2022). Computational evaluation of air jet cooling from a perforated air ducting system to mitigate heat stress of cows in free stalls. Computers and Electronics in Agriculture, 199, 107198.

Cao, M., Yang, R., Choi, C. Y., Rong, L., Zhang, G., Wang, K., & Wang, X. (2023). Effects of discharge angle of jet from a slot orifice on cooling performance for a perforated air ducting system in dairy cattle barn. Computers and Electronics in Agriculture, 210, 107890.

Cook, N. B., Mentink, R. L., Bennett, T. B., & Burgi, K. (2007). The effect of heat stress and lameness on time budgets of lactating dairy cows. Journal of dairy science, 90(4), 1674-1682.

Friedlander, A., Martinez, J. M., & Santos, S. A. (1994). A new trust region algorithm for bound constrained minimization. Applied Mathematics and Optimization, 30(3), 235-266.

He, X., Wang, J., Guo, S., Zhang, J., Wei, B., Sun, J., & Shu, S. (2018). Ventilation optimization of solar greenhouse with removable back walls based on CFD. Computers and Electronics in Agriculture, 149, 16-25.

Jung S., Chung, H., Mondaca, M.R., Nordlund, K.V., Choi, C.Y. (2023) Using computational fluid dynamics to develop positive-pressure precision ventilation systems for large-scale dairy houses, Biosystems Engineering. 227, 182-194.

Key, N., Sneeringer, S., & Marquardt, D. (2014). Climate change, heat stress, and US dairy production. USDA-ERS Economic Research Report, (175).

Kraft, D. (1988). A software package for sequential quadratic programming. Forschungsbericht-Deutsche Forschungs- und Versuchsanstalt fur Luft- und Raumfahrt. DFVLR-FB 88-28, DLR German Aerospace Center, 1988.

Le Cozler, Y., Allain, C., Xavier, C., Depuille, L., Caillot, A., Delouard, J. M., Delattre, L., Luginbuhl, T., & Faverdin, P. (2019). Volume and surface area of Holstein dairy cows calculated from complete 3D shapes acquired using a high-precision scanning system: Interest for body weight estimation. Computers and Electronics in Agriculture, 165, 104977.

Li, L., Cheng, Z., & Lange, C. F. (2018). CFD-based optimization of fluid flow product aided by artificial intelligence and design space validation. Mathematical Problems in Engineering, 2018.

Li, J., Narayanan, V., Kebreab, E., Dikmen, S., & Fadel, J. G. (2021). A mechanistic thermal balance model of dairy cattle. Biosystems engineering, 209, 256-270.

Liu, J., Li, L., Chen, X., Lu, Y., & Wang, D. (2019). Effects of heat stress on body temperature, milk production, and reproduction in dairy cows: A novel idea for monitoring and evaluation of heat stress—A review. Asian-Australasian journal of animal sciences, 32(9), 1332.

Mondaca, M. R., & Choi, C. Y. (2016a). A computational fluid dynamics model of a perforated polyethylene tube ventilation system for dairy operations. Transactions of the ASABE, 59(6), 1585-1594.

Mondaca, M. R., & Choi, C. Y. (2016b). An evaluation of simplifying assumptions in dairy cow computational fluid dynamics models. Transactions of the ASABE, 59(6), 1575-1584.

Mondaca, M. R. (2019). Ventilation systems for adult dairy cattle. Veterinary Clinics: Food Animal Practice, 35(1), 139-156.

Mondaca, M. R., Choi, C. Y., & Cook, N. B. (2019). Understanding microenvironments within tunnel-ventilated dairy cow freestall facilities: Examination using computational fluid dynamics and experimental validation. Biosystems engineering, 183, 70-84.

Norton, T., J. Grant, R. Fallon, and D. W. Sun. (2010). Improving the representation of ther-mal boundary conditions of livestock during CFD modeling of the indoor environment. Computer and Electronics in Agriculture 73:17-36.

Polsky, L., & von Keyserlingk, M. A. (2017). Invited review: Effects of heat stress on dairy cattle welfare. Journal of dairy science, 100(11), 8645-8657.

Rong, L., Nielsen, P. V., Bjerg, B., & Zhang, G. (2016). Summary of best guidelines and validation of CFD modeling in livestock buildings to ensure prediction quality. Computers and Electronics in Agriculture, 121, 180-190.

St.-Pierre, N. R., Cobanov, B., Schnitkey, G., (2003). Economic Losses from Heat Stress by US Livestock Industries. Journal of Dairy Science, 86(31). E52-77.

Tao, S., Orellana Rivas, R. M., Marins, T. N., Chen, Y. C., Gao, J., & Bernard, J. K. (2020). Impact of heat stress on lactational performance of dairy cows. Theriogenology, 150, 437e444. https://doi.org/10.1016/j.theriogenology.2020.02.048

USDA-NASS. (2017). Milk production. Retrieved from: http://usda.mannlib.cornell.edu/usda/nass/MilkProd//2010s/2017/MilkProd-02-21-2017.pdf

Van Os, J. M. (2019). Considerations for cooling dairy cows with water. Veterinary Clinics: Food Animal Practice, 35(1), 157-173.

Wang, X., Zhang, G., & Choi, C. Y. (2018). Evaluation of a precision air-supply system in naturally ventilated freestall dairy barns. Biosystems Engineering, 175, 1-15.

Wu, W., Zhai, J., Zhang, G., & Nielsen, P. (2012). Evaluation of methods for determining air exchange rate in a naturally ventilated dairy cattle building with large openings using CFD. Atmospheric Environment 63:179-188.

Zhou, B., Wang, X., Mondaca, M. R., Rong, L., & Choi, C. Y. (2019). Assessment of optimal airflow baffle locations and angles in mechanically-ventilated dairy houses using computational fluid dynamics. Computers and Electronics in Agriculture, 165, 104930.

# CHAPTER 5: CONCLUSIONS

## 5.1. Summary

The aim of this dissertation is to explore the potential of utilizing advanced sensor networks and simulation techniques to improve the control of ventilation in dairy barns, with a particular focus on refining techniques for alleviating heat stress and an ultimate goal of building a smarter animal-centric ventilation system. With the growing prevalence of data-centric technologies, the large amounts of data relevant to dairy barns will become more accessible to a wider range of stakeholders, including researchers, engineers, and farmers. This trend towards data-driven strategies for barn ventilation control and the possibility of fully automated dairy barn operations is becoming increasingly apparent and inevitable. The findings from this research can serve as crucial references for those who are working towards developing sophisticated systems that can counter heat stress and promote eco-friendly dairy practices. The key takeaways from this research include the following:

- The subcutaneous temperature at the base of a cow's ear is a reliable indicator of the animal's core body temperature, providing a more accurate assessment of heat stress than conventional environmental metrics.
- Real-time, wirelessly connected, rechargeable wearable biosensors are effective in consistently monitoring the subcutaneous temperature, paving the way for an all-encompassing, IoT-centric, animal-responsive ventilation control system.
- Machine learning-informed computational fluid dynamics (CFD) models can efficiently generate precise CFD simulation results, reducing the time and computational resources required.
- The simplified hardware requirements of data-oriented CFD models make CFD simulations more accessible to non-CFD specialists, such as producers and barn builders, by facilitating integration with user-centric online platforms.

- The PPPV system demonstrates enhanced cooling efficiency with reduced airflow compared to conventional crosswind ventilation systems, resulting in cost savings and decreased heat-induced stress for livestock.
- Integrating CFD with design optimization techniques reveals the potential to adeptly navigate and innovate within the realm of dairy barn ventilation strategies.

## 5.2. Future Work

To optimize cow cooling, a real-time monitoring of the cow's core body temperature and a targeted cooling ventilation system are essential. However, to fully harness their potential, a control scheme that seamlessly integrates these two elements is necessary. To develop this scheme, an experiment should be conducted using a pen-scale Positive Pressure Ventilation (PPPV) system, as outlined in Chapter 4. This system should be populated with cows equipped with ear tags for monitoring, as detailed in Chapter 2. The experiment should span at least two months, ideally during summer heat waves, to fine-tune the control scheme. Machine learning can be employed to optimize the system using various data points, including cow core body temperature, fan load, and plenum pressurization.

The CFD-ML tool can be further refined and generalized by enhancing the Dynamic Data-Driven Feature (DDF) training aspect. Currently, the DDF is constrained to a fixed computational domain size, regardless of its contents, and its performance is closely tied to the number of directions defined by the user. Rather than using a signed distance function to compute distances, an alternative machine learning approach could expedite the definition of DDF features, as this is the most computationally intensive step in the CFD-ML model. By expanding DDF to accommodate different computational boundary sizes, the tool can learn from any CFD simulations. Moreover, a more efficient CFD-ML tool could enable fluid simulation to be accessible via a mobile app, allowing producers to utilize it anywhere at a low computational cost.

# APPENDIX A: FOR CHAPTER 3

Table A.1. Model details for CNN1 2D. This model was used for both porous and solid cow-body cases.

| Layer | Kernel Size | Strides | Output Shape |
|---|---|---|---|
| Conv3D | (2,8) | (2,8) | (12,24,128) |
| Conv3D | (2,4) | (2,4) | (6,6,256) |
| Flatten | - | - | 9216 |
| Dense | - | - | 9216 |
| Reshape | - | - | (6,6,256) |
| Conv3DTranspose | (2,4) | (2,4) | (12,24,128) |
| Conv3DTranspose | (4,8) | (4,8) | (24,192,3) |

Table A.2. Model details for CNN2 2D.

| Layer | Kernel Size | Strides | Output Shape |
|---|---|---|---|
| Conv3D | (2,8) | (2,8) | (5,4,128) |
| Flatten | - | - | 2560 |
| Dense | - | - | 2560 |
| Dense | - | - | 256 |
| Dense | - | - | 128 |
| Dense | - | - | 36 |

Table A.3. Model details for CNN1 3D.

| Layer | Kernel Size | Strides | Output Shape |
|---|---|---|---|
| Conv3D | (4,16,4) | (4,16,4) | (6,12,5,128) |
| Conv3D | (2,4,5) | (2,4,5) | (3,3,1,256) |
| Flatten | - | - | 2304 |
| Dense | - | - | 2304 |
| Reshape | - | - | (3,3,1,256) |
| Conv3DTranspose | (2,4,5) | (2,4,5) | (6,12,5,128) |
| Conv3DTranspose | (4,16,4) | (4,16,4) | (24,192,20,4) |

Table A.4. Model details for CNN2 3D.

| Layer | Kernel Size | Strides | Output Shape |
|---|---|---|---|
| Conv3D | (5,8,7) | (5,8,7) | (2,4,2,128) |
| Flatten | - | - | 2048 |
| Dense | - | - | 1024 |
| Dense | - | - | 648 |

# APPENDIX B: FOR CHAPTER 4

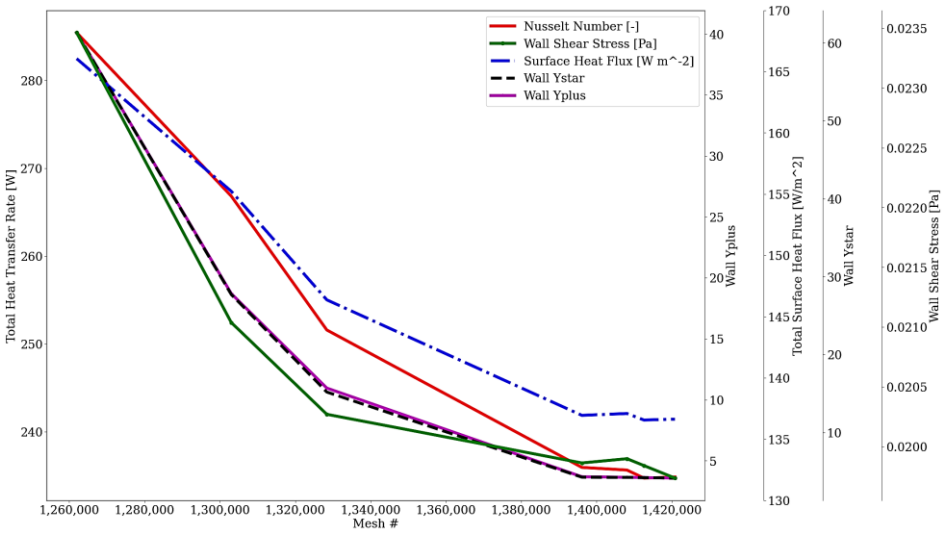


Figure B.1. Mesh testing with 5 CFD parameters.